UNIVERSITÀ DI PARMA

UNIVERSITA' DEGLI STUDI DI PARMA

DOTTORATO DI RICERCA IN

"Scienze del Farmaco"

CICLO XXXVI

Innovative Strategies for Non-invasive Treatment of Non-melanoma Skin Cancers

Coordinatore:

Chiar.mo Prof. Marco Mor

Tutore:

Chiar.ma Prof. Patrizia Santi

Dottorando: Luca Giulio

Anni Accademici 2020/2021 – 2022/2023

TABLE OF CONTENTS

METHODS ..... - 35-

RESULTS AND DISCUSSIONS .....- 53-

INTRODUCTION

1. Skin Cancers

Skin cancers are the most common group of cancers in the world, with more than 1.5 million new cases in 2020 [1]. According to the Skin Cancer Foundation, 1 out of 5 Americans will develop skin cancers by age 70 [2].

The main cause is the sun's harmful ultraviolet rays: despite small amounts of UV rays are beneficial for health and play an essential role in the production of Vitamin D, excessive exposure is carcinogenic to humans. The damage effects of UV radiation on the skin are thought to be caused by direct cellular damage and alterations in immunologic function [3]. In fact, skin cancer is defined as the out-of-control growth of abnormal cells in the epidermis, the outermost skin layer, caused by DNA damage (formation of cyclobutane pyrimidine dimers), gene mutations, immunosuppression, oxidative stress and inflammatory responses that trigger mutations. These mutations lead the skin cells to multiply rapidly and form malignant tumours.

Skin cancers are usually classified into melanoma and non-melanoma skin cancers (NMSCs), such as Basal Cell Carcinoma (BCC), Squamous Cell Carcinoma (SCC) and Merkel Cell Carcinoma (MCC), which are further and deeper detailed. In this classification, Keratoacanthoma (KA) should also be considered. Keratoacanthoma is a low-grade, rapidly growing, 1 to 2 cm dome-shaped skin tumour with a centralized keratinous plug [4]. It commonly occurs as an isolated lesion on sun-exposed skin in elderly patients. Many authors and the new World Health Organization Classification of skin tumours consider KA as an incipient variant of the cutaneous squamous cell carcinoma [5], although it is subject of debate [6][7].

1.1 Melanoma Skin Cancers

Melanoma is a cancer that develops from melanocytes, the skin cells that produce melanin pigment, which gives the skin its colour. Melanoma skin cancers are less common than non-melanoma skin cancers but are more dangerous due to their ability to spread to other organs more rapidly, if they are not treated at early stage. In fact, the estimated five-year

survival rate for US patients whose melanoma is detected early is about 99%, but drops to only 18% for stage IV metastatic melanomas [8].

It is very difficult to have a comprehensive view of warning signs because melanomas could be in different shapes, sizes and colours. There are different types of melanomas: the superficial spreading type, the lentigo maligna, the acral lentigious types and the nodular melanoma.

The most common type of melanoma is superficial spreading melanoma. Usually, it arises in an existing mole and it tends to grow on the surface of the skin for some time before penetrating more deeply. It may appear as a flat or slightly raised and discoloured, asymmetrical patch with uneven borders. Colours include shades of brown, black, red/pink, blue or white. It can also lack pigments and appear as a pink or skin-tone lesion (amelanotic). While it can be found nearly anywhere on the body, it is most likely to appear on the torso in men, the legs in women and the upper back in both.

The lentigo maligna type occurs in older people. It may look like a flat or slightly raised, blotchy patch with uneven borders. Colour is usually blue-black but can vary from tan to brown or dark brown.

The acral lentiginous melanoma is the most common type of tumor found in people of color. It often appears in hard-to-spot places including under the nails (subungual) and on the soles of the feet or palms of the hands.

The last type of melanoma is the nodular melanoma, the most aggressive. The tumor grows deeper into the skin more rapidly than other types and is most frequently found on the torso, legs and arms, as well as the scalp in older men. It is usually invasive at the time it is first diagnosed. This type is often recognized as a bump on the skin, usually blue-black in colour, but not uncommonly it can also appear as a pink to red bump [9].

1.2 Non-Melanoma Skin Cancers

Non-melanoma skin cancers (NMSCs) refer to a group of cancers that develop slowly in the upper layers of the skin. These types of cancers are more common than melanoma. The most common NMSCs are basal cell carcinoma (BCC) and squamous cell carcinoma (SCC),

which represent the majority, while Merkel cell carcinoma (MCC), sebaceous carcinoma, apocrine adenocarcinoma and other rare tumours are less frequent.

Although NMSCs are 18–20 times more frequent than cutaneous melanoma, there is little epidemiological data for those tumour types [10][11][12]. Only a few studies have examined the separate incidence of BCCs and SCCs, because in most European countries different types of NMSCs are not distinguished from each other in national cancer registry data. Both BCC and SCC result from the malignant transformation of keratinocytes and suppression of the cutaneous inflammatory response [13].

Basal cell carcinoma (BCC) predominantly manifests on sun-exposed areas, with 80% occurring on the head and neck and 15% on the trunk. These lesions exhibit slow growth, with rare instances of metastasis; however, untreated lesions can locally invade and destruct surrounding structures. Various histological subtypes of BCC exist. The classical nodular subtype appears as a pink, pearly papule with telangiectasia, a rolled edge, and potential central ulceration (known as rodent ulcer). Superficial BCCs present as slowly enlarging erythematous plaques, more common on the trunk, resembling conditions like psoriasis, Bowen's disease or discoid eczema. Morphoeic BCCs are more invasive, revealing late-stage pale, poorly demarcated plaques due to their nonspecific appearance.

On the other hand, squamous cell carcinoma (SCC) may manifest as ulcers or hardened keratinizing lesions in sun-exposed regions. SCCs can originate from pre-malignant lesions such as actinic keratoses (AKs) and Bowen's disease, also termed SCC in situ. AKs are indicators of UV-damaged skin and progress to invasive SCC in approximately 1–10% of cases.

To complete the overview, MCC is a rare, aggressive neuroendocrine tumor of the skin with increasing incidence. In 80% of diagnostic cases, Merkel cell polyomavirus is considered as the etiological agent in carcinogenesis [14].

1.3 Management of Non-Melanoma Skin Cancers

1.3.1 Non-Pharmacological Treatments

Among non-pharmacological options to treat non-melanoma skin cancers, surgery represents the treatment of choice.

Surgery is the removal of the tumor and surrounding tissue during a medical procedure. Which surgical procedure is used depends on the type of skin cancer and the size and location of the lesion. Mohs micrographic surgery (also known as complete margin assessment surgery) involves removing the visible tumor in addition to small fragments around the edge of the area where the tumor is located. Each small fragment is examined under a microscope until all the cancer is removed. This procedure is typically used for larger tumors, for those located in the head and neck region.

Similar treatment to Mohs surgery is represented by wide excision, which involves the removal of the tumor and some surrounding healthy skin and soft tissue, called a margin.
Another possibility for surgeons is curettage and electrodessication: following these procedures the skin lesion is removed with a curette, which is a sharp, spoon-shaped instrument. The area is then treated with an electric current that helps control bleeding and destroys any remaining cancer cells [15].

Radiation therapy has always played an essential role in the management of NMSC. This treatment consists of the use of high energy rays or other particles to destroy cancer cells. It may be used instead of surgery for skin cancers that that located in hard-to-treat places. Sometimes, it is recommended after surgery, especially for lymph nodes that are involved in the cancer, to help prevent relapses. The most common type of radiation treatment is called external-beam radiation therapy with high-energy photons or electrons (X-rays) delivered by a linear accelerator placed outside the body.

It can be used at any stage of the disease, with curative or palliative intent, as an exclusive or concomitantly with systemic treatment. Radiation therapy should only be avoided in rare genetic syndromes such as ataxia-telangiectasia, connective tissue disease (i.e., Verrucous carcinoma, LiFraumeni syndrome), and basal cell carcinoma/Gorlin syndrome [16].

Of great importance is photodynamic therapy: it uses a photosensitizing agent (methyl aminolevulinate or 5-aminolevulinic acid) activated by a light source such as X-rays, Ultraviolet rays, Near-Infrared rays and microwave light [17]. The photosensitiser produces photo-active porphyrins in malignant keratinocytes and illumination then results in the release of reactive oxygen species and free radical formation. Photodynamic therapy is not approved for SCC, due to the potential of metastasis and recurrence, but it is effective in the management of premalignant lesions [18] [19].

The last non-pharmacological treatment option is cryotherapy (also called freezing) that uses liquid nitrogen to freeze and destroy abnormal cells. It is usually used to treat precancerous skin conditions. Sometimes this procedure leaves a scar.

1.3.2 Pharmacological Treatments

1.3.2.1 Systemic Route of Administration

Systemic chemotherapy plays an important role in the management of NMSCs, in particular in the case of metastatic cancers. Cisplatin, cyclophosphamide, bleomycin, doxorubicin, methotrexate (MTX), and 5-FU are the most common therapeutical agents [20]. Data demonstrated that cisplatin-based treatments showed to be effective in advanced BCCs, both as a single agent or in combination with other cytotoxic agents. As confirmed by two extensive reviews on advanced BCCs, cisplatin alone or in combination with other agents yielded a response higher than 77%, a complete remission rate of over 35% and median survival over 20 months [21][22].

In the last years, immune modulators such and monoclonal antibodies, have demonstrated promising results; epidermal growth factor receptor (EGFR) inhibitors appear to be of great interest since EGFR is involved in the pathogenesis of SCC. National Comprehensive Cancer Network recommends chemotherapy as a possible supplement to radiation therapy in local, high-risk SCCs for patients who are non-surgical candidates [23].

In addition to these more common treatments, it has been observed that the ability of some antifungal agents to inhibit Hedgehog pathway should be effective to treat NMSCs.

Vismodegib and Sonidegib represent two Hedgehog pathway inhibitors used for the treatment of advanced BCCs [24].

Notably, it has been proved that an *off-label* use of intralesional MTX, widely used in oncology as anti-tumoral agent, gives very promising outcomes against KA and specified cases of SCC [25][26]. MTX is a folic acid analogue that irreversibly binds to dihydrofolate reductase, thereby blocking the formation of tetrahydro-folate and, subsequently, preventing the synthesis of the purine nucleotide thymidine, leading to a halt in DNA synthesis and to cell death [27]. By inhibiting DNA synthesis, MTX results also beneficial in rheumatoid arthritis and in certain inflammatory cutaneous disorders, such as psoriasis, although with variable efficacy [29][30]. To the best of our knowledge, MTX is usually administered by intralesional injection of 25 mg/ml or 12.5 mg/ml solutions [30][31]. Pain associated with this treatment may be controlled by the addition of lidocaine [32]. Across the studies, 74% to 100% of lesions resolved and serious systemic adverse effects were not reported. The most common observed side-effect is the injection-site pain [33][31][34][35]. Treatment intervals range from 7 to 38 days with patients requiring one to eight sessions. Korean patients require more treatment sessions albeit with shorter intervals compared to Caucasian patients [26]. It is postulated that ethnicity might affect the concentration of MTX required, possibly secondary to pharmacogenomics [36]. None of the patients reported in the studies had a relapse with follow-up periods varying from 6 weeks to 4 years. All treated cases achieved resolution with high patient satisfaction [37][30][32][26].

1.3.2.2 Topical Route of Administration

When surgical intervention and systemic treatments are not possible or rejected by the patient, topical treatment may be more appropriate and more effective. In fact, topical therapy is commonly recommended for patients presenting multiple clinical and subclinical lesions over a large anatomical area. Treatments with topical agents may also allow for higher drug levels at site of the tumor, with potentially lower toxicity to the patient than systemic agents [38].

Below, the drugs used in topical treatments are presented.

a. **Imiquimod** is an immunomodulator, acting as agonist of toll-like receptors; this leads to the activation of several cytokines and chemokines and these factors stimulate both

innate and acquired immune response pathways resulting in imiquimod-mediated antitumor responses. Imiquimod (Aldara®) was approved in 2004 for treatment of Ak and BCC, in patients not eligible for surgery or alternative treatments.

b. **5-Flurouracil (5-FU)** is an antimetabolite, leading to cell death. It is the commonly used topical agent to treat superficial BCC. A larger randomized controlled trial with 601 histopathologically-confirmed BCC compared the use of 5-FU with photodynamic therapy with methylaminolevulinic acid and topical imiquimod [39]. Both imiquimod and 5-FU were associated with less severe adverse events compared with photodynamic therapy.

c. **Ingenol mebutate** is a plant extract that has multiple mechanisms of action, including necrosis of cancer cells and subsequent activation of protein C kinase. The activation of protein C kinase contributes to the destruction of malignant cells and prevention of relapse. Ingenol mebutate is FDA approved for the treatment of Ak and it is used *off-label* for the treatment of superficial BCC. A randomized controlled trial conducted in 2016 showed a superficial BCC histologic clearance in 63% of patients [40]. Another important aspect is the short course treatment (once-daily for max three days), which ensure the adherence to treatment [41]. Adverse reactions may include erythema, pain, and oedema that typically resolve within 2 weeks [42].

d. **Dicolofenac**, a common nonsteroid anti-inflammatory drug, may be effective in reducing dysplastic keratinocytes. A topical gel formulation containing 3% diclofenac in 2.5% hyaluronic acid is currently available and FDA approved for the treatment of Ak.

e. **Photodynamic therapy** requires the use of a photosensitizing agent, the light (as X-rays, Ultraviolet rays, Near-Infrared rays or microwave light [17]) and the presence of oxygen. Methyl amino levulinate and 5-aminolevulinic acid are topical photosensitizer precursors used to treat NMSCs. When applied, these substances are converted into photoactive porphyrins preferentially in neoplastic cells. By proper light activation, photoactive porphyrins are excited to their higher energy state, which is subsequently transferred to oxygen molecules, resulting in the formation of cytotoxic free radicals and singlet oxygen. Considering that the cellular mechanism is not fully understood, both apoptosis and necrosis seems involved and influenced by intracellular localization of the photosensitizers and illumination parameters [19].

f. **Retinoids** are analogues of Vitamin A used to treat skin cancers, due to the interfering process of retinoids in growth and differentiation of keratinocytes, by the interaction with nuclear receptors (retinoic acid and retinoic X receptors). To date, no retinoids have been approved by the FDA, but they are successfully used in experimental models of keratinocyte carcinomas [43].

2. Structure of The Skin

The skin, or cutis, represents one of the main components of the integumentary system together with the skin appendages (hair, nails, glands). In an adult man, the extension of the skin can reach up to 2 m^2 and is considered a real organ with specific functions: coating, thermoregulation, physical, chemical and microbiological protection [44]. The skin is organized in three layers: the epidermis, the dermis and the hypodermis (Figure 1). The intricate structure of the skin displays notable regional variations in terms of epidermal and dermal thickness, the distribution of epidermal appendages and melanocyte content. While the skin on the palms and soles is non-hair bearing, the rest of the body is covered by hair-bearing skin. Embryologically, the epidermis and its appendages originate from the surface ectoderm, while the dermis and hypodermis emerge from the mesoderm. During the fourth week of embryonic development, a singular layer of ectoderm envelops the embryo, and above it lies a loosely organized stratum of undifferentiated mesoderm called mesenchyme. Around the sixth week, both ectoderm and the underlying mesoderm undergo proliferation and differentiation. The development of hair follicles, nails, and glands initiates during the third month. By the end of the third month, regular collagen bundles become evident in the dermis. The embryonic connective tissue beneath the dermis evolves into the subcutaneous layer, characterized by loose connective tissue featuring islands of fat [44].

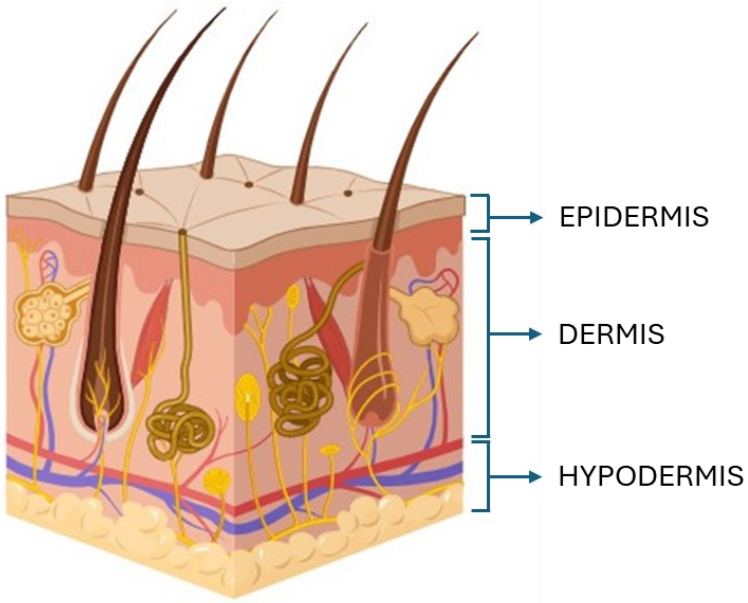

Figure 1: Structure of the skin. Partially created with BioRender.com.

2.1 The Epidermis

The normal epidermis is a continuously renewing stratified squamous epithelium. The primary cell type within the epidermis is the keratinocyte, accounting for approximately 95% of the epidermal cells. As keratinocytes progress from their attachment to the basement membrane toward the skin surface, they give rise to distinct morphological layers in the epidermis: the stratum basale or stratum germinativum, stratum spinosum, stratum granulosum, and stratum corneum (see Figure 2). On the palms and soles, an additional layer known as the stratum lucidum can be distinguished between the stratum corneum and stratum granulosum. Additionally, other cell types present in the epidermis include melanocytes, Langerhans cells, and Merkel cells [44].

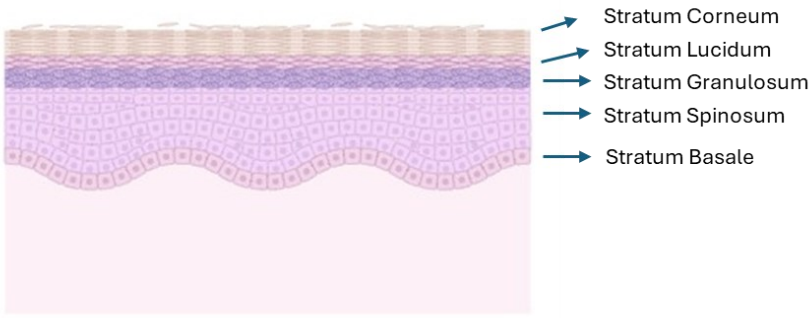

Figure 2: Layers of the epidermis. Partially created with BioRender.com.

The basal layer consists of a single layer of cuboidal cells resting on the basement membrane. Basal cells undergo division, leading to the formation of the next layer, known as the prickle cell layer or stratum spinosum. Typically, this layer is 3 to 4 cells thick and comprises polygonal cells with preformed keratin. Desmosomal attachments between the cells manifest as small spines, giving rise to the name stratum spinosum. Following this, the stratum spinosum is succeeded by the stratum granulosum, usually 1 to 4 cells thick, characterized by cytoplasmic keratohyalin granules. The outermost layer of the epidermis is the stratum corneum, consisting of flattened keratinocytes that have shed their nuclei and cytoplasmic organelles [45].

Melanocytes are derived from neural crest cells in the basal layer and migrate into the epidermis where they produce melanin. They are distributed among the basal keratinocytes with the ratio of 1 melanocyte to 4 to 10 basal cells. This ratio varies with anatomic location, with maximal density of melanocytes on genital skin. Melanin is produced from tyrosine by the enzymatic activity of tyrosine kinase and is stored in melanosomes. Melanosomes are transported along the dendritic processes of melanocytes to adjacent keratinocytes, where they form an umbrella-like cap over the nucleus, protecting it from the injurious effects of UV light [46].

Langerhans cells function as sentinel antigen-presenting cells that can capture invading viruses such as herpes simplex virus, varicella-zoster virus and human immunodeficiency virus. This interaction between Langerhans cells and viruses results in highly variable response (e.g. apoptosis and activation of T cells) [47]. The number of Langerhans cells increases during allergic reactions, such as contact hypersensitivity. With aging and chronic sun exposure, the

number of Langerhans cells decreases, which may play a permissive role in the development of cutaneous carcinoma in individuals who are elderly with sun-damaged skin [48].

Merkel cells are found in the basal layer of the epidermis and in the epithelial sheath of hair follicles. Merkel cells migrate from neural crest to the skin and have similar chemical and structural properties to an amine precursor uptake decarboxylation cell. They are associated with sensory nerve endings in the skin and may function as mechanoreceptors [47].

2.2 The Dermis

Dermis is found under the epidermis. It is constituted by two principal components: one superficial papillary layer and one deeper, called reticular layer (Figure 3).

The superficial papillary layer consists of loose connective tissue. This region contains the capillaries that supply the epidermis and the endings of the sensory nerves that innervate the receptors of the papillary layer and the epidermis. The papillary layer takes its name from the papillae of the dermis that deepen between the epidermal ridges.

The deeper reticular layer is constituted by a woven fibrous network of dense, irregular connective tissue that surrounded blood vessels, hair follicles, nerves, sweat and sebaceous glands. The name of the layer derives from the intertwining of the bundles of collagen fibers found in this region. Small group of collagen fibers ascend from the reticular dermis towards the papillary dermis, so that there is no clear line of demarcation between the two layers. The collagen fibers of the reticular layer also extend into the underlying subcutaneous layer.

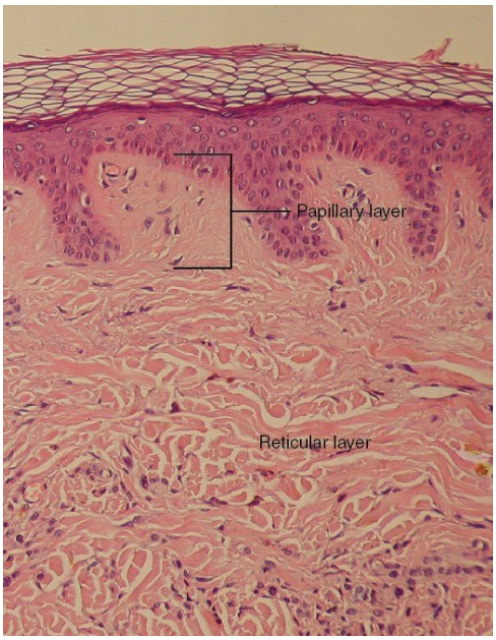

Figure 3: Layers of the dermis: Papillary and Reticular layers (credit: modification of work by "kilbad"/Wikimedia Commons)[49].

The dermis is not only composed of interstitial (like collagen fibers, elastic tissue and ground substance), but also of cellular components, like fibroblast, mast cells, plasma cells, limphocytes, dermal dendritic cell and histiocyte). It also contains blood vessels, lymphatic channels and sensory nerves. About 70% of the dry weight of dermis is made up of collagen. Elastic fibers are less tough than collagen fibers but guarantee flexibility to the skin. An extracellular ground substance containing glycosaminoglycans, such as hyaluronic acid, proteoglycans and glycoproteins is found between these fibrous components [50].

Dermal fibroblasts are the most abundant cellular component: they produce and organize the extracellular matrix of the dermis. They also communicate with each other and other cell types. Fibroblasts play a crucial role in regulating skin physiology and cutaneous wound repair. Normal adult human skin contains at least three distinct subpopulations of fibroblasts — papillary, reticular, and follicular. Phenotypic differences between these population are manifested in extracellular matrix production and organization, production of growth factors/cytokines, and participations in inflammatory responses [51].

Beyond skin support and protection, dermis plays a crucial role in thermoregulation through vasoactive vessels and glomus bodies. In addition, several mechanoreceptors are present in dermis. Nerve endings in the dermis surround hair follicles. These nerve endings sense hair movement and act as mechanoreceptors allowing sensation to extend beyond the skin's surface. Deep pressure receptors also exist [52].

3. Transdermal Drug Delivery

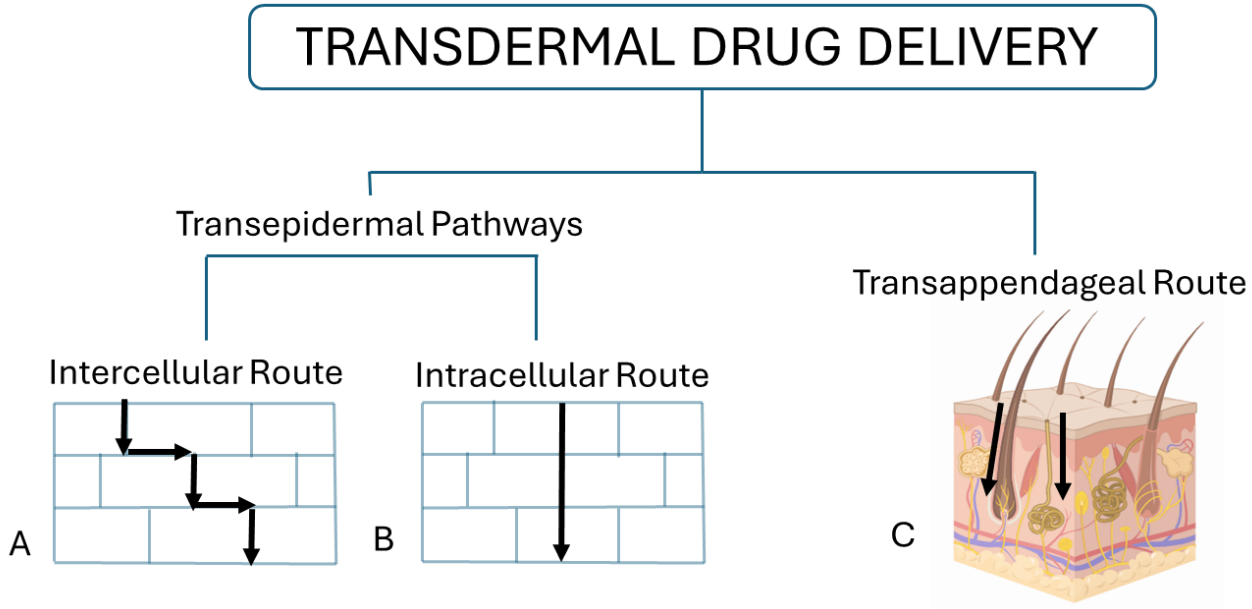

Figure 4: Types of transdermal pathways: transepidermal and tranappendageal routes. Partially created with BioRender.com.

The skin represents an attractive organ for local (topical, dermal) and systemic (transdermal) delivery of active substances. Molecules cross the stratum corneum barrier mainly through three pathways: the transepidermal pathways which include the intercellular and the transcellular routes and the transappendageal route.

The "brick and mortar" model of the stratum corneum is used to explain and predicted the permeability of penetrant molecules. Cornified dead cells are filled with keratin and compose the brick, while the mortar is composed of multiple stacks of lipid lamellae. This model considers passive diffusion driven by the concentration gradient of penetrant molecules.

Figure 4 shows the intercellular route (A), in which the drugs diffuse through the lipid matrix located between the corneocytes, while via the intracellular route (B), drugs diffuse through stratum corneum cells; in this last case, penetrants need to pass the lipid bilayers of the cell membranes. Although it is difficult to know exactly the mechanism of passage through the stratum corneum, it is possible to assume that hydrophobic molecules penetrate the routes through the lipid matrix in intercellular route, while hydrophilic ones prefer to pass through the corneocytes following intracellular route [53] [54]. Also in this last case, partial

penetration through intercellular pathway is necessary for allowing the passage from one corneocyte to another.

The diffusion of the drugs could also follow the transappendageal (follicular) route (C), since it is less studied than others due to the small presence of hair follicles, around 0.1% of total skin area.

Regardless the mechanism, in this model of passive diffusion, the transport of drug is controlled by their diffusion and partition coefficient inside the stratum corneum lipids and the retention by absorption to keratin of corneocytes. In the field of transdermal drug delivery, it is of great importance the "rule of 5" proposed by Lipinski; follow this empirical correlation, drug with molecular weight over 500 Da, LogP value over 5, the number of hydrogen bond acceptor major than 10 and the number of hydrogen donor over 5, poorly absorb through the skin. The use of advanced techniques like infrared spectroscopy, the Raman spectroscopy and the confocal microscopy supported this theory by analysing the fate of drugs into the skin and their interaction with skin components.

Of high interest that many studies by now suggest that the follicular pathway, in contrast to the conventional transepidermal pathways, is especially favourable for highly hydrophilic and high-molecular-weight substances [55], as demonstrated by Mitragotri [56] and reviewed by Barry [57].

4. Topical Dosage Forms for Skin Delivery

Topical products, widely used to manage skin diseases, have evolved from simple potions to sophisticated delivery systems. The effectiveness and the toxicity of topical products are influenced by several factors depending on the characteristics of the drug, the skin physiology, the product that contained the drug and the product perception by the patient in the consumer marketplace. The application of topical products could be aim to a transdermal administration or to treat the skin itself. As said previously, stratum corneum represents the main obstacle to drug penetration. In general, the first consideration in formulating a topical drug product is whether the drug to be used is sufficiently potent at local target site of action. Not all drugs are suitable for topical delivery. In 2021, date of publication of the article

published by Roberts et all. [58], at least 96 drugs are being used in topical delivery that meet these criteria and are applied in a range of dosage forms, including in patch, gel, ointment, and solution.

Topical dosage forms are classified into three major categories such as solid (powder and films), liquid (lotion) and semisolid (ointment, paste, emulsion, cream and gel) [59]. Since liquid formulations are attractive for other administration routes, usually they are not used in skin delivery due to their low viscosity which hinder their application in patients.

4.1 Solid Dosage Forms

The use of dusting powder, like talc, zinc oxide and starch, is reserved to relieve irritation or absorb moisture to reduce bacterial growth. While the use of dusting powders does not arouse great interest in research, for sure films represent an interesting and valid option for skin delivery of drugs.

Films can be referred as a thin and flexible layer of polymer with or without a plasticizer [60]. They are thin and flexible by their nature and for this reason can be perceived to be less obstructive and compliant for patients [60]. Compared to other drug delivery system, such as transdermal patches, are less irritating for the skin, show less pain when peeled off from skin and are easier to prepare [61]. In addition, they represent an improvement because they offer more flexibility and ease of use. PVA based films show great interest and have been widely used in skin delivery [62][63]. On the other side, PVA based films show some drawbacks such as the extreme water sensitivity and the swelling capacity upon hydration of PVA lead to instability of its physicochemical properties. These features leads to low adhesion and low patient compliance and make the research in this field attractive in order to overcome these limitations [61].

4.2 Semisolid Dosage Forms

For sure, due to physical characteristics, semisolid formulations are preferred over solids and liquids and find a lot of applications in skin delivery.

Pastes are semisolid dosage forms that contain a high percentage (often 50%) of finely dispersed solids with a stiff consistency intended for topical application. Gels, instead, are materials composed of a three-dimensional crosslinked polymer or colloidal network immersed in a fluid.

Hydrogels are gels that have water as their main constituent. Hydrogels suitable for transdermal drug delivery systems should possess excellent biocompatibility, biodegradability, elasticity, non-allergenicity, ease of application, soft consistency, and high-water content. Due to the hydration effects induced on the skin, hydrogels are utilized to increase the transport of drugs across the skin [64].

Emulsions, instead, are systems composed of at least two immiscible liquids, water and oil, one of which is usually uniformly dispersed as fine droplets throughout the other liquid phase by mechanical agitation process. Emulsions could be classified as oil-in-water (O/W) in which the water is the continuous phase or water-in-oil (W/O) in which the continuous phase is the oily phase. Emulsions are thermodynamically unstable and for this reason are stabilized by a surfactant: hydrophilic surfactants promote O/W emulsions, while lipophilic ones promote W/O emulsions. The dimension of droplets diameters vary a lot between different emulsions, but pharmaceutical and cosmetical emulsions are typically polydisperse with droplet sizes ranging from 0.1 to 100 μm [65]. Droplet size of the emulsion may influence the drug penetration through the skin, but the effect often is not clinically significant.

Emulsions can be designed to facilitate drug penetration into and/or through the skin. Their fine microstructure is better characterized, but the function of how each excipient (for example penetration enhancing agent) can influence drug bioavailability is not completely clear. In addition, the evaporation of volatile excipients can occur and so affect the drug permeation across the skin. Emulsion-based formulations have physically, chemically, and biologically superior compatibility with the skin compared with other topical and transdermal dosage forms, such as solutions, ointments and patches. Considering their composition, emulsions do not block the normal evaporation of the moisture, resulting in less discomfort. Compared to liquid formulations, the higher viscosity prevents running of the formulation during and after the application and better control the surface area of the application [65].

5. Approaches to Enhance Drug Permeation across Skin

There are different approaches to enhance the permeation of the drugs via transdermal route used to modify the barrier properties of the stratum corneum. As shown in Figure 5, there are different approaches to enhance the permeation of the drugs via transdermal route divided into passive/chemical or active/physical methodologies [66].

Passive methods include the optimization of the formulation, the use of vesicles and nanoparticles, the use of chemical enhancers, the formation of eutectic systems and eventually the chemical modification of the drug (prodrug). The active methods, instead, involve the use of an external energy which acts as a driving force for drug penetration into the skin.

Active methods include mechanical methods (microneedles), the use of ultrasounds and jet injection, the electrical methods (electroporation and iontophoresis) and the thermal ablation (heating through laser and radiofrequency) [67].

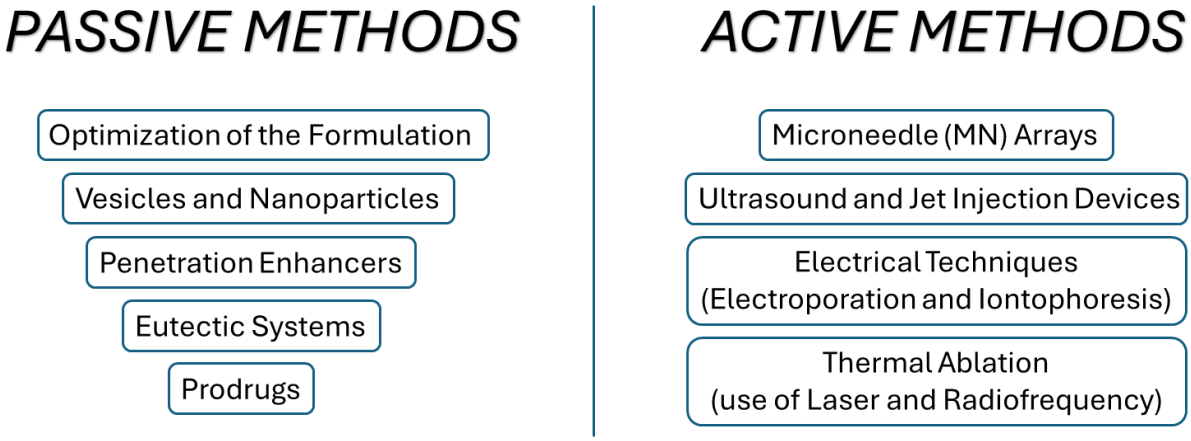

Figure 5: Transdermal drug delivery approaches to enhance drug permeability across skin: passive and active methods.

5.1 Passive Methods

Skin occlusion increases the water content of the stratum corneum up to 50%, and even a short-time occlusion results in significantly increased hydration. Occlusion enhances the percutaneous absorption of many but not all compounds and a correlation between the physical chemical characteristics of penetrants and increased permeability following occlusion is difficult [68]. For example, as reported by Zhai et all [69], the occlusion may increase penetration of lipid-soluble, non-polar molecules but seems to have less effect on polar molecules.

5.1.1 Optimization of the Formulation

Great results in transdermal delivery can be achieved by an appropriate choice of vehicle and the type of formulations. Vehicles can be important, as their effects on the skin can alter the interaction of the penetrant with the skin [70]. To optimize the vehicle of a formulation, several aspects should be considered: the solubility, release rate and stability of the active drug in the vehicle, the skin interactions between the vehicle and the skin and the drug, the anatomical localization, the skin type and the patient preferences [71].

For example, Grice et all demonstrated that a vehicle such as propylene glycol can alter the properties of the stratum corneum, so for example the solubility of the active ingredient minoxidil in the membrane is increased [72].

In addition to the components of the vehicle, it is worth remembering that often a simple change in properties, such as pH, viscosity, the relative amounts of oil, water or surfactant in emulsions, droplet size, ionic nature or the method of preparation, can influence the process of skin absorption.

Another important aspect is the type of formulation: as example, emulsions (O/W, W/O, W/O/W, O/W/O) or gels are important to adapt the hydrophilicity or lipophilicity of the drug with the vehicle [70].

5.1.2 Nanocarriers

To optimize drug penetration into the skin, nanocarriers have been introduced as an effective strategy. The most common nanocarriers used for the transdermal route are micelles, liposomes (which include also transfersomes and ethosomes), polymeric nanoparticles, solid lipid nanoparticles and dendrimers [73]. Their average diameter is the most important parameter which could determine the depth of penetration (mainly through follicular pathway), regardless of the type of carrier.

Micelles are colloidal systems constituted of amphiphilic molecules that in aqueous media form a core-shell structure when the concentration is above the CMC. Among all, polymeric micelles (10-200 nm) originated from self-assembly of amphiphilic block copolymers in aqueous solution. In comparison with micelles made of low molecular weight surfactants, polymeric micelles' main advantages can be found in their lower CMC and higher kinetic stability [74].

Liposomes, instead, are phospholipid-based vesicles (of size from 25 nm to 1,000 nm) organized in a bilayer structure, in which hydrophilic drugs can be incorporated in the aqueous compartment and hydrophobic drugs in the lipid component of the bilayer [75]. The structure and component of liposomes resemble cellular membranes, including phospholipid and cholesterol; liposomes, thanks to their structure and composition, can interact with the skin, although the precise mechanism has not been clarified. The addition of a single chain surfactant makes liposomes extremely elastic and flexible (transfersomes) [76]. Another class of liposomes are represented by ethosomes [75] which are used in transdermal field to promote the percutaneous penetration of drugs due to the presence of ethanol in the lipid bilayer which is known as an efficient penetration enhancer. Some of their characteristics are the small size, a stable structure and a high encapsulation efficiency [77].

Polymeric nanoparticles have attracted considerable interest in the transdermal field. Materials that commonly composed polymeric NPs could be natural, such as chitosan, dextran, heparin or hyaluronan or synthetic such as poly(lactic acid) (PLA), poly(glycolic acid) (PGA), and poly(lactic-co-glycolide) (PLGA), which have been approved by FDA and EMA Agencies [78].
General advantages of polymeric NPs as drug carriers include their potential use for controlled release, the ability to protect drug and other molecules with biological activity against the environment, improve their bioavailability and therapeutic index [79].

Solid lipid nanoparticles are colloidal carrier systems for controlled drug delivery, composed of physiological and biodegradable lipids, which organized in a solid lipid core matrix can solubilize lipophilic molecules. Lipid nanoparticles have lots of advantages for topical drug delivery such as biocompatibility and biodegradability, controlled and extended drug release profile, close contact and strong skin adhesion, skin hydration and film formation to increase skin and dermal penetration[80].

Dendrimers, instead, are hyper-branched organic compounds characterized via a three-dimensional structure possessing functional groups on the surface. Dendrimers have been found to provide advantages like improved drug solubility and controlled release of drugs, because of their water-solubility and biocompatibility. The dendrimers permeability through the skin is distinguished by physicochemical parameters, including composition, size of the generation, concentration, molecular weight and surface charge [81].

5.1.3 Penetration Enhancers

Chemical penetration enhancers facilitate drug permeation across the skin by increasing drug partitioning into the barrier domain of the stratum corneum or by altering the permeability of the barrier. In other terms, they are substances that temporarily changes the nature of the stratum corneum, so that drug transport through the skin is facilitated [82]. Penetration enhancer can act with one or more of these mechanisms of action: increasing fluidity of stratum corneum lipid bilayers, extraction of intercellular lipids, increasing drug's thermodynamic activity, increasing stratum corneum hydration, alteration of corneocyte proteins. The enhancer should be specific (increase the permeability without having other pharmacological activities in the body), non-toxic, non-irritating and non-allergenic. Penetration enhancers can be classified according to the origin (natural or semi-synthetic), to their chemical properties (small solvents and amphiphiles) or chemical characteristic of functional groups [83], because the classification according the mechanism of action is really difficult. Examples of commonly investigated penetration enhancers are alcohols, sulphoxides, azone, pyrrolidones, essential oils, terpenes and terpenoids, fatty acids, water and urea. Among drawbacks, penetration enhancers often cause skin irritation and are not always capable to achieve the desired skin permeability increase, then their ability to increase transport across skin is low and variable [84].

5.1.4 Eutectic Systems

A eutectic system is a blend of substances that melts and solidifies at a specific temperature that is lower than the melting points of the components. The application of these systems has been extensively studied. For example, EMLA® (eutectic mixture of local anesthetics) cream has been developed discovering that a specific mixture of lidocaine and prilocaine had a lower melting point than the melting point of the individual solid drugs, resulting liquid at room temperature [85].

The deep eutectic systems (DESs), instead, are a newer type of eutectic system that are different than the conventional eutectics in terms of their ability of lowering the melting point of the system to a greater extent, which is lower than the room temperature and the melting point of both components. In fact, they are mixtures composed of a hydrogen bond acceptor and a hydrogen bond donor that result in change delocalization and in a decrease in melting point. DES differs from ionic liquid due to the presence in the mixture of a variety of anionic and/or cationic species; instead, ionic liquid is composed primarily of one type of discrete anion and cation [86]. DESs exhibit the same physicochemical properties as ionic liquids, including low vapor pressure, inflammability, high tunability and conductivity. As reviewed by Wang and colleagues [87], DESs can act as stabilization agent, as surfactant and as solvents for active ingredients. Regarding their mechanisms of action, DESs exhibit lipid extraction function (main mechanism) or lipid fluidification effect. They result advantageous in terms of permeation for small compounds, such as nonsteroidal anti-inflammatory drug (ibuprofen) [88], biomacromolecules, such as insulin [89], polysaccharides [90] and siRNA [91].

5.1.5 Prodrugs

Prodrug design is a strategy that is used to increase the solubility and/or permeability of a compound resulting in the improvement of the penetration properties of the parent drug. To obtain prodrugs, molecules are in general derivatized; amino acid esters or amides are introduced into the hydroxyl, thiol, amine, or carboxylic acid functionalities. In the body, the prodrug is cleaved by the enzymes leading to the formation of the parent drug. Prodrugs show improved partition coefficient distribution, solubility (both in aqueous and oily phases), ionization, molecular weight, hydrogen bonding and melting point [92]. Although these

technological improvements, a prodrug is a new chemical entity and this leads to much longer studies and authorization processes for its approval.

5.2 Active Methods

5.2.1 Microneedle (MN) Arrays

MNs were developed to overcome some of the disadvantages commonly associated with hypodermic and subcutaneous injections, to address and improve patient compliance. These disadvantages include pain, possibility of transmitting diseases, erratic delivery and possibility of needle stick injuries. MN arrays represent minimally invasive drug delivery system: due to their small size, MN are not able to stimulate nerves and therefore they evade the generation of pain sensation resulting in a pain-free approach [93]. MN are micron-sized projections typically assembled on one side of a supporting base or patch. These micro projections generally range from 25 µm to 2,000 µm in length and from 50 µm to 250 µm in base width [94]. Various MN shapes have been developed, ranging from cylindrical, rectangular, pyramidal, conical, octagonal to quadrangular; this characteristic is crucial for skin penetration because they must insert into the skin without breaking.

Literature reports several examples of the use of MNs for the delivery of different drugs, from small hydrophilic molecules [95] to macromolecules, like heparins [96], insulin [97] and vaccines [98].

There are four main types of MNs: solid, coated, dissolvable and hollow MNs (Figure 6).

Solid MNs (a) are used for increasing the permeability of a drug formulation by creating micro-holes in the skin, followed by the application of a drug formulation (e.g., patch, gel). However, it is important to notice that a lot of dermatological conditions require drug delivery into large areas, which are difficult to address with MNs alone. Due to this reason, MN rollers are introduced: in this case MNs are mounted on a cylindrical surface and can be rolled across the skin, such that each MN may pierce the skin multiple times as the roller is passed on the skin surface [99].

In coated solid MNs (b), a layer of drug coats the surface of MNs; when applied, the drug dissolves fast into the skin. The use of these MNs results attractive especially for high molecular weight molecules, but drug delivery is limited due to small size of MNs.

Dissolvable MNs (c) are developed to have a rapid and controlled release of the drug incorporated within them. The materials from which the MNs are produced act as drug depots holding the drugs until the trigger for release occurs, i.e., dissolution in the case of dissolvable MNs or swelling in the case of hydrogel MNs. Dissolvable MN patches were successfully used to deliver both small and macro molecules.

Finally, hollow MNs (d) are used to puncture the skin and to release a drug following active infusion or diffusion of the liquid formulation through the needle pores.

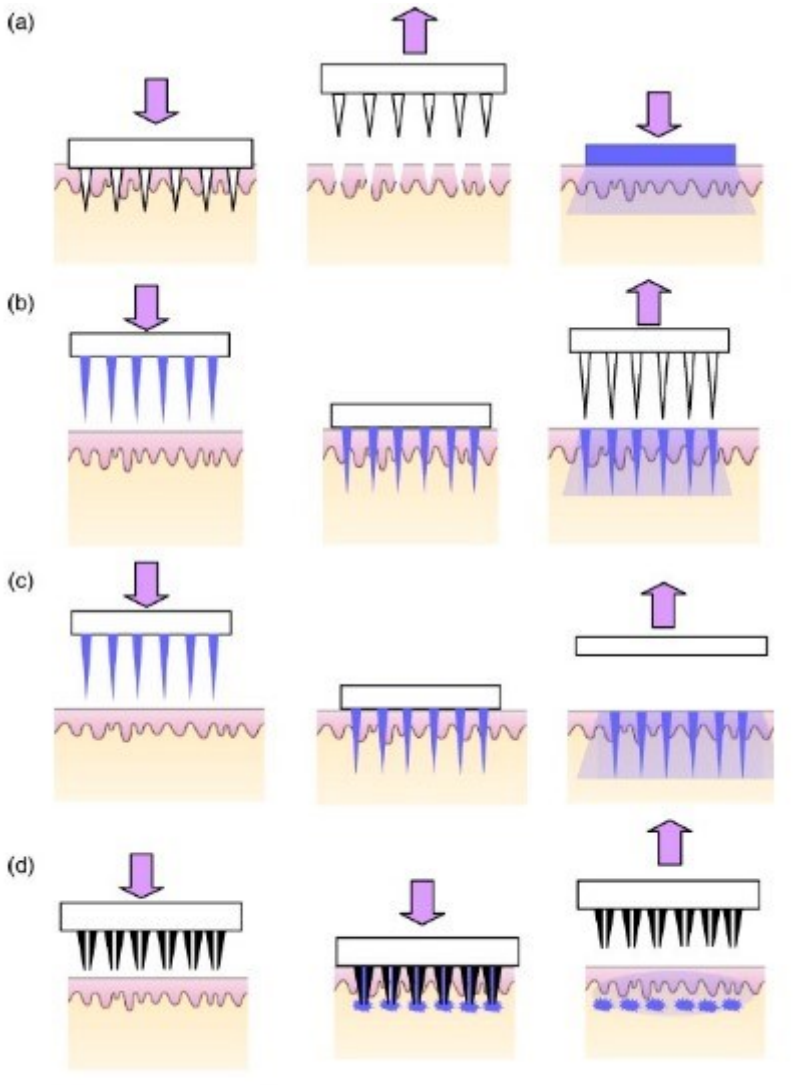

Figure 6: A schematic representation of different types of MNs used in transdermal drug delivery: a) solid, b) coated, c) dissolvable and d) hollow microneedles. Reprinted from [100].

5.2.2 Ultrasound and Jet Injection Devices

The use of ultrasounds has resulted in the increased delivery of various categories and classes of drugs, regardless of their electrical characteristics, by increasing skin permeability.

Ultrasound is an oscillating sound pressure wave that has long been used for many research areas including physics, chemistry, biology, engineering and others in a wide range of frequencies. Sonophoresis, or phonophoresis, can be defined as the application of ultrasound perturbation to the skin, at frequencies of 20 kHz–16 MHz sufficient to reduce its resistance, to increase drug permeation [101].

Considering jet injection, current liquid jet injectors are needle-free systems which use a high-velocity liquid stream (typically > 100 m s^{-1}) to deliver molecules across the skin into the intradermal, subcutaneous or intramuscular region, by changing pressure and orifice diameter [102].

5.2.3 Electrical Techniques: Electroporation and Iontophoresis

Electroporation uses electrical pulses of hundreds of volts, which result in the formation of aqueous pores in the lipid bilayers of the stratum corneum, as well as in the reversible disruption of cell membranes. Delivery of drugs is by passive diffusion through the pores due to the short duration of the pulses (msec) [103].

On the other side, iontophoresis involves the application of an electrical current of suitable intensity to drive charged permeants into the skin. The mechanism of iontophoresis is based on the physical phenomenon that “like charges repel and opposite charges attract”. For this reason, by using a negatively charged electrode, anionic drugs can cross the skin and oppositely, a positively charged electrode facilitates the transport of cationic drugs [104]. The drug permeation is caused by any one or combination of three main mechanisms: electro-repulsion, electro-osmosis and facilitate passive diffusion. Iontophoresis has minor effects on skin structure in short treatments, due to the low intensity of the applied electric current [103].

5.2.4 Thermal Ablation: Use of Laser and Radiofrequency

Thermal ablation is a method aimed to remove the stratum corneum by heating selectively the surface of the skin, without damaging deeper tissues, like epidermis and dermis.

Laser source is able to remove the stratum corneum by deposition of optical energy, which causes evaporation of water and formation of microchannels in the skin, allowing the passage of both hydrophilic and lipophilic drugs [105]. Anyway, the degree of barrier disruption achieved is controlled by wavelength, pulse length, tissue thickness, pulse energy, tissue absorption coefficient, pulse number, duration of laser exposure and pulse repetition rate [106].

Radiofrequency heating employs non disposable power supplies coupled to disposable heating elements. Through an electrode placed directly into the skin and a following application of high frequency alternating current (~100 kHz), pathways of microscopic dimensions are created in stratum corneum, allowing drugs permeation [107]. This method guarantees to localize the heating to a specific area of the skin and thus ablate the cells only in that region. Radiofrequency results effective for the delivery of hydrophilic drug and macromolecules [108].

AIM

The aim of the project was to develop innovative formulations for the topical administration of methotrexate in a non-invasive or minimally invasive way, to treat non melanoma skin cancers. In fact, it has been reported that an *off-label* use of intralesional methotrexate gives really promising outcomes against keratoachantomas and specified cases of squamous cell carcinomas. However, the use of intradermal drug injection is limited due to the drawbacks associated to this technique, such as the poor consistency of the injected volume, the invasive nature of hypodermic needle injections, the potential for needle-stick injuries and the risk of accidental subcutaneous injections.

To overcome these issues, topical formulations able to accumulate the drug in the skin were developed and studied, maximizing topical bioavailability and reducing transdermal absorption, to minimize the risk of systemic side effects.

Considering that the efficacy of topical treatments strictly depends on drug skin retention, the *first objective* was to develop an innovative and sensitive method for the quantification of the active ingredient in epidermis and dermis.

Given methotrexate toxicity, the *second objective* was to find a non-toxic model molecule with similar physicochemical and skin retention properties: folic acid resulted the molecule of choice. In addition, the *in vitro* skin behavior of both molecules was assessed in preliminary permeation experiments using a solution. To support retention and permeation data and to try to understand their mechanisms, two-photon microscopy technique was used as an innovative tool for drug visualization in the tissue based on its fluorescence properties.

The *third objective* was to study the effect of pre-treatment with microneedles mounted on a cylindrical surface (microneedle roller) on folic acid permeation and retention from solutions. In particular, the variables studied were a) the number of passes (1, 4 or 8 passes), b) the needle length (0.25, 0.50 or 0.75 mm) and c) the application time (2 or 6 hours).

The *fourth objective* was to develop a suitable topical formulation for the delivery of folic acid to the skin: among all, topical films based on hydrophilic polymers and semisolid formulations, e.g. hydrogels and emulsions, were formulated, characterized and *in vitro* tested to quantify the amount of folic acid retained in epidermis and dermis. The effect of microneedle pretreatment on these formulations was assessed as well. Beyond that, folic acid nanosupensions were prepared, loaded in soluble microneedle of different lengths and tested *in vitro,* in comparison with the application of dried discs of the same formulation.

Finally, the best performing formulation was replicated with the active drug methotrexate to confirm the potential of the developed system to reach the desired targets, resulting in a promising therapeutical strategy to treat non-melanoma skin cancers.

MATERIALS

- Acefylline (Sigma-Aldrich, Steinheim, Germany; purity ≥ 99%)
- Acetonitrile (Sigma-Aldrich, St. Louis, Missouri, USA)
- Adipic Acid (Fluka Chemika, Buchs, Switzerland)
- Ammonium acetate (Sigma-Aldrich, Steinheim, Germany)
- Anhydrous Sodium Acetate (Merck KGaA, Germany)
- Caffeine (ACEF Spa, Fiorenzuola D'Arda, Italy; purity 99 %)
- Carbopol 934 (ACEF Spa, Fiorenzuola D'Arda, Italy)
- Cetomacrogol 1000 (ACEF Spa, Fiorenzuola D'Arda, Italy)
- Cetostearylic Alchol (Galeno srl, Carmignano, Prato, Italy)
- DURO-TAK® 87-2852 (Henkel Corporation, Bridgewater, NY, USA)
- EDTA disodium salt (Merck, Darmstadt, Germany)
- Ethanol (Sigma-Aldrich, St. Louis, Missouri, USA)
- Eudragit® E 100 (Rohm, Darmstadt, Germany)
- Folinic Acid calcium salt (Sigma-Aldrich, Steinheim, Germany; purity ≥ 99%)
- Glacial Acetic Acid (VWR Chemicals, Rosny-sous-Bois, France)
- Glycerol (Merck, Darmstadt, Germany)
- Hydroxypropyl-β-cyclodextrin (Sigma-Aldrich, Steinheim, Germany)
- LABRAFIL® M 2130 CS (Gattefossè, 69804 Saint-Priest Cedex, France)
- Lauric Acid (Fluka Chemika, Buchs, Switzerland)
- Liquid paraffin (ACEF Spa, Fiorenzuola D'Arda, Italy)
- Methanol (Sigma-Aldrich, St. Louis, Missouri, USA)
- Monobasic Potassium Phosphate (Sigma-Aldrich, Steinheim, Germany)
- Olive oil (Carapelli Spa, Firenze, Italy)

- PEG400 (poly(ethylene glycol); MW: 380–420 g/mol; Eigenmann & Veronelli S.p.a., Milano, Italy)
- Phosphoric acid 85% (Sigma-Aldrich, Steinheim, Germany)
- Polyvinyl alcohol (MW: 89.000-98.000, 99+% hydrolyzed, Sigma-Aldrich, Steinheim, Germany)
- Polyvinylpyrrolidone (Kollidon® 30 and Kollidon® 90, Sigma-Aldrich, Steinheim, Germany)
- Polyvinylpyrrolidone (MW 10000; Sigma-Aldrich, Milan, Italy)
- Propylene glycol (ACEF Spa, Fiorenzuola D'Arda, Italy)
- Sodium Chloride (ACEF Spa, Fiorenzuola D'Arda, Italy)
- Sodium hydroxide pellets (Carlo Erba Reagenti, Milano, Italy)
- Sodium Monoacid Phosphate (Alfa Aesar GmbH, Karlsruhe, Germany)
- Sorbitol (Merck, Darmstadt, Germany)
- Stearic acid (ACEF Spa, Fiorenzuola D'Arda, Italy)
- Stringy Vaseline (Galeno srl, Carmignano, Prato, Italy)
- TEFOSE® 63 (Gattefossè, 69804 Saint-Priest Cedex, France)
- TWEEN 80 (Merck, Darmstadt, Germany)
- Water (Arium® comfort, Sartorius, Goettingen, Germany)

1. Methotrexate (MTX)

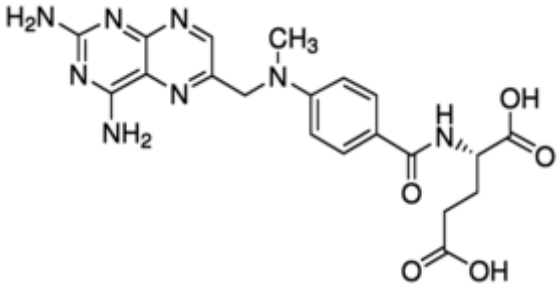

IUPAC NAME: (2S)-2-[[4-[(2,4-diaminopteridin-6 yl) methylmethylamino] benzoyl]amino] pentanedioic acid

MOLECULAR FORMULA: $C_{20}H_{22}N_8O_5$ *XH_2O

MOLECULAR WEIGHT: 454.4 g/mol (anhydrous)

XLoGP3: - 1.8

TOPOLOGICAL POLAR SURFACE AREA: 211 Å

ASPECT: yellow powder

MELTING POINT: 195 °C

SOLUBILITY: Insoluble in water , alcohol, chloroform, ether; slightly soluble in dilute hydrochloric acid; solubility pH-dependent, so neutral or basic solutions are required for its solubility [22].

pKa: 2.7; 4.1; 5.5 [109]

MANUFACTURING COMPANIES

- Methotrexate Sigma Aldrich (≥ 98 %-HPLC), trihydrate
- Methotrexate Hangzhou Dayangchem Co. (Hangzhou City, PRC)

2. Folic Acid (FA)

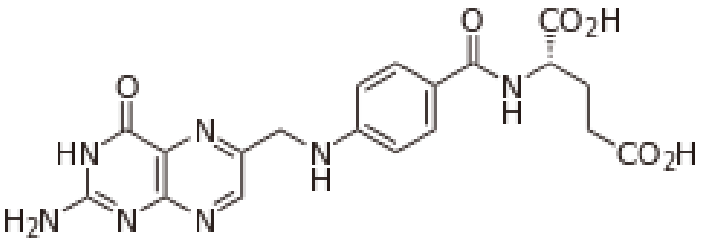

IUPAC NAME: (2S)-2-[[4-[(2-amino-4-oxo-3H-pteridin-6-yl)methylamino]benzoyl]amino] pentanedioic acid

MOLECULAR FORMULA: $C_{19}H_{19}N_7O_6$

MOLECULAR WEIGHT: 441.4 g/mol

XLoGP3: - 1.1

TOPOLOGICAL POLAR SURFACE AREA: 209 Å

ASPECT: yellow powder

MELTING POINT: 250 °C

SOLUBILITY: Slightly soluble in methanol, less in ethanol and butanol; insoluble in acetone, chloroform, ether, benzene; relatively soluble in acetic acid, phenol, pyridine and in solution of alkali hydroxides and carbonates.

pKa: 2.4; 3.5; 4.6 [110]

MANUFACTURING COMPANY: Sigma Aldrich (≥ 97% - HPLC)

METHODS

1. Preparation of Porcine Tissues

The skin used for the experiments was obtained from pig ears, sourced from a local abattoir and transported to the laboratory immediately after slaughter. The ears were washed with cold water and, with the help of a scalpel, portions of suitable size to cover the permeation area of the Franz cells (0.6 cm^2) were cut and separated from the cartilage. In all the fragments, hairs were cut with scissors and the hypodermis was removed.

Some tissues, prepared as previously described, were further treated to separate the epidermis from the dermis. To this end, the full thickness skin was heated with a hair drier for 30 seconds and then the epidermis was detached from the dermis using a flat spatula.

All samples were frozen at -20°C for not more than 3 months. Before use, skin specimens were thawed at room temperature in 0.9% NaCl saline solution.

2. Thermal Analysis of MTX

Characterisation of the thermal behaviour of MTX were performed by differential scanning calorimetry DSC (Mettler DSC 821e STARe, Mettler-Toledo S.p.A., Novate Milanese, Italy) and TGA (thermogravimetric analysis).

For DSC analysis, about 3 mg of methotrexate (obtained from the two different Companies) were weighted in sealed and pierced crucibles and were then subjected to a thermal programme from 0 °C to 340 °C, at a scan rate of 5 °C/min under a dynamic nitrogen atmosphere (200 ml/min).

TGA was performed using a TG50 (Mettler-Toledo S.p.A., Novate Milanese, Italy) driven by STARe software. Samples of 4 mg of MTX (Hangzhou Dayangchem Co.) were analysed in aluminium pans with a pierced cover. The analysis was performed from 25 °C to 240 °C at 5 °C/min under a nitrogen atmosphere.

3. UV-VIS Analysis

UV-VIS spectra of MTX and FA (25 µg/ml solutions) were recorded to determine the wavelength for HPLC-UV analysis. A spectrophotometer JASCO V-570 (SN: 0296331) instrument and quartz cuvettes (light path: 10 mm; type-NR: 108.002.25) were used. The solutions in different solvents were analysed:

a) Extraction solvent: a mixture composed of 87:13 (% v/v) of 50 mM sodium acetate (pH 6.6) and methanol;
b) Receptor fluid in permeation experiments, i.e. pH 7.4 PBS.

The corresponding blank solvents were analysed as well.

4. Fluorescence Analysis

Fluorescence measurement on a FA solution was performed with a FLS1000 Edinburgh Fluorometer. Emission spectrum was collected on diluted solutions of FA in pH 7.8 PBS, with absorbance lower than 0.1 to avoid inner filter effects. The excitation wavelength was 320 nm and the fluorescence spectrum was duly corrected for the excitation intensity and the detector sensitivity.

5. Solubility Studies

An excess amount of powder was placed into a vial containing 5 ml of selected solvent or mixture at room temperature. After 24, 36, 48, 65 or 72 h, an aliquot of the solution was centrifuged (15,000 rpm; 15 min) and the surnatant, after appropriate dilution, was analysed using the validated HPLC- method.

6. Two-Photon Electron Microscopy Analysis

Two-photon microscopy analysis of folic acid (FA) was performed on the skin after contact with a solution of the drugs for 6 hours. Briefly, the full thickness skin was mounted on a Franz-type vertical diffusion cell (0.6 cm^2). The donor was filled with 417 µl/cm^2 of 12.5 mg/ml of FA solution (pH 7.8), while the receptor was filled with pH 7.4 PBS under magnetic stirring. The same experiment was performed also using a pH 7.8 PBS solution in donor compartment as a control. Skin samples were analysed with a Two-Photon Microscope Nikon A1R MP+ Upright equipped with a femtosecond pulsed laser Coherent Chameleon Discovery (~ 100 fs pulse duration with 80 MHz repetition rate, tunable excitation range 660–1320 nm). A 25× water dipping objective with numerical aperture 1.1 and 2-mm working distance was employed for focusing the excitation beam and for collecting the two-photon excited fluorescence (TPEF) and the second harmonic generation (SHG) signals. TPEF/SHG signal was directed by a dichroic mirror to a series of two non-descanned detectors (high sensitivity GaAsP photomultiplier tubes) allowing fast image acquisition. The two detectors are preceded by optical filters allowing the simultaneous acquisition of two separated channels: blue channel (415–485 nm) and green channel (506–593 nm). Imaging overlay of the two channels and processing was performed by the operation software of the microscope. Additionally, a third GaAsP photomultiplier detector, connected to the microscope through an optical fiber and preceded by a dispersive element, was used to record the spectral profile of the TPEF/SHG signal (wavelength range 430 to 650 nm with a bandpass of 10 nm). For microscope observations of skin samples, performed right after dismounting the tissue from the Franz-type cell, the tissues were placed in a dedicated plexiglass holder and saline solution was used to dip the objective and to avoid dehydration. Samples were excited at 820 nm. Images were acquired with a typical field of view of 500 µm × 500 µm.

The visualization of 0.5 mm microneedle was acquired by exciting the sample at 820 nm, keeping the gains of the two detectors (blue and green) at the same value. The three-dimensional visualization was reconstructed from 252 scans, collected every 2 microns apart.

7. Preparation of Topical Films

7.1 Polyvinyl Alcohol-Polyvinylpyrrolidone Films

PVA (191.75 mg) was dissolved in 6.5 ml of water under magnetic stirring at 80 °C for one hour. The solution was then cooled to room temperature, replenishing the evaporated water. Then, the polymer PVP (k30 or k90) (126.75 mg) and the plasticizer propylene glycol (34 mg) were added and stirred until complete solubilization. 30 mg of FA were dissolved in the previous solution in the presence of 120 µl of sodium hydroxide solution 1 N. The final formulation was then poured into a Petri dish (55 mm diameter) and allowed to dry overnight at 37 °C [111]. The loading of FA in dried film was 77.5 mg/g.

7.1.1 Release Experiments

Drug-loaded PVA-PVP k30 or k90 films (0.6 cm^2, n = 4) were placed in vials containing 5 ml of pH 8 PBS at room temperature under magnetic stirring. Samples of 0.3 ml were taken at 1, 5, 15, 30, 60, 90 and 120 min and replaced with the same volume of fresh PBS. Collected samples were analyzed by HPLC-UV using a previously validated method to determine the amount of FA released (see Methods paragraph 11). The collected data were processed as released percentage of the drug, calculated with respect to the drug content experimentally determined.

7.1.2 Mechanical Characterization

To measure the mechanical properties, a strip of 10 × 70 mm was cut from each prepared film. Breaking force and elasticity were assessed at breaking point using an electronic dynamometer (Instruments J. Bot; Barcelona, Spain) [111] and setting a load cell weight of 5 Kg. These parameters allowed to determine approximately the resistance and elongation of the different films under evaluation [112]. Each strip was held between the two clamps of the dynamometer for analysis: the upper clamp is mobile while the lower one is static. The strip

was pulled at a rate of 50 mm/min. The tensile strength and elongation at breaking point were calculated following eq. (1) and (2) [112].

$$\text{Tensile strenght}\left(\frac{\text{N}}{\text{mm}^2}\right) = \frac{\text{Break force (N)}}{\text{Cross sectional area } (mm^2)} \quad (1)$$

$$\text{Elongation } (\%) = \frac{Increase\ in\ lenght\ at\ break\ point\ (mm)}{Original\ length\ (mm)} \cdot 100 \quad (2)$$

7.2 DURO-TAK® Films

A topical film containing DURO-TAK® and FA was prepared mixing 0.14 g of the active ingredient with 19.86 g of the adhesive at room temperature. Due to low solubility of FA in the adhesive solvents (ethyl acetate, hexane, isopropanol, 2,4-pentanedione and toluene), the resulted formulation was non-homogeneous. The formulation was anyhow laminated with a film casting knife (BYK Gardner, Silversprings, MD, USA) with a gap 0.6 mm and dried in the oven at 80 °C for 30 minutes, but it resulted not uniform.

7.3 PVP k90-PEG 400 Films

PVA was hydrated in the appropriate volume of water to a final concentration of 20% (w/w). The mixture was slowly stirred overnight using a magnetic stirrer and then heated at 90 °C to solubilize the polymer (P1). PVP k90 (21%, w/w) was dissolved in a mixture of PEG400:water (15:85, w/w) (P2).

Following the formulation reported by Padula et all. [113], 62% of P1 were mixed with 27% of P2. 4% of sorbitol (70% w/w water solution) was then added, together with 2% of Folic Acid and 5% sodium hydroxide solution 2N. All the percentages are expressed as percentage w/w. The formulation was slowly stirred overnight at room temperature. The obtained mixture was laminated on siliconized paper using a film casting knife (BYK Gardner, Silverspring, MD, USA – gap 0.6 mm) and dried at room temperature in the dark for 24h.

The loading of FA in the dried films was 75.5 mg/g.

7.4 PLASTOID® Films

Two films were prepared, according to the content of Folic Acid.

PLASTOID® E 35 H was prepared according to the protocol of Rofarma: Eudragit® E 100 (15.9%, w/w), lauric acid (9.2%, w/w) and adipic acid (1.8%, w/w) were added to hot water (72.1%, w/w, temperature ~80°C). The mixture was stirred, maintaining the temperature at ~80°C, until a clear solution was formed. The solution was then cooled to 60 °C, and glycerol (1.0%, w/w) was added. The mixture was then gradually cooled to room temperature while stirring [114][115].

27.3% of PLASTOID® E 35 H was mixed with 62.6% of PVA water solution (20% w/w, prepared as indicated before). When a clear solution was formed, 4.0% of sorbitol water solution (70% w/w), 1.0% (or 2.0%) of FA and 5.0% (or 4.0%) of water were then added. The mixtures were stirred overnight at room temperature, spread on siliconized paper using a film casting knife (BYK Gardner, Silverspring, MD, USA; gap 0.450 mm) and oven-dried at 80 °C for 30 min. The films were covered with a second siliconized paper and sealed in aluminium pouches.

The loading of FA in the dried films was 41.3 mg/g and 80.8 mg/g.

8. Preparation of Semisolid Formulations

8.1 Hydrogels

8.1.1 PVA- and PVP-based Hydrogels

Two hydrogels containing the hydrophilic polymers PVA and PVP k30 were prepared. The first one was prepared as followed: 4.11% of PVA were hydrated in water and the mixture was slowly stirred overnight using a magnetic stirrer and then heated at 90 °C to solubilize the polymer. Subsequently, 2.72% of PVP k30, 0.73% propylene glycol, 0.64% of Folic Acid and 0.0026% of sodium hydroxide solution 1 N were solubilized together to form a clear homogeneous hydrogel (H1).

The second one was prepared maintaining the same ratio PVA/PVP of the other but increasing the percentage of the polymers. Therefore, 9.14% of PVA were hydrated in water and the mixture was slowly stirred overnight using a magnetic stirrer and then heated at 90 °C to solubilize the polymer. Subsequently, 6.02% of PVP k30, 4.82% propylene glycol, 0.33% of FA and 0.13% of sodium hydroxide (salt) were solubilized together to form a clear homogeneous hydrogel (H2). All the percentages are expressed as percentage w/w.

8.1.2 Carbopol® 934 Hydrogel

Carbopol® gel was prepared dissolving 0.8% Carbopol® 934, prewetted with 4.8% propylene glycol, in 90% of water and 0.2% of EDTA disodium salt. When Carbopol® 934 was completely dissolved, 1.24% of FA (12.4 mg/g) were added in the presence of 3.1% of NaOH 2.5 N to allow the formation of a gel. All the percentages are expressed as percentage w/w.

8.2 O/W and W/O Emulsions

8.2.1 Preparation of FA TEFOSE® O/W Emulsion

FA TEFOSE® O/W emulsion was prepared weighting TEFOSE® 63, LABRAFIL® M2130 CS, olive oil and cetostearyl alcohol in the same becker. A solution containing FA and sodium hydroxide was prepared and added to other excipients. The becker was subsequently heated at 75-80 °C. The emulsion was stirred at 350-500 rpm for 5 minutes maintaining this temperature. The mixture was cooled down until 25 °C while stirring (350 rpm).

The final concentration of the excipients and drug was 9.72% of TEFOSE® 63, 2.43% OF LABRAFIL® M2130 CS, 6.48% of olive oil, 1.62% of cetosterayl alcohol, 0.59% of sodium hydroxide, 1.25% of FA and 77.92% of water. All the percentages are expressed as percentage w/w.

8.2.2 Preparation of MTX TEFOSE® O/W Emulsion

MTX TEFOSE® O/W emulsion was prepared weighting TEFOSE® 63, LABRAFIL® M2130 CS, olive oil and cetostearyl alcohol in the same becker. A solution containing MTX and sodium hydroxide was prepared and added to other excipients. The becker was subsequently heated at 75-80 °C. The emulsion was stirred at 350-500 rpm for 5 minutes maintaining this temperature. The mixture was cooled down until 25 °C while stirring (350 rpm).

The final concentration of the excipients and drug was 9.72% of TEFOSE® 63, 2.43% OF LABRAFIL M2130 CS, 6.48% of olive oil, 1.62% of cetosterayl alcohol, 0.59% of sodium hydroxide, 1.25% of MTX (anhydrous form) and 77.92% of water. All the percentages are expressed as percentage w/w.

8.2.3 Preparation of FA Stearic Acid O/W Emulsion

Stearic acid was melted into a becker at 70 °C (oily phase). FA was solubilized in water, in the presence of sodium hydroxide and glycerin in a second becker (water phase). The water

phase was heated at 70 °C and then the two phases were mixed using a homogenizer (Ultra-Turrax T8, Deutschland, Germany) at 15,000 rpm for 5 minutes. The obtained O/W emulsion was cooled (25 °C) under continuous magnetic stirring.

The final concentration of the excipients and drug was 13.83% of stearic acid, 27.65% of glycerin, 0.99% of sodium hydroxide, 1.23% of FA and 56.30% of water. All the percentages are expressed as percentage w/w.

8.2.4 Preparation of FA W/O Emulsion

An oily phase composed by vaseline, liquid paraffin and cetostearyl alcohol (surfactant) was obtained by melting these excipients at 70 °C. In a second becker, the co-surfactant cetomacrogrol 1000 was solubilized in water; FA was added and solubilized in the presence of a small amount of sodium hydroxide (added as 5 N solution). The water phase was then heated at 70 °C, mixed with the oily phase and cooled at room temperature under continuous stirring. The final concentration of the excipients was 36.28% of solid vaseline, 14.47% of liquid paraffin, 17.37% of cetosteryl alcohol, 4.25% of cetomacrogol 1000, 1.25% of FA, 0.45% of sodium hydroxide and 25.93% of water. All the percentages are expressed as percentage w/w.

8.3 Rheological Analysis

Viscosity was measured using HAAKE™ RheoStress™1 (Thermo Fisher Scientific, Waltham, MA, USA), cone and plate type, equipped with a cone 222-1269 C35/2. The cone has a diameter of 35 mm and the formed angle is 2 DEG. The rheometer is composed of a thermostat plate (25 °C), connected to a heated bath, over which the sample will be placed. The software used is “RheoWin Job Manager”.

9. Preparation of Soluble PVP Microneedles

9.1 Preparation of FA Nanosuspension

A FA nanosuspension was produced via a wet ball media milling approach, employing a 2:1 (% w/w) ratio of drug to stabilizer. The drug was dispersed in a 1% w/w water solution containing TWEEN 80 (0.5% w/w) using an Ultra Turrax T25 basic (IKA, Werke, Staufen, Germany) for 15 minutes at 15,000 rpm. Subsequently, the resulting suspension was transferred into 1.5 ml conical tubes containing about 0.4 g of yttrium-stabilized zirconia–silica beads (Silibeads® Typ ZY Sigmund Lindner, Warmensteinach, Germany) with a particle size of 0.1–0.2 mm. The mixture was oscillated at 3,000 rpm for a total of 105 minutes (7 cycles of 15 minutes each, with 5 minutes of rest between cycles) using a bead-milling cell disruptor device (Disruptor Genie®, Scientific Industries, Bohemia, NY, USA). The resulting nanosuspension was then separated from the milling beads through sieving.

9.2 Particle Size Analysis

The average diameter and polydispersity index (PDI) of FA-nanosuspensions were determined by Dynamic Light Scattering (DLS) using a Zetasizer nano. A helium–neon laser (633 nm) at an angle of 173° was used to backscatter the samples, maintained at temperature value of 25 °C. The analysis by means of the M3-PALS (Phase Analysis Light Scattering) technique allowed the determination of the Zeta potential value. The analysis was performed before nanosuspensions dilution with distilled water. The measurements were made in triplicate.

9.3 Preparation of Soluble Microneedles

The solvent casting technique was used to fabricate soluble microneedle. Initially, FA nanosuspension was blended with PVP by combining 0.8 g of PVP and 0.04 g of glycerol with 1 ml of FA suspension, followed by gentle stirring overnight to achieve a homogeneous mixture. Subsequently, 60 µl of this dispersion were evenly applied to the microneedle template (MPatch™ Microneedle Templates ST-14 (10 × 10 array, H = 0.5 mm, base = 0.2 mm, pyramid) and ST-29 (10 × 10 array, H = 0.8 mm, base = 0.2 mm, pyramid), Micropoint Technologies Pte Ltd., Singapore) for the initial deposition. The template was then placed in a 50 ml falcon tube and subjected to centrifugation using a NEYA 8 BASIC centrifuge (Neya Centrifuges, Carpi, Italy) at 4,000 rpm for 15 minutes to fill the needle part of the array and eliminate air bubbles. Following centrifugation, the template was left to dry overnight. Subsequent cycles of deposition–centrifugation–drying were conducted by adding 50 µl of blank PVP solution to completely fill the template and form the base of the array. After the final deposition, the template was left to dry at 25 °C for 3 days in a light-protected glass desiccator jar. The arrays were delicately removed from the templates using double-sided tape, and then vacuum-packed for storage until use.

For comparative analysis, the same formulation was pipetted onto a flat support and allowed to dry overnight, resulting in FA-nanodispersion discs.

10. *In vitro* Permeation Experiments

In vitro permeation studies were conducted across porcine ear skin. The tissue was mounted on Franz's type diffusion cells (DISA, Milan, Italy), with a diffusional area of 0.6 cm^2. The receptor compartment (volume of about 4 ml) was filled with degassed pH 7.4 PBS, kept under magnetic stirring, and the cell was placed in a thermostatic bath set at 37 °C. The formulations were applied to the skin before assembling the cell (films, MNs, Carbopol®

hydrogel and emulsions) or placed on the skin in the donor comportment (solutions and PVA- and PVP-based hydrogels). Donor compartment was covered with Parafilm®.

Samples of 300 µl were collected from the receptor side every hour and replaced with the same amount of fresh PBS. At the end of the experiments the receptor solution was sampled, and the skin surface was washed four times with 500 µl of pH 7.4 PBS (in the experiments with solutions) or water (in the experiments with formulations). The washing solutions were collected in a volumetric flask and then diluted with the appropriate volume of water (or pH 7.4 PBS, in the case of solutions). The skin was cut in correspondence of the permeation area and heat-separated into epidermis and dermis. The drug present in the epidermis was extracted using the validated method (see Methods, paragraph11).

For dermis extraction, 10 µl of MTX solution (223.43 µg/ml in extraction solvent) in the case of FA experiments or 10 µl of FA solution (250 µg/ml in extraction solvent) in the case of MTX experiments was applied to each sample as internal standard; after 1 h, FA/MTX extraction was performed in the validated conditions (see Methods paragraph 11).

10.1 Permeation with Solutions

10.1.1 Comparison between Methotrexate and Folic Acid Solutions

Infinite dose conditions were obtained applying 417 µl/cm^2 of 12.5 mg/ml of FA solution (pH: 7.8) or in alternative of 417 µl/cm^2 of 12.5 mg/ml MTX solution (pH 7.8) in donor compartment. The donor was covered with Parafilm® to avoid solvent evaporation.

Finite dose conditions were obtained applying 15 µl/cm^2 of FA solution (12.5 mg/ml; pH: 7.8) or in alternative 15 µl/cm^2 of MTX solution (12.5 mg/ml; pH 7.8) in donor compartment. The donor was not covered with Parafilm® to allow solvent evaporation.

The permeation time was 6h.

10.1.2 Evaluation of the Number of Passes of Microneedle Rollers

To evaluate the effect of the number of passes of microneedle rollers (1, 4 or 8), the skin specimen was placed on a flat surface and the roller (TinSky® 0.5 mm needle length) was passed back and forth for 1, 4 or 8 times, trying to apply an even pressure. Then the skin was mounted on the diffusion cell and the permeation experiment with a solution of FA 12.5 mg/ml in pH 7.8 PBS in infinite conditions was carried out (see above). The permeation time was 6 h.

10.1.3 Evaluation of the Needle Length of Microneedle Rollers

To evaluate the effect of needle length of microneedle rollers (TinSky®: 0.5 mm and 0.75 mm and Luollove®: 0.25 mm), the skin specimen was placed on a flat surface and the proper roller was passed back and forth for 4 times, trying to apply an even pressure. Then the skin was mounted on the diffusion cell and the permeation experiment with a solution of FA 12.5 mg/ml in pH 7.8 PBS in infinite conditions was carried out (see above). The permeation time was 6 h.

10.1.4 Kinetic Studies on Folic Acid Solutions

To evaluate the effect of the application time, the permeation time was reduced to 2 h. The skin specimen was placed on a flat surface and the proper roller (TinSky®: 0.5 mm or 0.75 mm or Luollove®: 0.25 mm) was passed back and forth for 4 times, trying to apply an even pressure. Then the skin was mounted on the diffusion cell and the permeation experiment with a solution of FA 12.5 mg/ml in pH 7.8 PBS in infinite conditions was carried out (see above).

10.2 Permeation with Formulations

The effect of the application of the formulations or soluble MN arrays on the skin in passive condition and in the condition of pretreatment with MN rollers (in the case of formulations) was investigated. The following paragraphs illustrate and describe the various experimental conditions.

10.2.1 Permeation with Topical Films

Circles of films of 0.6 cm^2 area were cut using a punch and then applied on full thickness skin surface using a tweezer. The skin was pre-wetted with a proper amount of water before film application. The skin was then mounted on a Franz's type diffusion cell (DISA, Milan, Italy) in non-occlusive conditions (or occlusive conditions, if specifically indicated) and the experiments were carried out as indicated before.

10.2.1.1 PVA-PVP k30 Films

Since PVA-PVP k30 films were not self-adhesive, two different conditions were tested: the skin was pre-wetted with 167 µl/cm^2 or 15 µl/cm^2 of water before film application. Films were applied in non-occlusive conditions.

10.2.1.2 PLASTOID® Films

PLASTOID® films were applied before pre-wetting the skin with 15 µl/cm^2. Topical PLASTOID® films 80.8 mg/g of FA were tested in non-occlusive conditions, while films with a FA concentration 41.3 mg/g were applied both in non-occlusive and occlusive conditions. In the latter, a polyester film (SCOTCHPATCH® heat sealeble 9723, thickness: 66 µm) was applied on the surface of the film.

10.2.2 Permeation with Hydrogels

10.2.2.1 Permeation with PVA- and PVP-based Hydrogels

PVA- and PVP- based hydrogels, prepared as described in Methods par 8.1.1, were tested in 6 h permeation experiments as indicated before. Infinite conditions were realized by applying average volumes of about 183 µl/cm^2 in the case of hydrogel H1 or 350 µl/cm^2 in the case of hydrogel H2 in the donor compartment.

10.2.2.2 Permeation with Carbopol® 934 Hydrogel

Carbopol® 934 gel containing FA, prepared as described in Methods paragraph 8.1.2, was tested in 6 h *in vitro* permeation experiment in infinite dose conditions, by applying 95 mg/cm^2 of the formulation.

10.2.3 Permeation with Emulsions

FA emulsions and the MTX TEFOSE® O/W emulsion prepared as described in Methods paragraph 8.2 were tested in 6 h *in vitro* permeation experiments, in infinite dose conditions. An average amount of 92 mg/cm^2 of the formulation was applied on the skin using a spatula and then mounted on the diffusion cell and the experiment was carried out as previously indicated.

10.2.4 Permeation with Soluble Microneedles

Soluble microneedles prepared as described in Methods par 9 were tested in 6 h permeation experiments. After skin thawing, the skin was wiped with a paper towel and the arrays were applied by manual pressing. The skin was then mounted on the diffusion cell and the experiment carried out as previously indicated.

10.3 Statistical Analysis

Statistical analyses were performed with GraphPad Prism and reported through stars significant changes compared to the respective control (Dunnet one-way ANOVA test; *: $p < 0.01$ and **: $p < 0.001$) and through bars significative variations between the same group (Tukey's one-way ANOVA test). In the presence of two population groups, analyses were performed applying Student's t test (*: $p < 0.01$ and **: $p < 0.001$).

11. Analytical and Extraction Method

Analyses were performed using an HPLC–UV system (Infinity II 1260, Agilent Technologies, Santa Clara, CA, USA), equipped with a Phenomenex Jupiter C_{18} column, 5 µm, 150 x 4.6 mm, 300 Å, maintained at 30 °C. The mobile phase, pumped at 1 ml/min, was a mixture of 50 mM sodium acetate pH 3.6 and methanol (87:13, v/v). The injection volume was 50 µl, and absorbance was monitored at 290 nm [116]. The retention times of Folic Acid and Methotrexate were respectively ~5 min and ~8.5 min.

Extraction Method was validated for the extraction of Methotrexate from the skin layers [116]. Basically, blank epidermis and dermis were spiked with known amount of Methotrexate (5, 10, 15 µl of a standard solution 446.90 µg/ml in pH 7.4 PBS). A 10 µl aliquot of Folic Acid solution (250 µg/ml in extraction mixture) was applied to dermis samples. After 1 h of contact, samples were extracted with 1 ml of an appropriate extraction mixture (50 mM sodium acetate pH 6.6 and Methanol; 87:13, v/v) overnight at room T. Subsequently, samples were centrifuged at 15,000 rpm for 10 min. The recovery of the two analytes (Methotrexate and the internal standard Folic Acid) from samples was determined with respect to the amount applied, determined by direct injection of the spiked solution in the absence of skin tissue.

To validate the extraction method of Folic Acid from the skin layers, blank isolated tissues (epidermis and dermis) were spiked with known amounts of Folic Acid (10 µl of standard solutions 100 µg/ml, 250 µg/ml and 500 µg/ml in pH 7.4 PBS). A 10 aliquot of Methotrexate solution (223.43 ug/ml in extraction mixture) was applied to dermis samples.

After 1 h of contact, samples were extracted with 1 ml of an appropriate extraction mixture (50 mM sodium acetate pH 6.6 and methanol; 87:13, v/v) overnight at room temperature. Subsequently, samples were centrifuged at 15,000 rpm for 10 min. The recovery of the two analytics (Folic Acid and the internal standard Methotrexate) from samples was determined with respect to the amount applied, determined by direct injection of the spiked solution in the absence of skin tissue.

RESULTS AND DISCUSSIONS

1. Drug Characterization

1.1 Methotrexate

1.1.1 UV-VIS Analysis

Methotrexate spectra were recorded in both extraction solvent and receptor fluid (Figure 7).

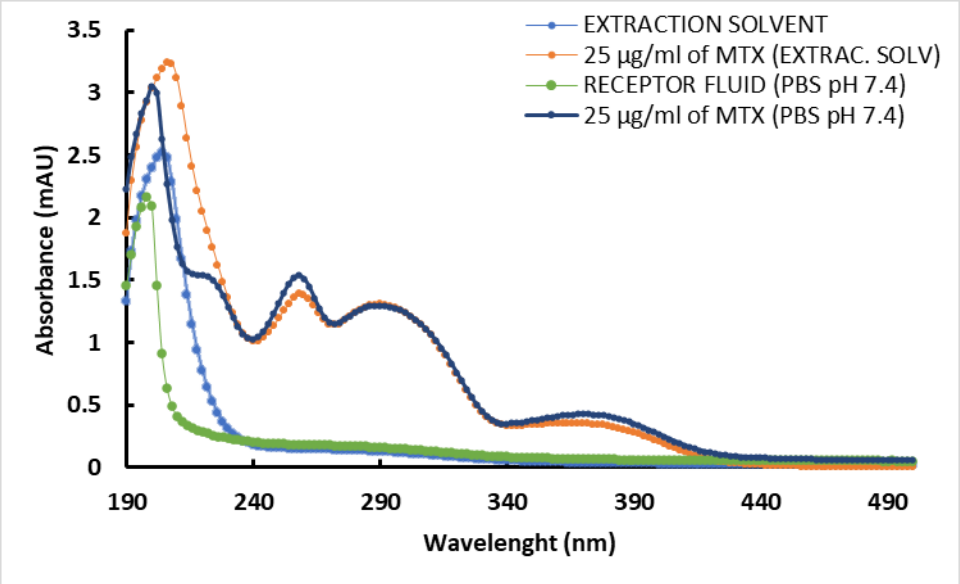

Figure 7: UV-VIS spectra of methotrexate solutions in different solvent and respective blank solutions.

The peaks of absorption are at 260 and 290 nm and their position is not affected by the medium in which the drug is solubilized. The wavelength of 290 nm was selected for HPLC analysis.

1.1.2 Analytical Method

Based on the research work published by Von Zuben et all [117], the first attempt for MTX detection and quantification was conducted using 50 mM ammonium acetate buffer (pH 6.6) and methanol (77:23, v/v) as mobile phase. Figure 8 reports as a title of example the chromatogram of 25 µg/ml MTX solution in pH 7.4 PBS. The analysis was performed using an

HPLC-UV based system (Infinity II 1260, Agilent Technologies, Santa Clara, CA, USA), equipped with a Phenomenex Jupiter C_{18} column, 5 µm, 150 x 4.6 mm, 300 Å, maintained at 25 °C. The mobile phase, pumped at 1 ml/min, was a mixture of 50 mM ammonium acetate pH 6.6 and methanol (77:23, v/v). The injection volume was 50 µl, and absorbance was monitored at 313 nm. The retention time was about 3.5 min. The linearity range was evaluated for the range 0.05-50 µg/ml and the LLOD resulted to be 0.025 µg/ml.

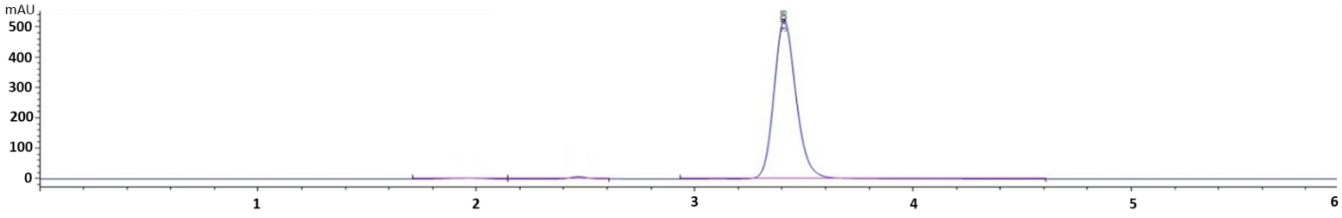

Figure 8: Chromatogram of 25 µg/ml MTX solution quantified with the analytical method cited above.

Although this method should be used as analytical quantification of MTX, further methods have been developed due to its inapplicability in developed extraction method from the skin. Moving toward the internal standards used for the validation of the extraction of MTX from skin layers, further development have been settled to allow the drug and the selected internal standard in the same analytical run. When caffeine was firstly tested as possible internal standard for the quantification of MTX in dermis samples, the analytical analysis was slightly changed using as elution mixture 50 mM sodium acetate buffer pH 3.6 (with glacial acetic acid) and methanol (87:13, v/v), the temperature of the column was 30 °C and the wavelength was settled at 279 nm. The column, the flux and the injection volume were maintained. The retention times of the internal standard caffeine and of methotrexate were respectively ~6 min and ~8.2 min, as shown in Figure 9 A.

When the attention moved towards the acefylline, the only variation in the analytical method compared to the caffeine analysis was the pH of the water phase which increased to reach a value of pH 7.2 to delete the interference of the ionization state of this internal standard observed at acidic pH. Acefylline was eluted after ~3.2 min and Methotrexate after ~7.8 min (Figure 9 B).

Folic Acid and Methotrexate, instead, were detected in the same analytical run using the conditions reported in Methods paragraph 11 and an example of chromatogram obtained analysing FA (2.5 µg/ml) and MTX (2.5 µg/ml) is reported in Figure 9 C.

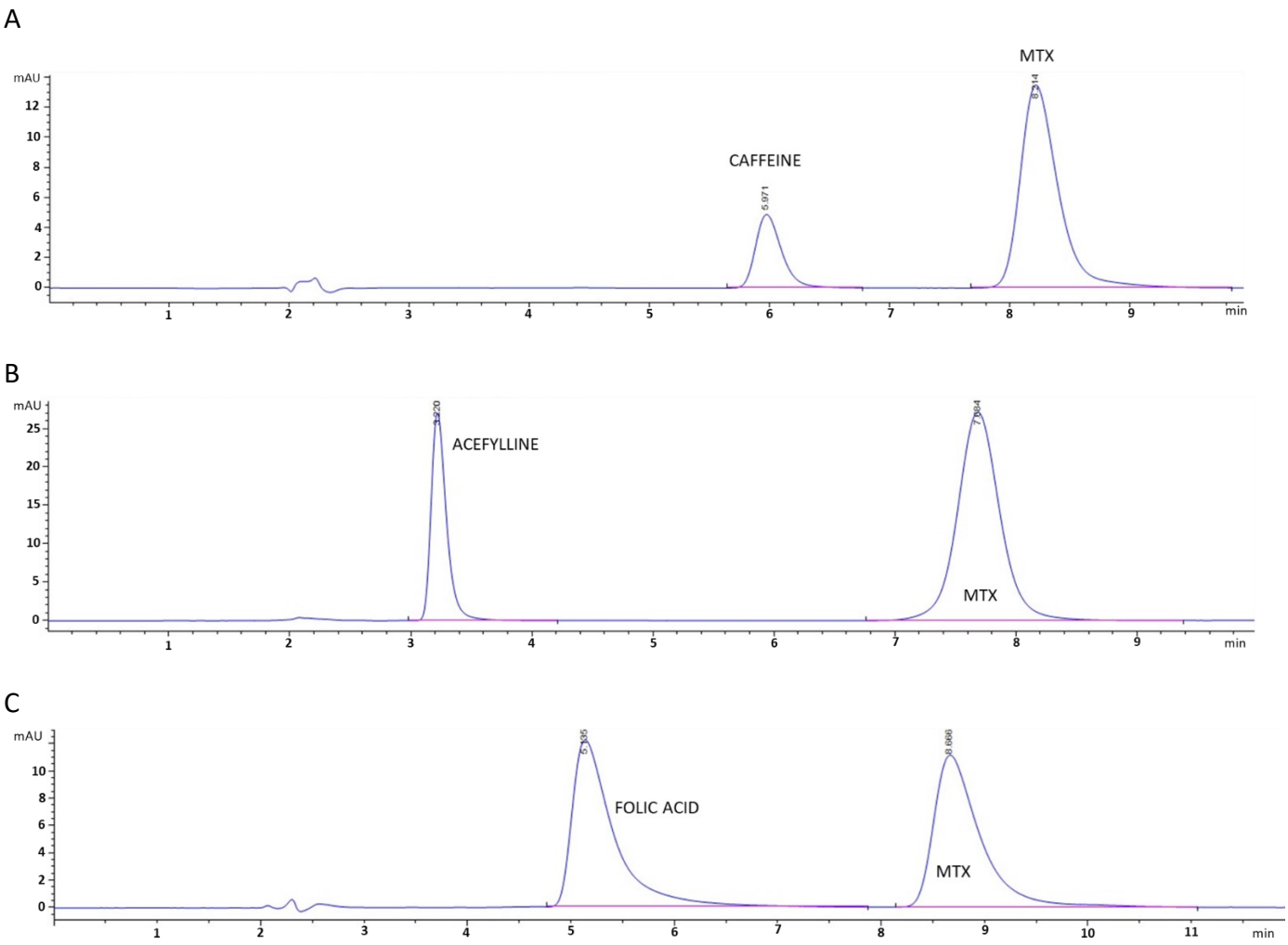

Figure 9: Representative chromatogram of caffeine (0.5 µg/ml) and methotrexate (2.5 µg/ml) solution (A), representative chromatogram of acefylline (25 µg/ml) and methotrexate (5 µg/ml) solution (B) and representative chromatogram of folic acid (2.5 µg/ml) and methotrexate (2.5 µg/ml) solution (C).

The quantification of the internal standard FA and the drug MTX was validated using an analytical method, following the guidelines outlined by the European Medicines Agency (EMA) for bioanalytical method validation (EMA, 2012). The validation included assessments of selectivity, linearity, lower limit of quantification (LLOQ), accuracy, and precision.

Table 1 shows the calibration data, including the equations of linear regression of the calibration curves in the receptor fluid and in the extractive solvent. In all cases, the correlation coefficient (R^2) was major than 0.999. Accuracy, assessed in accordance with EMA guidelines, demonstrated satisfactory results at each concentration level, with RE below 15% (or 20% for LLOQ). The LLOQ for MTX, which corresponds to the lowest concentration of the calibration curve that can be quantified with adequate accuracy (RE <20%) and precision (RSD <20%), was determined as 0.11 µg/ml (for the extraction solvent) and 0.05 µg/ml (for pH 7.4 PBS).

Table 1 also summarizes within-day and between-day accuracy (RE) and precision (RSD) results. Overall, RE ranged from 1.25 to 17.76%, while RSD ranged from 0.02 to 5.41%, both falling below the acceptable threshold of 15% (or 20% for LLOQ).

Stability assessments, conducted storing the samples at 4 °C for 15 days, indicated that the recovery of MTX for all tested concentrations remained within the 100 ± 15% of the nominal value, as required by guidelines. Based on these results (data not shown), it can be concluded that samples can be stored at 4 °C for a period of 2 weeks.

Table 1: Calibration data, within and between day accuracy and precision in the optimized conditions.

Medium	Regression equation	Nominal concentration (µg/ml)	Fitted value (µg/ml)	Within-day		Between-day	
				RE %	RSD %	RE %	RSD %
Receptor fluid	$y = 154.65x - 1.0084$ ($R^2 = 1$)	0.05	0.05 ± 0.00	9.99	4.98	7.19	0.02
		0.11	0.11 ± 0.01	4.14	5.41	1.31	0.02
		0.22	–	–	–	–	–
		0.45	–	–	–	–	–
		2.23	2.18 ± 0.06	3.52	3.55	1.77	0.87
		4.47	–	–	–	–	–
		8.94	8.79 ± 0.22	2.61	3.11	1.47	1.14
Extraction solvent (with IS)	$y = 0.4126x - 0.0113$ ($R^2 = 0.9997$)	0.11	0.12 ± 0.00	12.16	2.74	13.76	4.18
		0.21	0.22 ± 0.01	3.08	2.05	6.71	3.18
		0.43	–	–	–	–	–
		2.12	–	–	–	–	–
		4.25	4.21 ± 0.15	3.02	3.35	2.53	2.39
		8.49	8.49 ± 0.23	1.91	2.51	2.02	2.28
Extraction solvent (without IS)	$y = 155.72x - 5.163$ ($R^2 = 0.9999$)	0.11	0.13 ± 0.00	5.60	2.73	17.76	2.35
		0.21	0.23 ± 0.00	5.52	1.46	7.85	1.84
		0.43	–	–	–	–	–
		2.12	–	–	–	–	–
		4.25	4.18 ± 0.11	12.50	2.87	1.33	1.63
		8.49	8.39 ± 0.11	11.78	1.04	1.25	1.79

1.1.3 Skin Extraction and Quantification

To find a proper extraction method for drug quantification in skin layers, the first attempt was carried out using a mixture composed of 50 mM ammonium acetate buffer (pH 6.6) and MeOH (77:23, v/v) as both the mobile phase and extractive solvent. Samples were left in contact overnight at room temperature and under these conditions the recovery percentage was quantitative only from epidermis, while for dermis the value not exceeding

60%. To improve the amount recovered in dermis specimens, the effect of pH, the variation of the percentage of aqueous phase and organic solvent, the temperature and the effect of sonication were investigated. The recovery percentage of MTX in dermis samples was lower than 80% for all the conditions tested. The hard challenge of extracting MTX from the dermis should be explained with its considerable thickness (about 1 – 2 mm), average weight (134 mg/cm^2) and hydrophilicity; it acts as a sort of reservoir for the hydrophilic drug MTX. After all the attempts reported in Table 2, it was necessary to find a suitable internal standard (IS). Different ISs were proposed in literature in order to extract MTX in biological fluids, such as 1,3,7-thremethiluric acid and ferulic acid for human serum [118][119], caffeine [120] and 2,4-diaminopteroic acid [121] from rat or human plasma, respectively. Sparfloxacin was proposed by Ullah and colleagues [122] to extract MTX in different biological fluids, while ibuprofen [122] for the extraction of the drug from urine samples.

A suitable IS for the extraction of MTX in the skin should guarantee the same recovery percentage of the drug MTX once applied in dermis samples following the same treatment with the same appropriate extraction solvent. As reported in the Table 2, caffeine and acefylline were firstly tested in different conditions, but the recovery percentage of the drug and the IS was not the same. The attention shifted to Folic Acid (FA), owing its very high structural similarities and physicochemical characteristics compared with the drug MTX (Table 3).

Using an extraction mixture composed of 50 mM sodium acetate buffer (pH 6.6) and methanol (87:13, v/v), left in contact with the dermis overnight at room temperature, ensured an equivalent recovery of both MTX and FA. Both analytes were subsequently determined in the same HPLC analytical run (see Methods-paragraph 11). For the validation of the extraction method in dermis, 2.5 µg of FA (corresponding to the application of 10 µl of a 250 µg/ml solution in extraction mixture) was chosen on the basis of the amount of MTX recovered in the skin in a preliminary permeation experiment.

The recovery of MTX from skin layers was determined with respect to the amount applied, determined by direct injection of the spike solution in the absence of skin layer samples. Then, the amount of drug extracted was plotted as a function of the amount added. The recoveries and regression lines equations of epidermis and dermis samples obtained are reported in Figures 10 and 11. MTX recovery was quantitatively (100 ± 15% of the nominal values) at all concentration levels tested, so the proposed methods could be defined, according

to the EMA guidelines on bioanalytical method validation (EMA, 2012), as accurate and precise.

Table 2: Development of an extractive method for dermis (mean value ± SD). 10 µl of 50 µg/ml MTX solution (and where indicated of the IS solution) were applied to the tissue; after 1 h of contact, 1 ml of the specified extraction solution was added and left in contact overnight at room temperature. Before analysis, all samples were centrifuged (15,000 rpm; 10 min). AAB: 50mM ammonium acetate buffer; SAB: 50mM sodium acetate buffer; MeOH: methanol; ACN: acetonitrile; EtOH: ethanol.

MOBILE PHASE (v/v)	EXTRACTIVE SOLUTION (v/v)	SONICATION (30 min)	Proposed IS (amount added - µg)	Recovery (%)	SD
AAB pH6: MeOH (77:23)	AAB pH6: MeOH (77:23)	Yes	-	54.09	0.60
AAB pH6: MeOH (77:23)	AAB pH6: MeOH (77:23)	-	-	47.19	1.55
AAB pH6: MeOH (77:23)	AAB pH6: MeOH (77:23)	Yes (50°C)	-	61.71	10.67
AAB pH6: MeOH (77:23)	AAB pH6: MeOH (60:40)	-	-	Loss in peak resolution	-
AAB pH6: MeOH (77:23)	AAB pH6: ACN (77:23)	-	-	Loss in peak resolution	-
AAB pH6: MeOH (77:23)	AAB pH7.4: MeOH (77:23)	-	-	76.50	10.87
AAB pH6: MeOH (77:23)	AAB pH3.6: MeOH (77:23)	-	-	53.57	18.13
AAB pH6: MeOH (77:23)	AAB pH7.5: MeOH (77:23)	Yes (50 °C)	-	60.35	5.35
AAB pH6: MeOH (77:23)	AAB pH7.5: MeOH (90:10)	Yes	-	55.39	0.86
AAB pH6: MeOH (77:23)	AAB pH7.5 100%	Yes	-	48.64	5.88
AAB pH6: MeOH (77:23)	AAB pH7.5: EtOH (77:23)	Yes	-	Loss in peak resolution	-
SAB pH3.6: MeOH (87:13)	SAB pH3.6: MeOH (87:13)	Yes (30°C)	Caffeine (0.55 µg)	62.47 (MTX)	7.92 (MTX)
				86.95 (IS)	4.99 (IS)
SAB pH3.6: MeOH (87:13)	SAB pH3.6 (100%)	-	Caffeine (0.55 µg)	63.13 (MTX)	3.51 (MTX)
				88.91 (IS)	1.96 (IS)
SAB pH7.2: MeOH (87:13)	SAB pH2.4: MeOH (87:13)	-	Acefylline (1 µg)	Loss in peak resolution (MTX and IS)	-

SAB pH7.2: MeOH (87:13)	SAB pH7.2: MeOH (87:13)	-	Acefylline (1 µg)	52.27 (MTX)	5.67 (MTX)
				85.29 (IS)	2.04 (IS)
SAB pH3.6: MeOH (87:13)	SAB pH3.6: MeOH (87:13)	-	Folic acid (0.50 µg)	54.17 (MTX)	4.41 (MTX)
				31.04 (IS)	2.45 (IS)
SAB pH3.6: MeOH (87:13)	SAB pH3.6: MeOH (87:13)	-	Folic acid (0.44 µg)	57.38 (MTX)	12.65 (MTX)
				40.03 (IS)	12.44 (IS)
SAB pH3.6: MeOH (87:13)	SAB PH3.6: MeOH (75:25)	-	Folic acid (0.44 µg)	49.05 (MTX)	6.64 (MTX)
				32.55 (IS)	11.98 (IS)
SAB pH3.6: MeOH (87:13)	SAB pH3.6 (100%)	-	Folic acid (0.44 µg)	64.15 (MTX)	9.53 (MTX)
				37.33 (IS)	5.42 (IS)
SAB pH3.6: MeOH (87:13)	SAB pH4.5: MeOH (87:13)	-	Folic acid (0.50 µg)	41.49 (MTX)	4.39 (MTX)
				27.50 (IS)	2.57 (IS)
SAB pH3.6: MeOH (87:13)	SAB pH2.5: MeOH (87:13)	-	Folic acid (0.50 µg)	79.65 (MTX)	12.33 (MTX)
				35.42 (IS)	10.29 (IS)
SAB pH3.6: MeOH (87:13)	SAB pH6.6: MeOH (87:13)	-	Folic acid (0.50 µg)	48.74 (MTX)	2.62 (MTX)
				45.73 (IS)	2.50 (IS)
SAB pH3.6: MeOH (87:13)	SAB pH6.6: MeOH (87:13)	-	Folic acid (2.5 µg)	50.92 (MTX)	3.77 (MTX)
				45.30 (IS)	2.71 (IS)
SAB pH3.6: MeOH (87:13)	SAB pH6.6: MeOH (87:13) containing FA (2.5 µg/ml)	-	-	59.85 (MTX)	7.84 (MTX)
				80.60 (IS)	1.02 (IS)

Table 3: Comparison between physicochemical data of Methotrexate and Folic Acid.

	METHOTREXATE	**FOLIC ACID**
	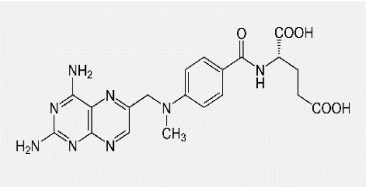	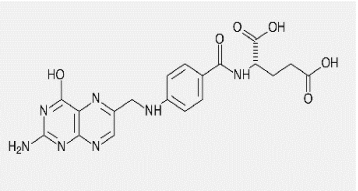
Molecular weight (g/mol)	454.4	441.4
pKa (25°C)	2.7; 4.1; 5.5	2.4; 3.5; 4.6
XLogP3	-1.8 [123]	-1.1 [124]
TPSA (Å²)	211 [123]	209 [124]

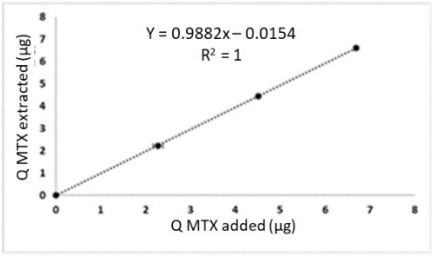

EPIDERMIS			
MTX added (µg)	MTX recovered (µg)	Recovery %	SD
2.28 ± 0.11	2.21 ± 0.04	96.99	1.86
4.51 ± 0.04	4.45 ± 0.03	98.42	0.63
6.69 ± 0.05	6.60 ± 0.06	98.67	0.84
Regression equation: y = 0.9882x – 0.0154			
Correlation coefficient: 1.0000			

Figure 10: Recovery percentage of Methotrexate (MTX) from epidermis in the optimized extraction conditions. Data expressed as mean ± SD.

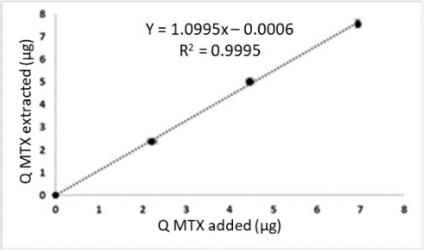

DERMIS				
MTX added (µg)	FA added (µg)	MTX recovered (µg)	Recovery %	SD
2.21 ± 0.10	2.5	2.38 ± 0.11	107.33	5.16
4.47 ± 0.09	2.5	5.02 ± 0.17	112.35	3.74
6.94 ± 0.03	2.5	7.58 ± 0.17	109.20	2.46
Regression equation: y = 1.0995x – 0.0006				
Correlation coefficient: 0.9995				

Figure 11: Recovery percentage of Methotrexate (MTX) from dermis in the optimized extraction conditions. Data expressed as mean ± SD.

A 6 h permeation experiment in finite dose condition was performed to test the analytical and extraction method developed using porcine skin tissues as biological membrane. The donor compartment was filled with 15 µl/cm^2 of 25 mg/ml commercial MTX solution (VELOS®, Difa-Cooper S.p.a.). At the end of the permeation experiment, the donor compartment was washed 4 times with 500 µl of pH 7.4 PBS buffer and MTX extracted in skin tissues was quantified as validated (results are reported in Figure 12). The total amounts of MTX recovered was 96.5 ± 1.4% of the applied dose, which is in line with the requirements of guidelines of the Organisation for Economic Co-operation and Development (2004), demonstrated the suitability and the usefulness of the methods proposed to develop new MTX topical formulations.

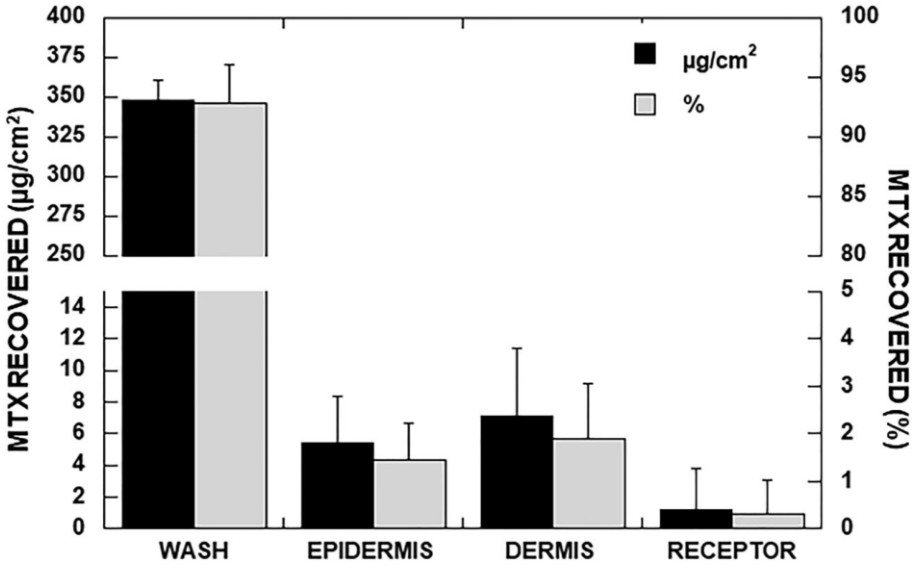

Figure 12: MTX recovered in porcine skin tissues (expressed both as µg/cm² and percentage of applied dose) at the end of 6 h permeation experiment in finite dose condition. Data expressed as mean ± SD. N: 5. Image obtained from [116].

1.2 Folic Acid

1.2.1 UV-VIS Analysis

Folic Acid spectra were recorded in both extraction solvent and receptor fluid (Figure 13).

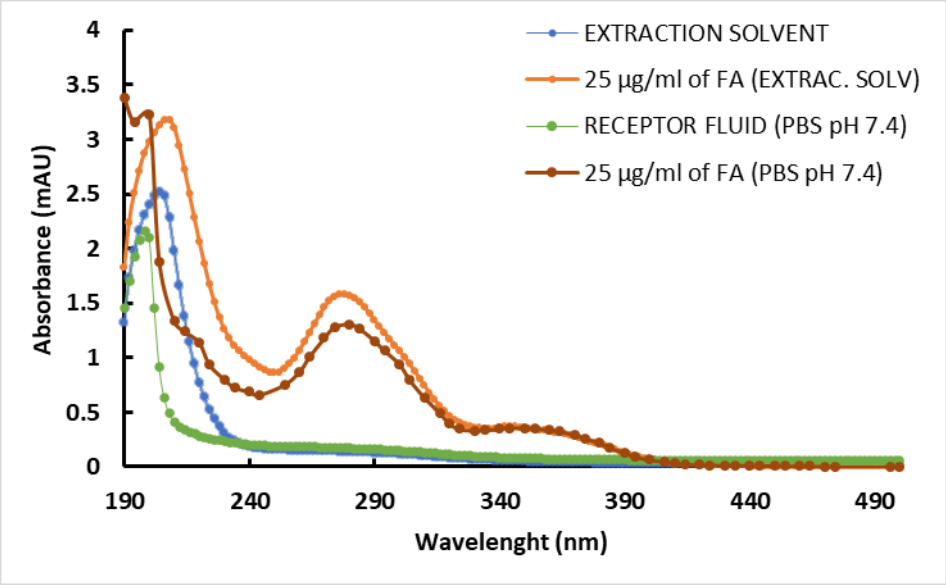

Figure13: UV-VIS spectra of FA solutions in different solvent and respective blank solutions.

The peak of absorption is at 280 nm and its position is not affected by the medium in which the drug is solubilized. To detect both MTX and FA simultaneously, the wavelength of 290 nm was finally selected for HPLC analysis.

1.2.2 Fluorescence Analysis

Figure 14 shows the absorption and emission spectra of a diluted solution of FA in pH 7.8 PBS.

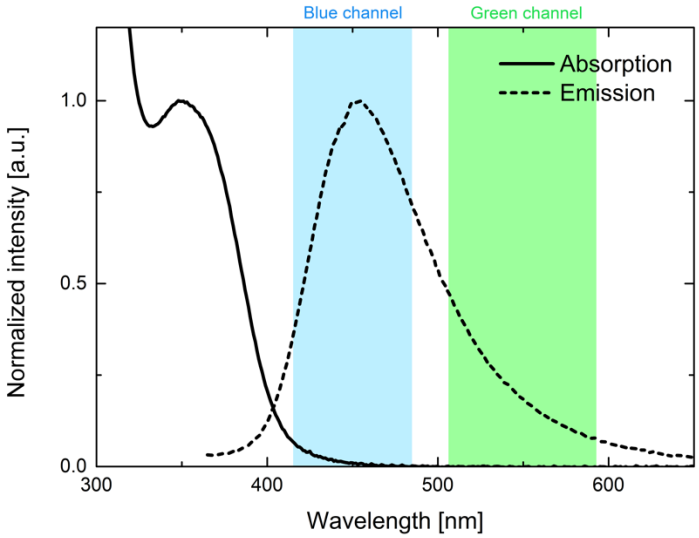

Figure 14: Absorption and emission spectra of FA in PBS buffer. The spectral ranges of the blue and green channels of the two-photon microscope detectors are also shown.

The image also shows the spectral ranges of the green and blue channels of the two-photon microscope detectors. FA solution shows an emission maximum in the blue area.

1.2.3 Solubility

The European Pharmacopoeia 12.0 reports FA as practically insoluble in water. Table 4 reports the solubility values obtained at 37°C from experiments conducted by different research groups. A minimal solubility value occurring at pH value close to 3: FA in fact exists as uncharged molecule in aqueous solution within the pH range of 2.4 to 3.5 [125].

Table 4: Solubility studies at 37°C of Folic Acid in different pH conditions. Adapted from [125].

Literature	pH of buffer	Solubility (mg/ml)
Younis [126]	1	29×10^{-3}
	3	0.840
	4	1.050
	7	5.330
	10	19.47
Bellavinha et al. [127]	1.2	9×10^{-3}
	4.5	19×10^{-3}
	6.8	4.340
Hofsäss [125]	1.2	15.95×10^{-3}
	3.0	1.46×10^{-3}
	4.5	63.6×10^{-3}
	6.8	≥ 6.47

Since the data published in literature are inconsistent, the solubility of this drug was further evaluated in different water or organic solvents or mixtures (Table 5).

Table 5: Experimental solubility values of FA at room temperature in different solvent or mixtures.

Solvent/Mixture	**Time (h)**	**Solubility (µg/ml ± SD)**
pH 2 PBS (Eu. Ph.)	24	3.44 ± 0.02
pH 5.2 PBS (Eu. Ph.)	24	≈130.01
pH 5.5 PBS (Eu. Ph.)	24	≈287.06
pH 6 PBS	24	3,364.43 ± 88.76
pH 7 PBS	24	6,139.07 ± 70.45
pH 8 PBS	24	30,573.84 ± 5.61
20 mM TPGS	24	10.19 ± 2.92
Water:propylene glycol (70:30, v/v) pH 2	24	≈7.60
Water:propylene glycol (70:30, v/v) pH 4	24	≈8.17
Water:propylene glycol (70:30, v/v) pH 5	24	≈83.98
Ethanol	65	12.34 ± 0.53
Isopropanol	65	456 ± 0.09
Methanol *	72	44.9 ± 4.16
Methanol + lecithin 2.5%	48	60.0 ± 3.95
HPBCD 0.75%	36	73.75 ± 3.86
HPBCD 1.12%	36	67.05 ± 9.93
HPBCD 2.24%	36	98.81 ± 4.36
Olive oil	48	< 220.00

**: supernatant was filtered (0.22 µm) after centrifugation. HPBCD: Hydroxypropyl-β- Cyclodextrin.*

From the experimental data obtained, it is possible to confirm that the solubility of FA is pH-dependent and improves by increasing the pH of the medium. The addition of HPBCD does not improve its solubility, as well as the use of polar organic solvents.

1.2.4 Analytical Method

The analytical method for the quantification of methotrexate and folic acid is reported in Methods paragraph 11.

1.2.5 Skin Extraction and Quantification

Based on the observation found in the validation of the extraction method of methotrexate in the skin, MTX was tested as internal standard for the extraction of Folic Acid from the dermis layer. An extraction mixture composed by 50 mM sodium acetate buffer (pH 6.6) and methanol (87:13, v/v), left in contact with dermis overnight at room temperature, guaranteed a similar recovery of FA and MTX. The two analytes were determined in the same analytical run (see Methods-paragraph 11). Method was validated with 2.23 µg of Methotrexate (corresponding to the application of 10 µl of a 223.43 µg/ml solution in extraction mixture) added as internal standard. The recovery percentages of FA are shown in Figures 15 and 16.

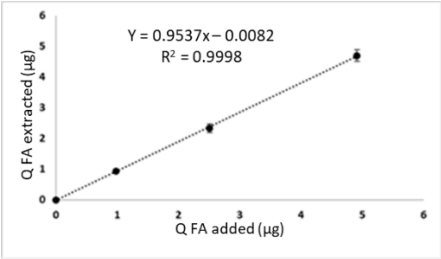

EPIDERMIS			
FA added (µg)	FA recovered (µg)	Recovery %	SD
0.98 ± 0.01	0.94 ± 0.02	96.20	2.47
2.51 ± 0.04	2.34 ± 0.14	93.31	5.51
4.91 ± 0.03	4.70 ± 0.19	95.59	3.88
Regression equation: y = 0.9537 x – 0.0082			
Correlation coefficient: 0.9998			

Figure 15: Recovery of Folic Acid from isolated epidermis in the optimized extraction conditions (mean value ± SD).

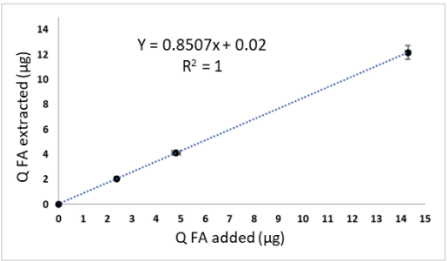

DERMIS				
FA added (µg)	IS added (µg)	FA recovered (µg)	Recovery %	SD
2.38 ± 0.06	2.23	2.06 ± 0.16	86.71	6.58
4.81 ± 0.17	2.23	4.12 ± 0.18	85.61	3.73
14.30 ± 0.10	2.23	12.18 ± 0.56	85.17	3.92
Regression equation: y = 0.8507 x + 0.02				
Correlation coefficient: 1				

Figure16: Recovery of Folic Acid from isolated dermis in the optimized extraction conditions (mean value ± SD).

Although compliant with the guidelines, to improve the recovery percentage in dermis and to eliminate the use of toxic MTX, Folinic Acid (calcium salt) was tested as possible internal standard, due to high similarities in physicochemical characteristics, as shown in the following Comparison Table (Table 6).

Table 6: Main physicochemical characteristics of Folic Acid and Folinic Acid (calcium salt).

	FOLIC ACID	**FOLINIC ACID (Ca^{++})**
	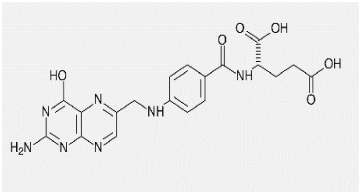	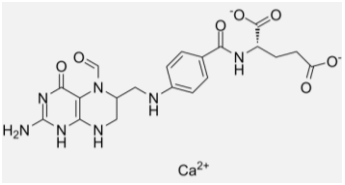
Molecular weight (g/mol)	441.4	511.5
pKa (25°C)	2.4; 3.5; 4.6	3.1; 4.8; 10.4
XLogP3	-1.1 [124]	-1.2 [128]
TPSA ($Å^2$)	209 [124]	216 [128]

Three different amounts (1, 2.5 and 4 µg/sample) of the internal standard Folinic Acid (calcium salt) were tested in order to find the higher recovery percentage of these two molecules in dermis samples in the presence of an extraction mixture composed by 50 mM sodium acetate buffer (pH 6.6) and methanol (87:13, v/v), left in contact with the dermis overnight at room temperature. Unfortunately, the recovery was not quantitative (data not shown).

Further attempts were conducted, such as the variation of the pH in the aqueous phase or the proportion between aqueous phase and organic phase in the extraction mixture, but the results did not show an improvement in the recovery (data not shown).

The last attempt aimed to investigate the effect of the partial disintegration of the dermis, obtained applying sonication with a homogenizer (Ultra-Turrax T8, Deutschland, Germany), but the obtained samples were not analysed with HPLC-UV based method due to the jellification of the samples.

1.2.6 Thermogravimetric (TGA) Analysis and Dynamic Scanning Calorimetry (DSC) Analysis

The characterization of the thermal behavior of the powders was performed by DSC analyses (Figure 17) and TGA (Figure 18).

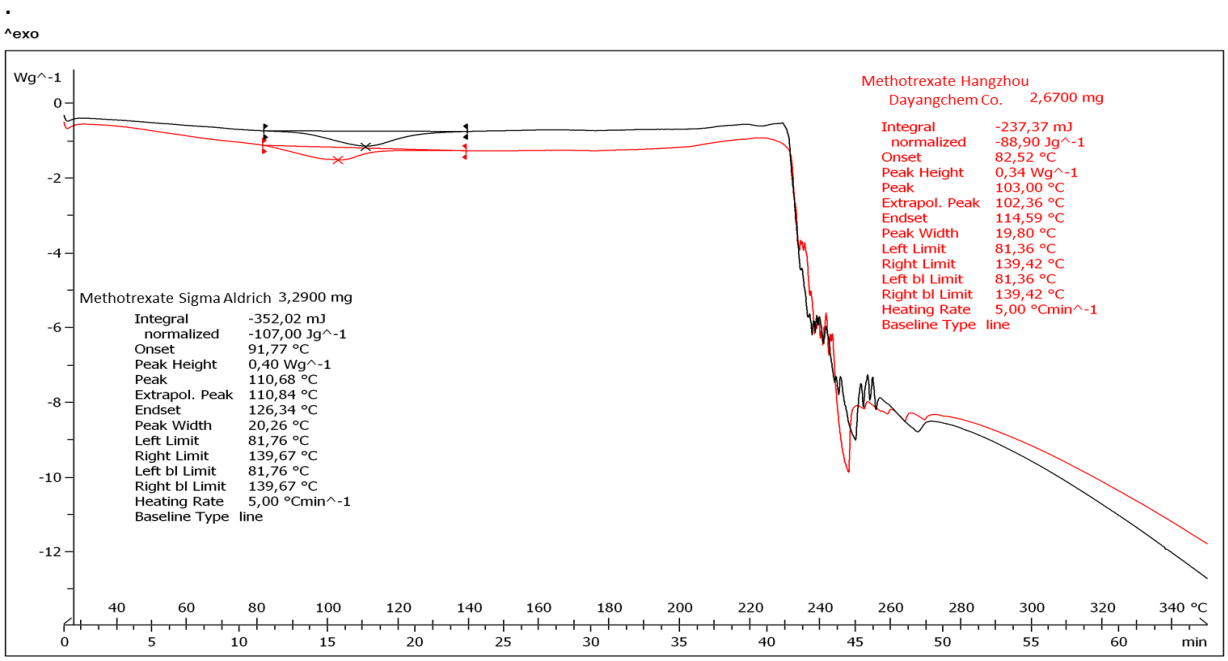

Figure 17: DSC analysis of methotrexate Sigma Aldrich and Dayangchem Co.

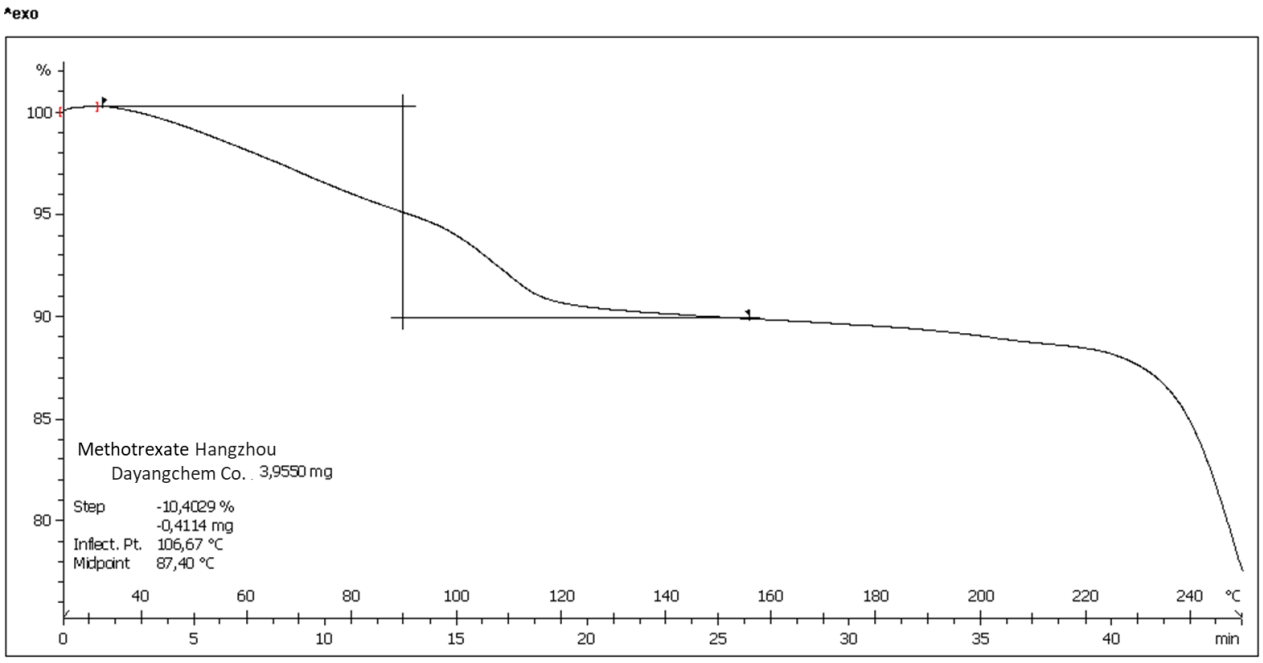

Figure 18: TGA analysis of methotrexate powder Hangzhou Dayangchem Co.

A weight loss of 10.40% at temperature of about 100 °C, demonstrated that also methotrexate Hangzhou Dayangchem Co. was a trihydrate powder, as declared for methotrexate Sigma Aldrich.

2. Preliminary Permeation Experiments

In vitro permeation experiments (6 h) were conducted on full thickness skin in finite and infinite dose conditions without any pretreatment, from solutions (12.5 mg/ml in pH 7.8 PSB) of the two drugs.

The bar graphs in Figures 19 report the amount of MTX or FA (expressed as µg/cm^2) retained in epidermis (Panel A), in dermis (Panel B), globally in the skin (Panel C) and permeated through the skin (Panel D).

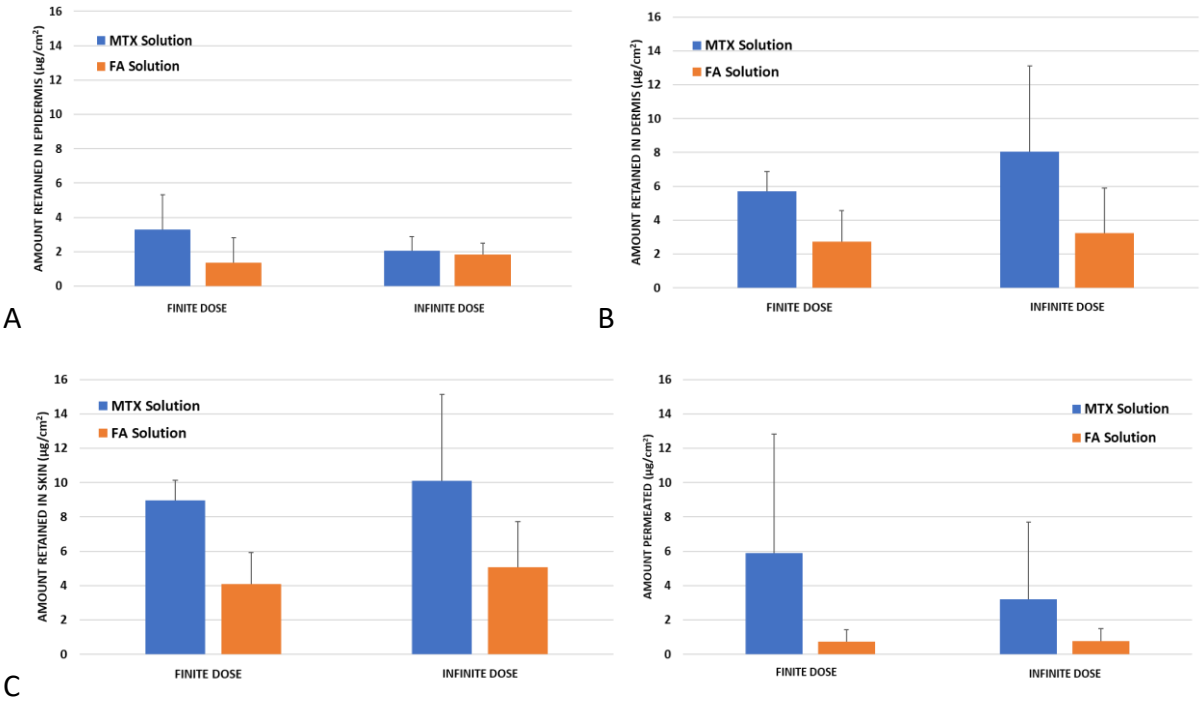

Figure 19: Amount of FA retained in epidermis (A), dermis (B), globally in the skin (C) and permeated through the skin (D) expressed as µg/cm² after 6 h permeation experiments in finite or infinite dose conditions in the presence of a solution of the drugs 12.5 mg/ml. All data are expressed as mean ± SD. N ≥ 4 for MTX and ≥ 6 for FA solutions.

Considering the amount retained in the skin layers and the amount permeated, the differences between MTX and FA were not statistically significant ($p > 0.01$), probably due to

the high variability especially of MTX experiments (the number of replicates was ≥ 4 for MTX and ≥ 6 for FA). This high variability might be explained considering a possible tropism of both MTX and FA for hair follicles, which are differently distributed in biological samples.

Based on these observations and considering the high similarities in their physicochemical properties, FA was used as a model drug for preliminary investigations, thus reducing the use of highly toxic MTX powder.

3. Formulation Development

3.1 Films

3.1.1 Characterization of PVA-PVP Films

The PVA-PVP films obtained through casting technique method were homogeneous, had good flexibility and were opaque. Figure 20 shows the images of PVA-PVP k30 (A) and PVA-PVP k90 (B) films.

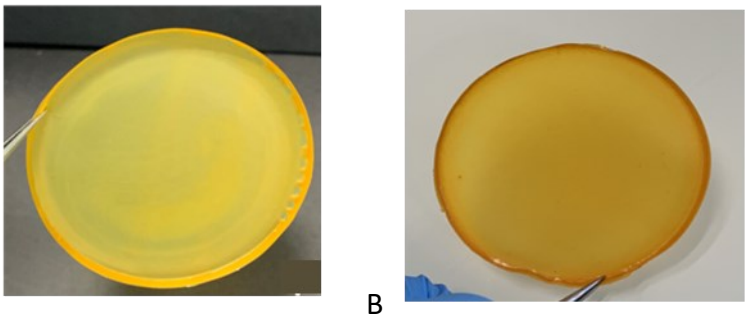

A B

Figure 20: Images of PVA-PVP k30 (A) and PVA-PVP k90 (B) films.

The mean weight was 14.90 ± 2.01 mg/cm^2 and the mean thickness (measured by Absolute Digimatic, Mitutoyo, Milano, Italia; model ID-C112BS; serial number 02101, 0.001-12.7 mm) was 101.3 ± 5.2 µm for PVA-PVP k30 films. For the PVA-PVP k90 films, the mean weight was 11.28 ± 1.20 mg/cm^2, while the mean thickness was 105.7 ± 7.3 µm.

3.1.1.1 Release Studies

In vitro release studies were performed to confirm that PVA-PVP films were able to release their load when placed in contact with an aqueous media. The release profiles of FA are shown in Figure 21.

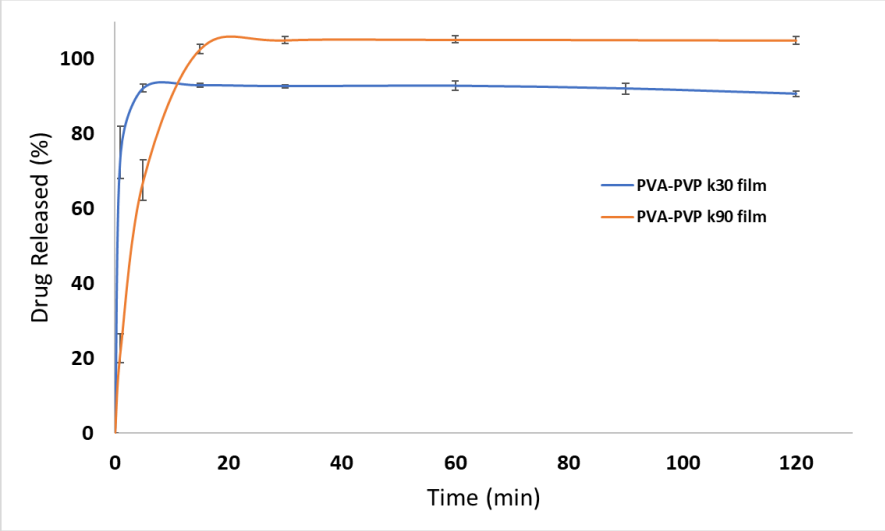

Figure 21: Percentage of FA released after 120 min in pH 8 PBS at room temperature of PVA-PVP films. All data are expressed as mean ± SD (n:4), calculated with respect to drug loading.

All FA loaded in the film was released in the first 15 minutes, without significative differences between the curves of the films formulated with PVP k30 or PVP k90.

3.1.1.2 Mechanical Characterization

The data obtained from evaluation of the mechanical properties of the films, namely breaking strength and elongation, are shown in Figures 22 and 23.

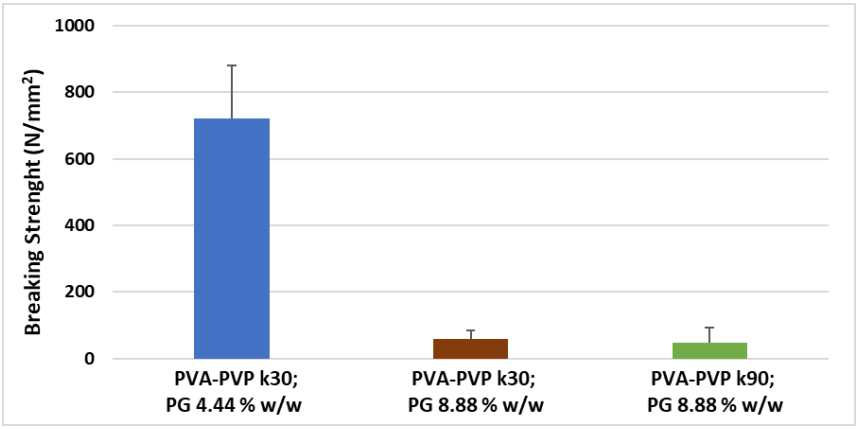

Figure 22: Breaking strength (N/mm²) obtained for PVA-PVP k30 or k90 films in the presence of different propylene glycol (PG) concentrations. Data expressed as mean ± SD. N ≥ 5.

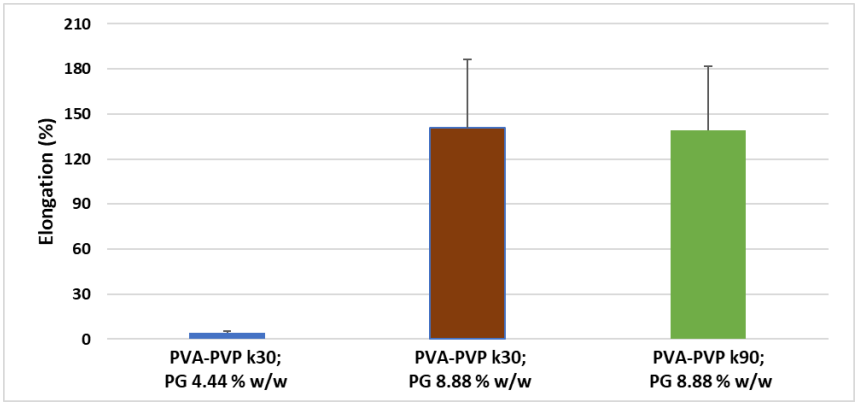

Figure 23: Percentage elongation obtained for PVA-PVP k30 or k90 films in the presence of different propylene glycol (PG) concentrations. Data expressed as mean ± SD. N ≥ 5.

In Figure 22, breaking strength (N/mm^2) can be observed for different films prepared with different grade of PVP or in the presence of different amounts of PG. The highest value is 720.2 ± 161.3 belonging to PVA-PVP k30 film in the presence of a halved amount of PG, while PVA-PVP films with different grade of PVP in the presence of 8.88% of PG show a marked decrease in breaking strength values. Analysing bar graphs in Figure 23, the elongation percentage of the PVA-PVP k30 film with the lower content of PG is lower than 5%. Doubling the amount of PG in the formulations, the elongation percentage increases a lot, with no significative variations between PVP grade films. PG was necessary to guarantee film elasticity: films with 8.88 % of PG stretched up to 140.7% (for grade 30) or 139.1% (for grade 90) of their original sizes.

3.1.2 Characterization of PLASTOID® Films

PLASTOID® containing films were prepared although the drug was not completely solubilized in the formulation before drying.

As shown in Figure 24, even after drying small spots, probably of FA, are still present in the film.

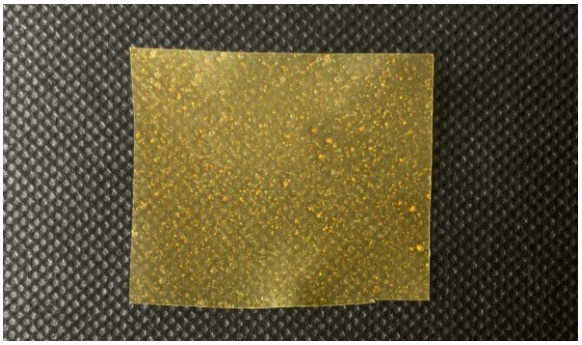

Figure 24: Image of the PLASTOID® containing film (80.8 mglg of FA).

As reported in a previous paragraph (Results paragraph 1.2.3), FA solubility is pH dependent and its solubility increases in alkaline conditions; however, the addition of sodium hydroxide to PVA/PLASTOID® mixture leads to precipitation of Eudragit E100.

The mean weight of PLASTOID® films (FA concentration 80.8 mg/g) was 6.50 ± 0.15 mg/cm^2, while the mean weight of PLASTOID® films (FA concentration 41.3 mg/g) was 7.46 ± 0.20 mg/cm^2. The two films, containing different amounts of FA, were tested in skin permeation experiments despite the presence of undissolved drug.

3.1.3 Characterization of DURO-TAK® Films

DURO-TAK® 87-2852 is an acrylate copolymer which contains 33.5% of solids. According to Henkel selection product guideline, DURO-TAK® 87-2852 shows moderate peel adhesion and tack properties and very good shear resistance properties. FA was added in DURO-TAK® 87-2852, but the resulting dispersion was completely non-homogeneous. After lamination and drying, the film (FA 20 mg/g) was completely non-homogeneous and could not be used in permeation experiments.

3.1.4 Characterization of PVP k90-PEG400 Films

Contrary of previous formulations, PVP k90-PEG400 film was homogeneous, opaque (Figure 25) and showed good elasticity, but it was not adhesive. It was firstly tested in permeation experiments (*in vitro* analysis) prewetting the tissue with 15 µl/cm^2 of water, but it immediately detached from the skin. It was supposed that the presence of FA in the dried film could negatively impact on its adhesivity and, based on this observation, the film was discarded.

Figure 25: Image of PVP k90-PEG400 film. The concentration of FA was 75.5 mg/g.

3.2 Semisolid Formulations

3.2.1 Characterization

After their preparation, semisolid formulations were characterized in terms of pH, appearance and consistency. Table 7 summarizes these characteristics.

Table 7: Characterization of developed semisolid formulations.

Formulation	Composition	Aspect	pH
Hydrogel H1	4.06% PVA 2.68% PVP k30 0.78% propylene glycol 2.47% NaOH 1N 89.37% water 0.64% (6.4 mg/g) FA	Homogeneous, solution-like behaviour	8.40
Hydrogel H2	9.14% PVA 6.02% PVP k30 4.82% propylene glycol 0.13% NaOH (salt) 79.56% water 0.33% (3.3 mg/g) FA	Homogeneous	9.25
Carbopol® Hydrogel	0.8% Carbopol 934 4.8% propylene glycol 0.2% EDTA 3.1% NaOH 2.5N 90% water 1.24% (12.4 mg/g) FA	Homogeneous	5.90
TEFOSE® O/W Emulsion	9.72% TEFOSE® 63 2.43% LABRAFIL® M2130 CS 6.48% olive oil 1.62% cetostearyl alcohol 0.59% NaOH (salt) 77.92% water 1.25% (12.5 mg/g) FA	Homogeneous	7.80
Stearic Acid O/W Emulsion	13.83% stearic acid 27.65% glycerine 0.99% NaOH (salt) 56.30% water 1.23% (12.3 mg/g) FA	Grainy appearance	6.45
W/O Emulsion	36.28% stringy vaselin 14.47% liquid paraffin 17.37% cetostearyl alcohol 4.25% cetomacrogol 1000 0.45% NaOH (salt) 25.93% water 1.25% (12.5 mg/g) FA	Homogeneous	9.80

3.2.2 Rheological Analysis

Topical delivery systems need to have adequate rheological characteristics to facilitate product application and spreading: for this reason, most of them possess viscoelastic flow properties [129]. The results of the rheological analysis of the prepared formulations are illustrated in Figure 26: in particular, Panel A reports the viscosity values with increasing shear rate in the interval 1-50 s^{-1} (the insert shown the magnification of the low viscosity formulations) whereas Panel B reports the log elaboration of the data: to have an arbitrary

shear rate value for the comparison between the different formulations, this re-elaboration allows to obtain the Log viscosity value at Log shear rate equal to zero.

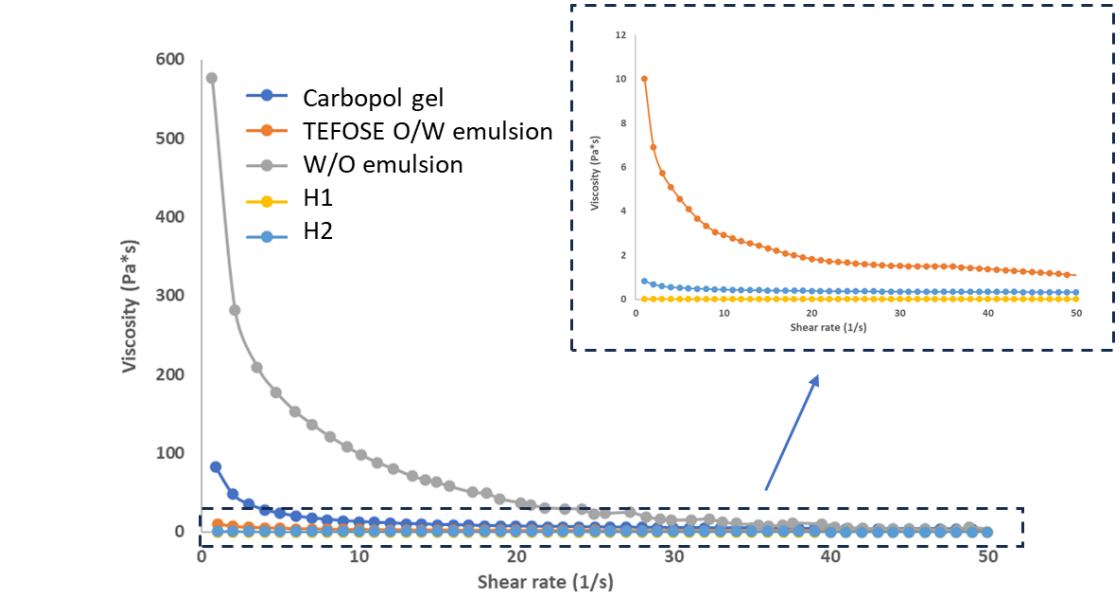

A

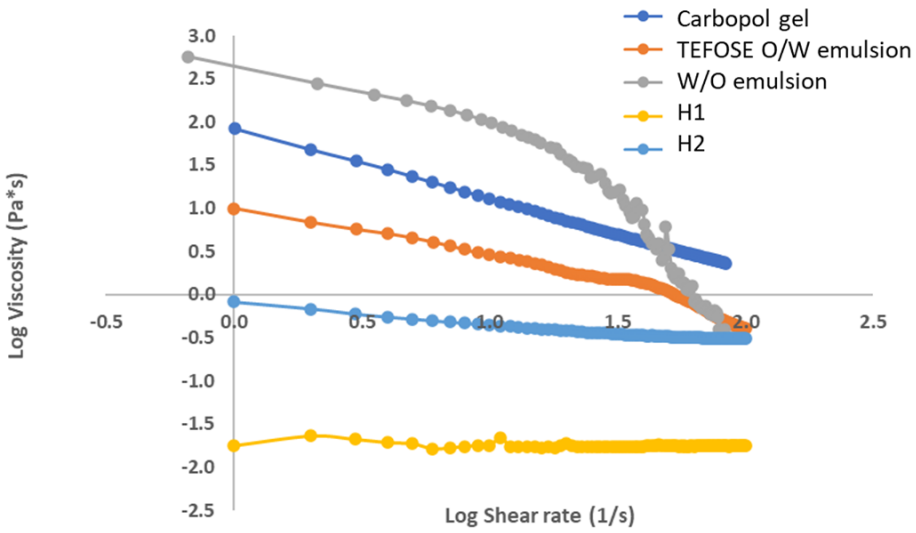

B

Figure 26: Rheological analysis of the developed semisolid formulations (Panel A) and logarithmic elaboration (Panel B).

All formulations showed pseudoplastic behaviour, that means decreasing viscosity with increasing shear rate, except for H1 hydrogel, which is classified as a Newtonian fluid. As shown in the logarithmical analysis, an increase in polymer concentration (H2 hydrogel) corresponded to an increase in viscosity value, but it is still not suitable for an application *in vivo*.

On the contrary, Carbopol® gel and the W/O emulsion showed the highest values of viscosity; in fact, as observed during their fabrication processes, they resulted stiff

formulations, which are difficult to apply to the skin. TEFOSE® O/W emulsion showed an intermediate viscosity profile compared to the other formulations.

Rheological analysis demonstrated that the latter formulation resulted promising for the topical application on the skin surface.

3.3 Microneedle Arrays

3.3.1 Characterization of FA nanosuspension

DLS analysis showed an average nanocrystal diameter of 132.3 nm, with a polydispersity index (PDI) of 0.21 (narrow size distribution). Samples revealed a substantially negative value (-38.6 mV) as Zeta potential, indicative of nanosuspension stability.

Table 8: DLS characterization of FA nanosuspension at the day of preparation. Mean ± SD (n:3).

Mean Diameter (nm)	PDI	Zeta Potential (mV)
132 ± 3.3	0.21 ± 0.00	- 38.6 ± 0.4

3.3.2 Characterization of Microneedle Arrays

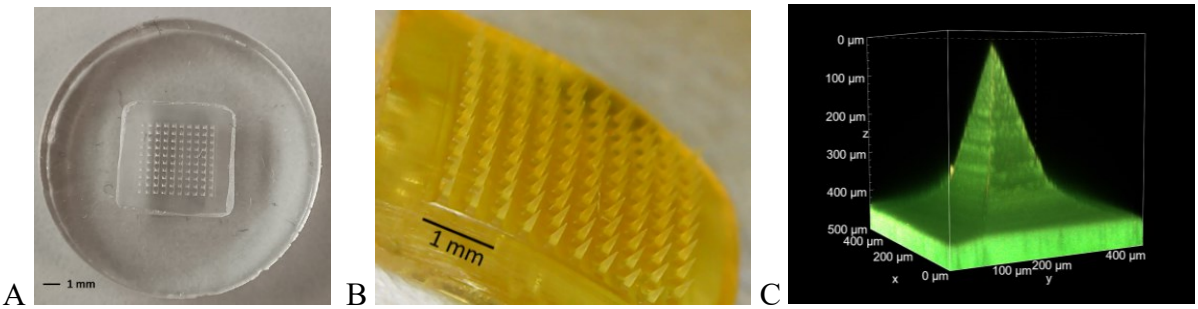

Figure 27: A) representative image of MPatch™ Microneedle Template ST-14, B) image of soluble microneedles array (obtained with Jiusion USB Digital Microscope) and C) two-photon microscopy visualization of a single microneedle (excitation wavelength 820 nm).

As can be seen in Figure 27 B, microneedle arrays are formed correctly from the template (Figure 27 A) and 100 microneedles arranged in 10 x 10 matrix are obtained, with the shape of each microneedle clearly visible. To further investigate their structure, a single microneedle was visualized with two-photon microscope (Figure 27 C) exciting the sample at

820 nm: a regular pyramidal shape can be seen, with sharp ends of the needles. The scale on the z axis confirms that needles are 0.5 mm long.

4. Skin Permeation and Retention

4.1 Folic Acid

4.1.1 Microneedle Roller Application on Solution

4.1.1.1 Evaluation of the Number of Passes of Microneedle Rollers

Microneedle (MN) rollers are minimally invasive devices that bypass the stratum corneum barrier, which represents the main obstacle to drug penetration into the skin. In contrast to MN patches, MN roller devices enable the treatment of broader skin areas [130]. These handheld devices feature stainless-steel micro-needles mounted on a roller. They can be used to create micro wounds, which trigger collagen production during the skin repair process. They can also be used in conjunction with topical skin medications to improve the penetration of active ingredients [131].

In the present study, the number of passes of MN roller 0.5 mm needle length in pretreatment of the skin was investigated, as reported in Methods paragraph 10.1.2.

The graphs in Figure 28 report the amount of FA (expressed as $\mu g/cm^2$) retained in epidermis (Panel A), in dermis (Panel B), globally in the skin (Panel C) and permeated through the skin (Panel D).

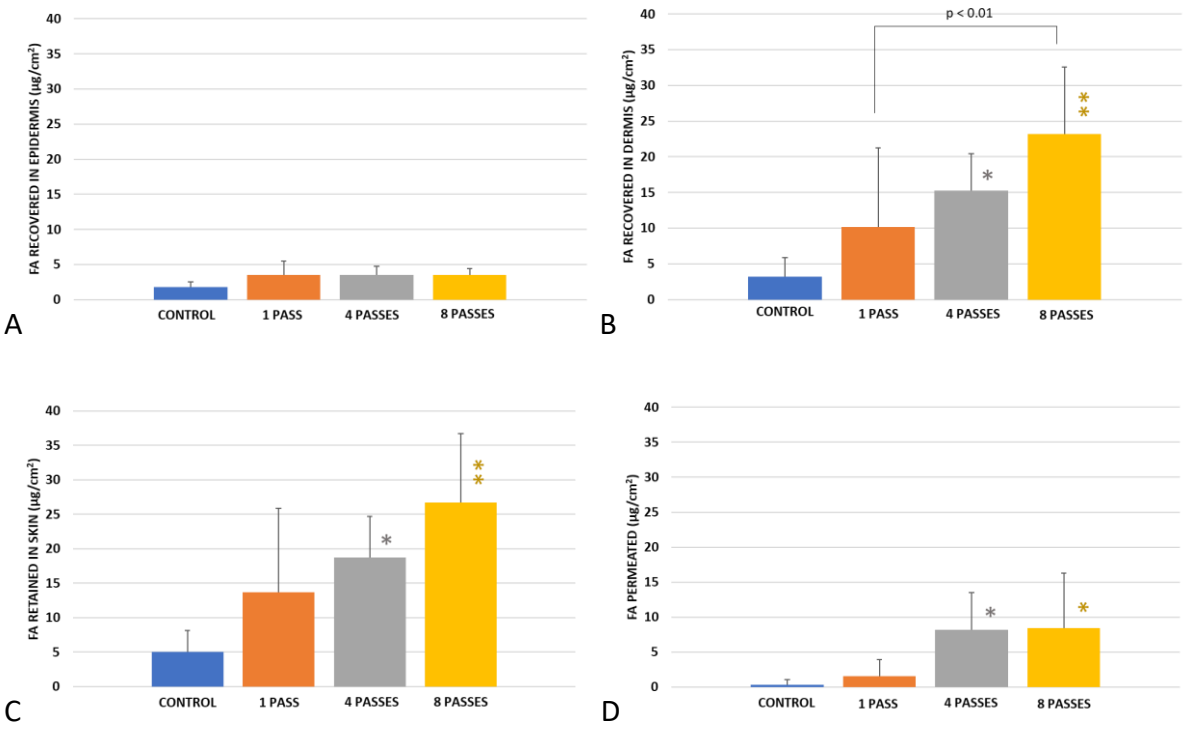

*Figure 28: Amount of FA retained in epidermis (A), dermis (B), globally in the skin (C) and permeated through the skin (D) expressed as µg/cm² after a 6 h permeation experiment in infinite dose conditions after a pretreatment with different number of passes of 0.5 mm MN roller. All data are expressed as mean ± SD (n ≥ 8). *: p < 0.01 and **: p < 0.001, compared to control.*

In untreated conditions (control), FA skin retention was very low, as was low the amount permeated across the skin. According to the physicochemical characteristics, FA is a very hydrophilic compound and cannot overcome the very hydrophobic barrier represented by the stratum corneum.

Panel A shows that when the skin was pretreated with microneedle rollers the epidermis retention was only slightly affected. On the contrary, microneedles application (4 and 8 passes) increased considerably dermis retention (Panel B), that gave the main contribution to the overall skin retention (Panel C). The effect of micro perforation of the skin was evident also in the amount permeated, which increased with pretreatment with 4 or 8 passes.

Considering the overall effect of the number of passes, a slight increase was observed with a single pass, but 4 passes were required to obtain a statistically significant effect. Since there were no significative variations between 4 or 8 passes, the following experiments were performed with 4 passes.

4.1.1.2 Evaluation of the Needle Length of Microneedle Rollers

The effect of pretreatment of the skin with MN rollers with different needle lengths- 0.25, 0.5 and 0.75 mm- was investigated. The full thickness skin was pretreated with 4 passes of MN roller along a single axis before the application of FA solution 12.5 mg/ml in infinite dose conditions, as described in Method paragraph 10.1.3.

The graphs in Figure 29 report the amount of FA (expressed as µg/cm^2) retained in epidermis (Panel A), in dermis (Panel B), globally in the skin (Panel C) and permeated through the skin (Panel D).

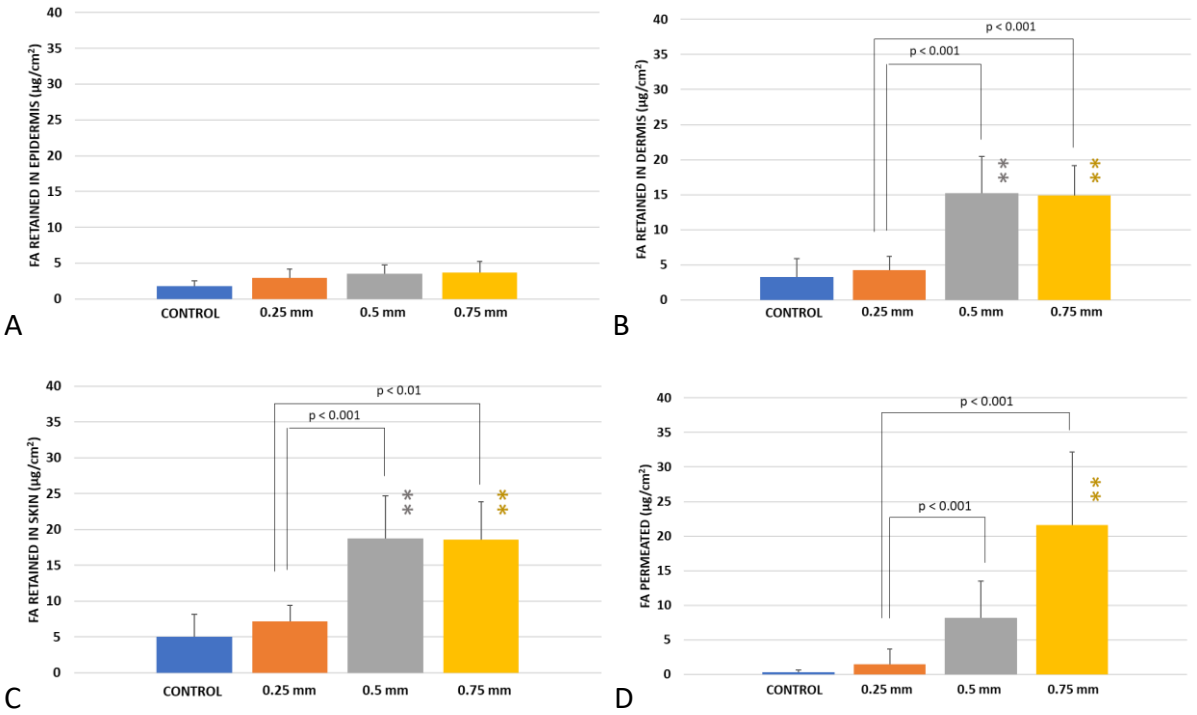

*Figure 29: Amount of FA retained in epidermis (A), dermis (B), globally in the skin (C) and permeated through the skin (D) expressed as µg/cm^2 after a 6 h permeation experiment in infinite dose conditions after a pretreatment with different needle length MN rollers. All data are expressed as mean ± SD (n ≥ 8). *: p < 0.01 and **: p < 0.001, compared to control.*

Considering the total amount retained in the skin (Panel C; Figure 29), 0.25 mm MN rollers did not produce any enhancement in FA skin retention, which improved significantly when the needle length increased up to 0.75 mm. No significative differences ($p < 0.01$) were observed on the amount retained between 0.5- and 0.75-mm needle length.

Analysing the amount of FA permeated across the skin (Panel D; Figure 29), there was an increase proportional with needle length; in fact, a pretreatment with 0.75 mm MN roller

allowed a permeation of more than twice the value obtained with 0.5 mm, with an increase in toxic effects derived from the systemic absorption.

Again, the epidermis (Panel A; Figure 29) and the dermis (Panel B; Figure 29) distributions show that the epidermis retention was slightly affected by microneedles application, whereas dermis gave the main contribution to the overall skin retention.

Since there were no significative variations between 0.5 and 0.75 needle length in terms of FA retained in the skin, the following experiments were performed using 0.5 mm MN roller. This choice allows also to reduce the amount of FA permeated across the skin.

4.1.1.3 Kinetic Studies

Figure 30 shows the permeation profiles obtained when the skin was pretreated with different needle length MN rollers. From the linear portion of the permeation profiles (from 4 to 6 hours) the flux (J) was calculated, as the slope of the regression line. From the intercept on the x axis the time lag (h) was calculated as well. The permeability coefficient (P) was obtained using the following relationship:

$$P=J/CD$$

where CD (µg/ml) was the donor concentration and J (µg/(cm^2*h)) was FA flux across the skin. In untreated conditions (control), the amount found in receptor fluid was zero in 8 out of the 10 cells; a similar situation was found when using 0.25 mm MN roller.

FA flux and P were proportional to needle length, but no significative difference were observed, probably because of the high variability of the data. Analysing the time lag, it reduced from almost 3 hours (0.5 mm needle length) to close to two hours (0.75 mm MN roller). This reduction resulted significative with $p < 0.001$.

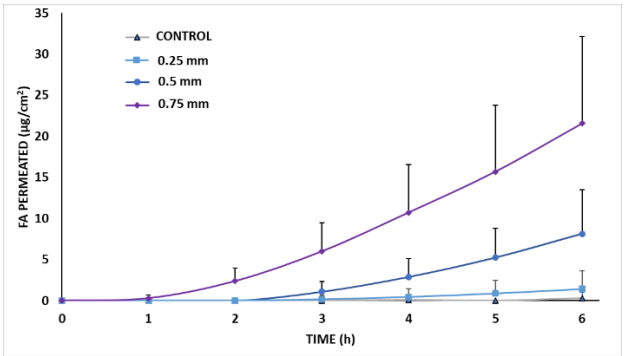

	J (µg/(cm²*h))	t lag (h)	P * 10⁴ (cm/h)
CONTROL	-	-	-
0.25 mm	-	-	-
0.5 mm	2.47 ± 1.76	2.92 ± 0.14	2.22 ± 1.28
0.75 mm	5.42 ± 2.39	2.16 ± 0.37	4.34 ± 1.91

Figure 30: Permeation profiles obtained when the skin was pretreated with different needle length MN rollers and values of the flux, P and time lag. Mean ± SD (n ≥ 8).

Permeation curves shows that FA was found in receptor fluid after 2 h, so the experimental time was reduced to 2 h to evaluate the effect of contact time on FA retention and permeation. The experiments were performed as before (infinite dose condition, FA solution 12.5 mg/ml), using 0.25, 0.50 mm and 0.75 mm MN rollers.

The graphs in Figure 31 report the amount of FA (expressed as µg/cm^2) retained in epidermis (Panel A), in dermis (Panel B), globally in the skin (Panel C) or permeated through the skin (Panel D).

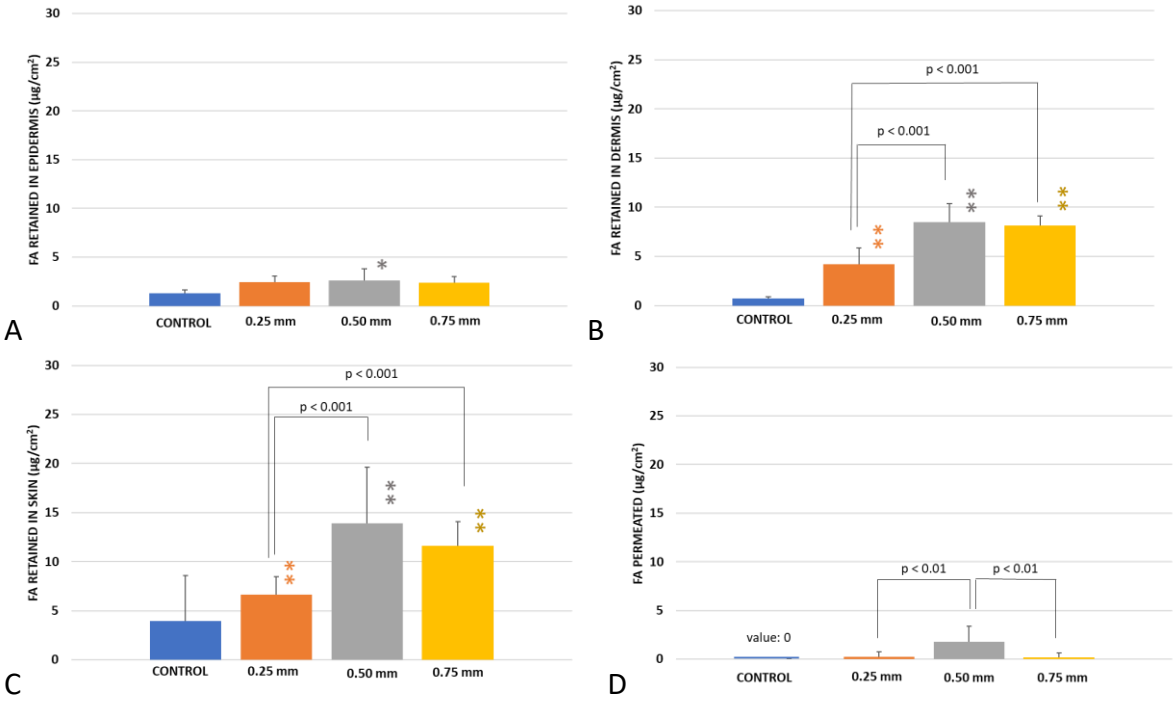

*Figure 31: Amount of FA retained in epidermis (A), dermis (B), globally in the skin (C) and permeated through the skin (D) expressed as µg/cm^2 after a 2 h permeation experiment in infinite dose conditions after a pretreatment with different needle length MN rollers. All data are expressed as mean ± SD (n ≥ 7). *: p < 0.01 and **: p < 0.001, compared to control.*

From the data obtained, FA permeation was very fast and after two hours the amount found in the receptor fluid (Panel D, Figure 31) was close to zero for all the conditions

(untreated and treated samples). After 2 h, 0.75 mm MNs did not improve significantly the amounts retained in the skin compared to 0.5 mm (Panel C, Figure 31). Also in this case, the differences in the amounts of FA retained in the skin were attributed to dermis (Panel B, Figure 31) and the contribution of the amounts retained in epidermis on overall balance was the same for each condition tested (Panel A, Figure 31).

4.1.1.4 Ratio "Retained VS. Permeated"

A further elaboration was to calculate the ratio between the amount retained in the skin and the amount permeated: the higher the ratio, the higher will be the efficacy of the formulation, with limited risk of systemic absorption. This calculation was possible only when the amount permeated was different from zero, so it was determined only for 0.50 and 0.75 mm MNs.

As reports in the Figure 32, the pretreatment with 4 passes of MN roller 0.5 mm before the application of the solution for 2 h gave the higher ratio compared to 6 h.

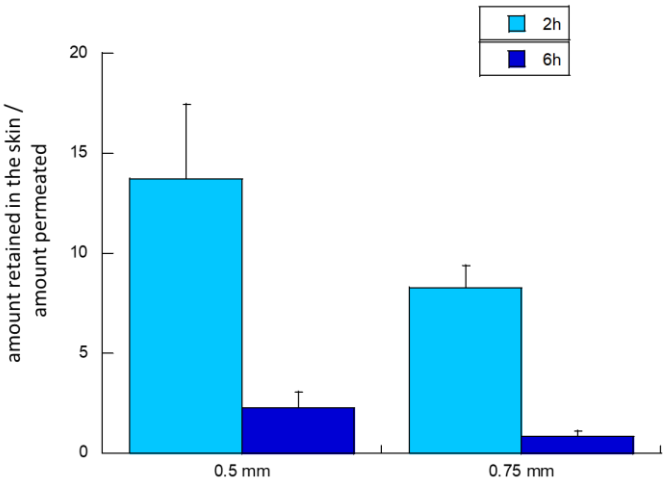

Figure 32: Ratio "retained/permeated" for the pretreatments (4 passes) with 0.5- and 0.75-mm MN rollers following 2- or 6-hours in vitro permeation experiments. Mean ± SD.

In the two cases analyzed, the pretreatment with MN roller 0.5 mm provided a higher ratio than the pretreatment with 0.75 mm. Considering the application time, although from a numerical point of view the ratio data are greater for the two-hour condition, the subsequent experiments were performed at 6 hours, as more similar to the residence time *in vivo* of the developed formulations.

4.1.1.5 Two-Photon Microscopy Analysis

The effect of a potential retention of FA in hair follicle was investigated analysing the skin following 6 h permeation experiments applying in donor compartment:

a) 417 µl/cm^2 of pH 7.8 PBS (BLANK - Figure 33, A);

b) 417 µl/cm^2 of 12.5 mg/ml of FA solution (PASSIVE - Figure 33, B);

c) 417 µl/cm^2 of 12.5 mg/ml of FA solution, applied after a pretreatment (4 passes) with MN roller 0.5 mm (TREATED - Figure 33, C1 and C2). Two different hair follicles were studied to verify the reproducibility.

All samples were studied in the absence of water between the objective and the tissue to avoid the back-diffusion of FA and the rehydration of the tissue, which could influence the results.

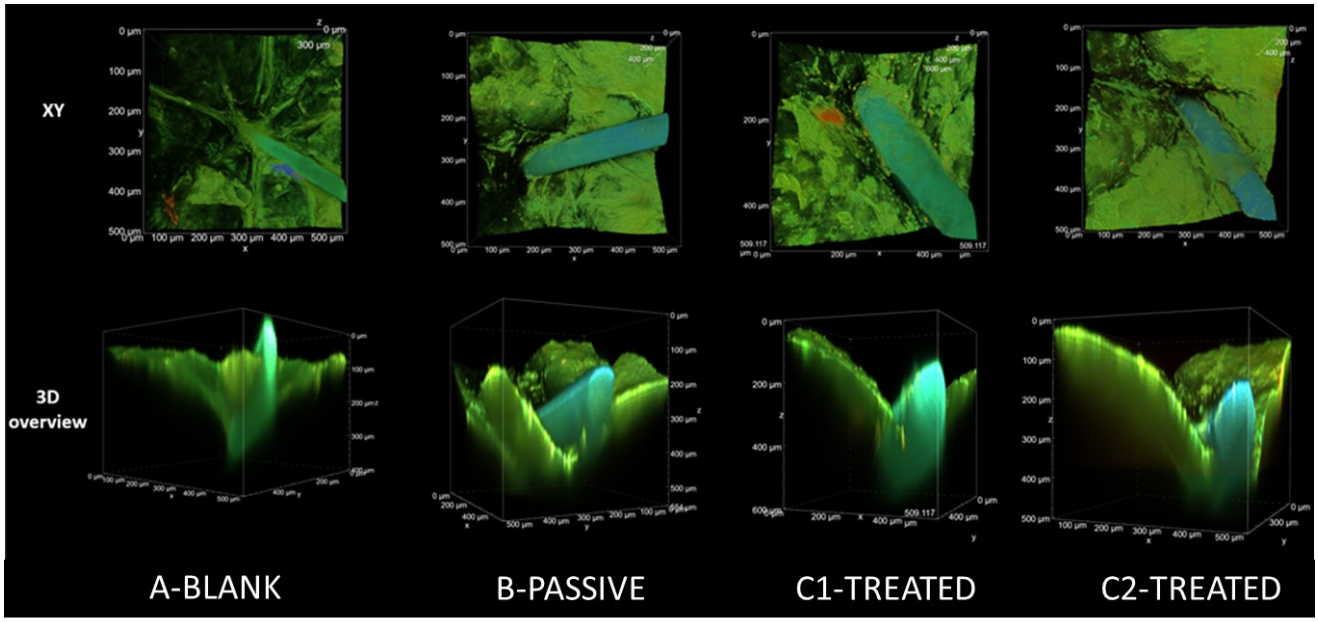

Figure 33: Volume renderings of skin tissues reconstructed from Z-stack, acquired with an excitation wavelength of 820 nm, power of 10% and detector gain 100 for all the channels.

Based on the fluorescence analysis data, skin samples exposed to FA are expected to show a more pronounced blue component than the green one, which was instead associated to the autofluorescence of the skin samples.

As observed from the three-dimensional renderings, in the current experimental conditions the presence of FA in the tissue do not offer any type of contrast compared to the autofluorescence of the blank samples. The only exception is the hair follicle, which has a slightly unbalanced signal towards the blue channel, that is typical of FA.

By comparing the emission spectra acquired in the samples discussed above, it is possible to observe a slight blue-shift for the bands of the samples treated with FA (Figure 34). For comparison, it is indicated the spectrum of FA solution (12.5 mg/ml in PBS pH 7.8).

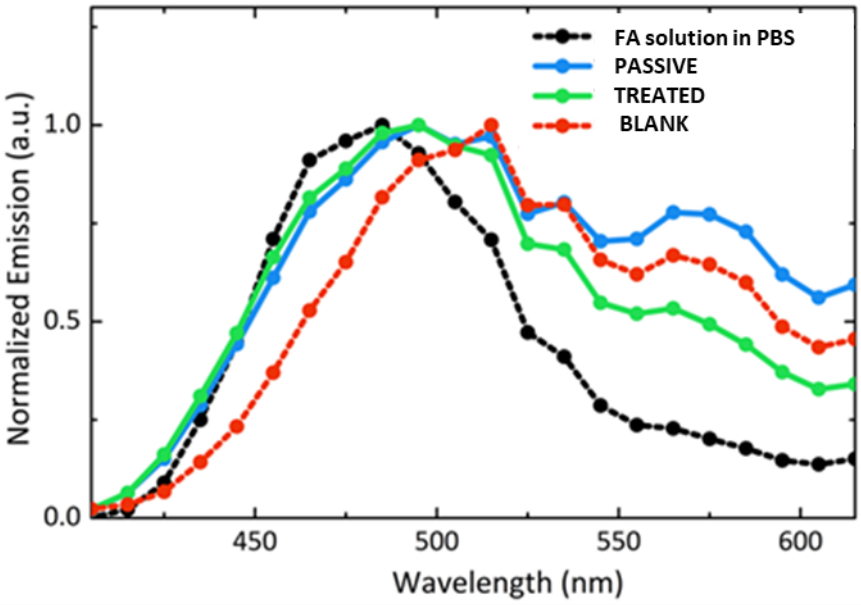

Figure 34: Emission spectra of different samples obtained excited at 820 nm.

Although the spectra give a good indication of the presence of FA in passive and treated tissues, the intensity of the fluorescence signal observed in these samples was only slightly higher than that observed in blank tissue. This result could indicate that the concentration of the fluorophore (FA) of interest was quite low in the tissue or that its emissivity in this environment was rather low and comparable to autofluorescence.

The autofluorescence of the tissue could vary depending on how much the focal plane was occupied by the epidermis or the hair follicle, as they present different signals. Figure 35 shows two emission spectra acquired in specific regions of a blank tissue highlighted by coloured cycles, compared with the average spectrum collected from the whole field of view.

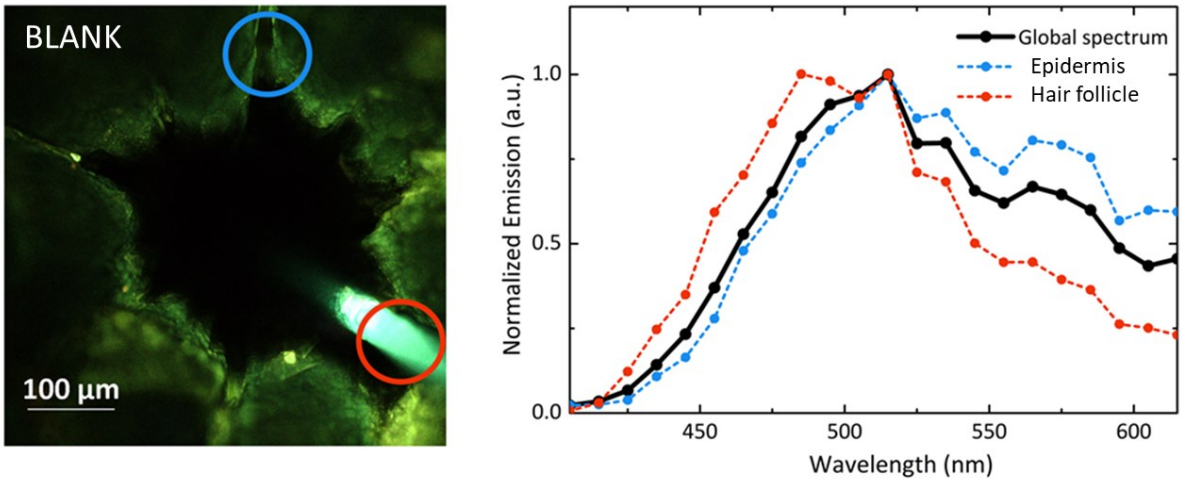

Figure 35: Emission spectra in two different regions (epidermis and hair follicle) in a blank tissue. Two different contributes were highlighted: epidermis in blue and the hair follicle in red. The image and the spectra were obtained excited the sample at 820 nm.

The same comparison could be replicated in the presence of a tissue been in contact with FA; in this case the analysis was performed in treated samples (Figure 36). The emission spectrum of a FA solution (12.5 mg/ml) in PBS is reported.

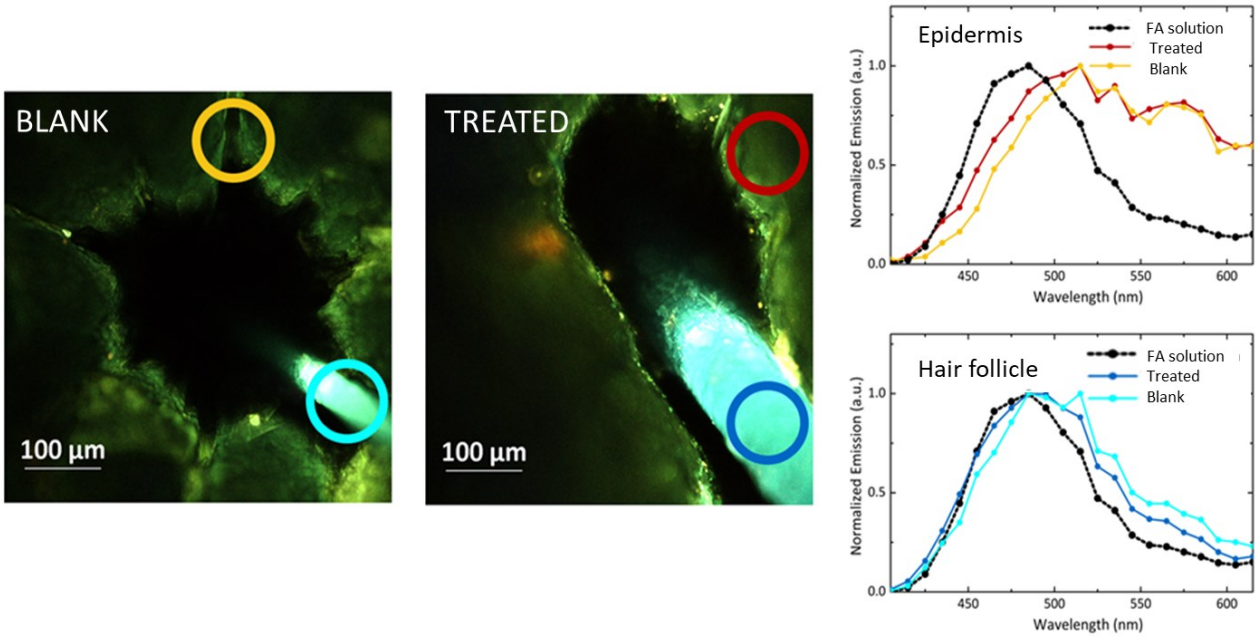

Figure 36: Comparison between the emission spectra and corresponding images of blank and treated tissue. Contributes of two different areas of the skin (epidermis and hair follicles) are shown. The epidermis in brown (treated) and yellow (blank) and the hair is blue (treated) e and light blue (blank). The Images and the spectra were obtained exciting the samples at 820 nm.

Also considering the separate emissions of the epidermis and the hair follicle alone, no significative variations are observed, except a slight blue-shift in the case of treated samples, indication of the presence of FA.

The data obtained supported the accumulation of the drug in passive and treated tissues. However, further studies will be necessary to reduce as much as possible the autofluorescence signal and to further investigate the preferential accumulation of FA in the hair follicle.

4.1.2 Microneedle Roller Application on Films

4.1.2.1 PVA-PVP k30 Film

After its characterization, PVA-PVP k30 film was tested *in vitro,* in 6 h permeation experiments. Since PVA-PVP k30 film was not self-adhesive, the skin was wetted with two different amounts of water (15 µl/cm^2 or 167 µl/cm^2) before the application of the film with a spatula. The bar graphs in Figure 37 report the amount of FA (expressed as µg/cm^2) retained in epidermis (Panel A), in dermis (Panel B), globally in the skin (Panel C) or permeated through the skin (Panel D).

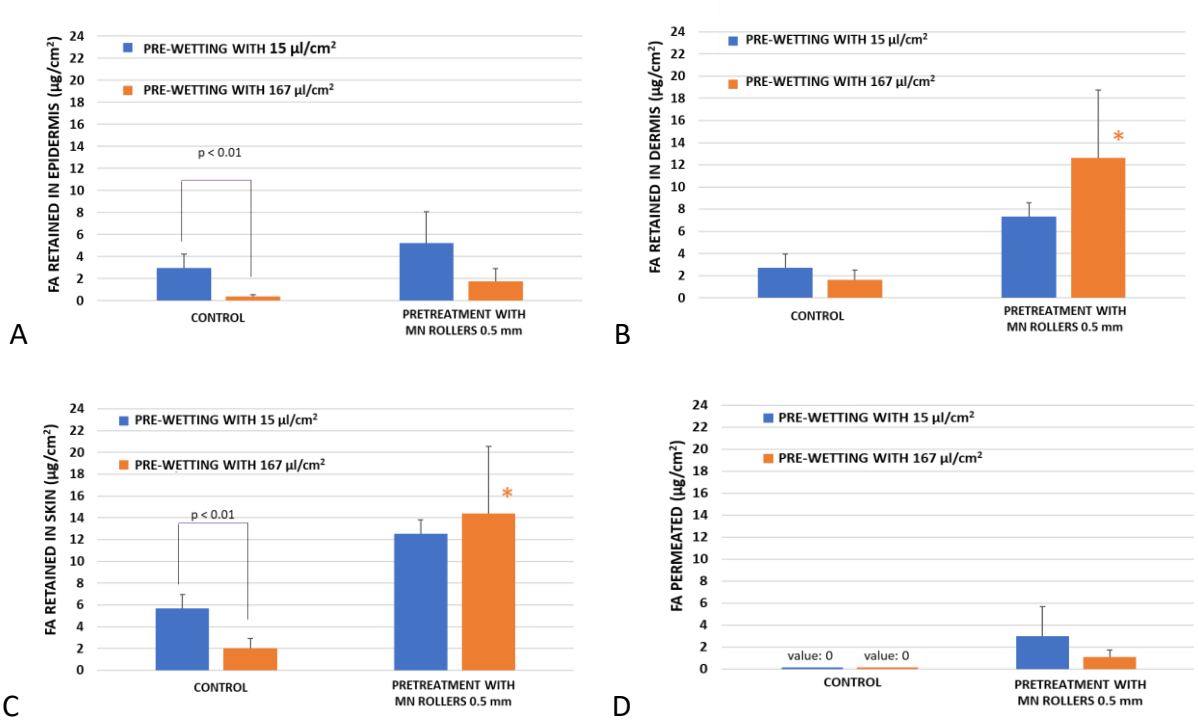

*Figure 37: Amount of FA retained in epidermis (A), dermis (B), globally in the skin (C) and permeated through the skin (D) expressed as µg/cm^2 after a 6 h permeation experiment after the application of PVA-PVP k30 film in the presence of different pre-wetting conditions. All data are expressed as mean ± SD (n ≥ 3). *: p < 0.01 and **: p < 0.001, compared to control.*

When the tissue was pre-wetted with 15 µl/cm^2 of water, skin contact and adhesion of the film was not achieved completely, whereas pre-wetting with 167 µl/cm^2 the film completely adhered to the skin at least initially (although during the experiment, it tended to detach and partially to solubilize). In the latter case, the amount of FA retained was higher and significantly different from respective control. No differences were observed taking into account the amount permeated.

Considering the average weight of this film (14.90 ± 2.01 mg/cm^2), an average amount of 0.7 mg of FA was applied on the skin in the donor compartment. To evaluate the efficiency of the film, these data were compared with those obtained from a 12.5 mg/ml solution in infinite conditions (3 mg of FA applied on the skin). In fact, although the concentration of FA in the film was higher than in the solution (77.5 mg/g VS 12.5 mg/ml), the amount applied was lower due to film thickness. The skin was pretreated with MN roller with different needle lengths and the statistical analysis was performed as described in Methods, paragraph 10.3. The graphs in Figure 38 report the amount of FA (expressed as µg/cm^2) retained in epidermis (Panel A), in dermis (Panel B), globally in the skin (Panel C) and permeated through the skin (Panel D).

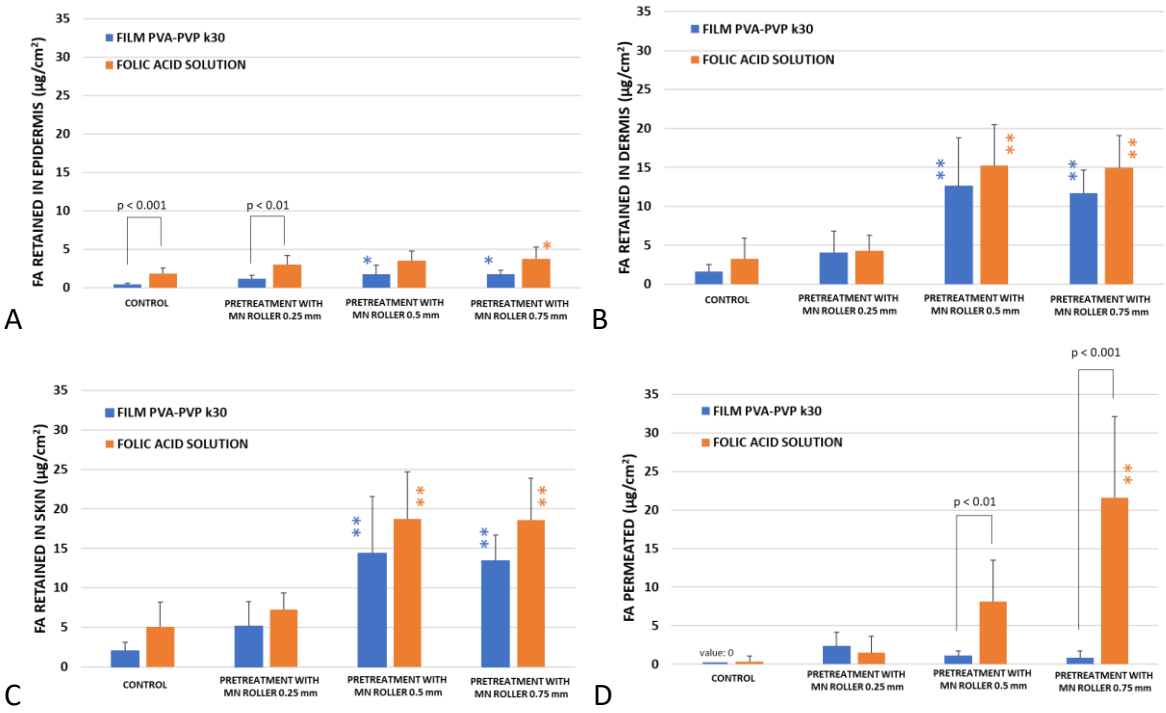

*Figure 38: Amount of FA retained in epidermis (A), dermis (B), globally in the skin (C) and permeated through the skin (D) expressed as µg/cm^2 after a 6 h permeation experiment after the application of PVA-PVP k30 film (167 µl/cm^2 water pre-wetting) and a FA solution in infinite dose condition. All data are expressed as mean ± SD (n ≥ 5). *: p < 0.01 and **: p < 0.001, compared to control.*

Film and solution produced similar results in terms of skin retention, with respect of MN length pretreatment (with a few exceptions for epidermis retention). However, a very evident difference was found for skin permeation: as shown in Panel D, the amount of FA permeated across the skin was significantly lower for the film compared to the solution, with both MN length. The ratio retained to permeated was 10.85 ± 4.13 and 8.20 ± 4.26 for the film (0.5 and 0.75 mm MN, respectively) and 3.01 ± 1.58 and 1.12 ± 0.76 for the solution.

It has to be underlined, however, that the application of the film with such an amount of water (167 µl/cm^2) lead to the formation of a solution and cannot be considered as a suitable formulation for patient use.

4.1.2.2 PLASTOID® Films

Adhesive films containing PLASTOID® with two different FA concentrations (80.8 mg/g and 41.3 mg/g) were tested after a pre-wetting of the tissue with 15 µl/cm^2 of water. PLASTOID® film 41.3 mg/g of FA was also tested in occlusive conditions. Figure 39 shows the amount retained in epidermis (Panel A), dermis (Panel B), globally in the skin (Panel C) and the amount permeated through the skin (Panel D) after 6 h *in vitro* permeation experiment, in comparison with the data obtained from the FA solution (12.5 mg/ml).

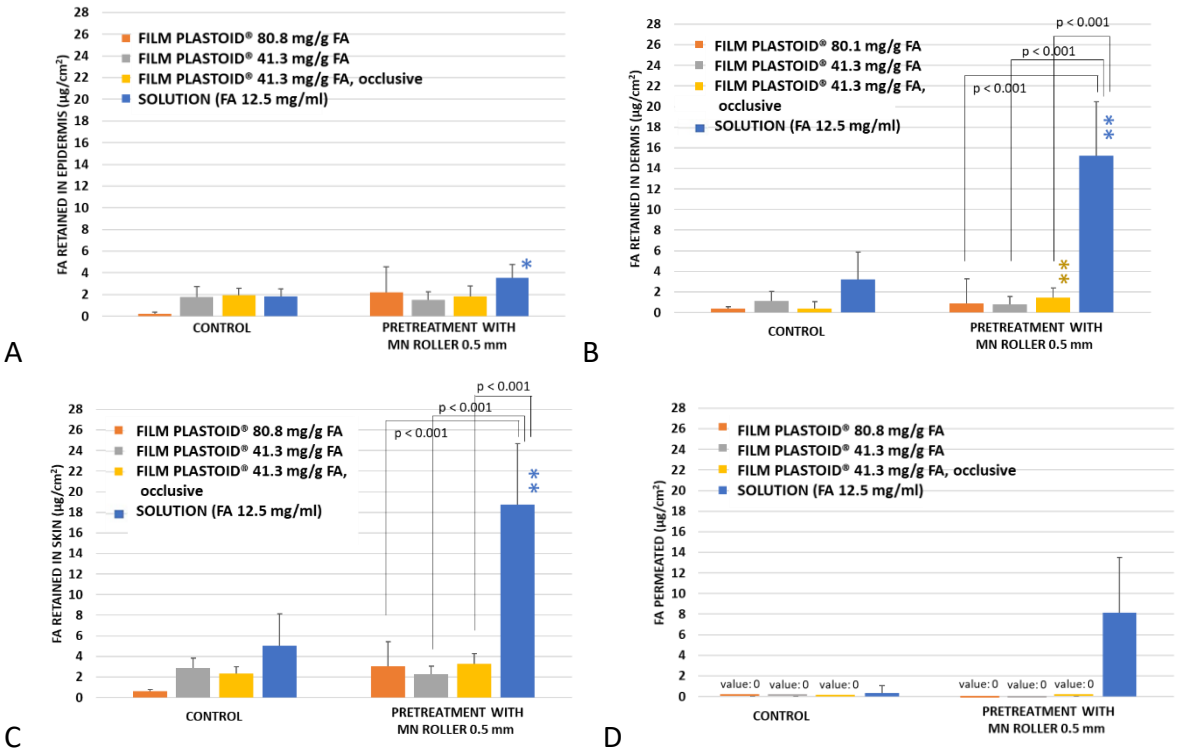

*Figure 39: Amount of FA retained in epidermis (A), dermis (B), globally in the skin (C) and permeated through the skin (D) after 6 h in vitro permeation experiments after the application of PLASTOID® films. All data are expressed as mean ± SD; n: 3 for PLASTOID® films 80.8 mg/g of FA, n ≥ 6 for PLASTOID® films 41.3 mg/g of FA. *: p < 0.01 and **: p < 0.001, compared to control.*

It was observed that there were no significative variations between the formulations analysing the amount retained in epidermis (Panel A, Figure 39), while FA retained in dermis (Panel B, Figure 39) after the application of topical films containing the adhesive PLASTOID® was significative lower than the amount of drug retained after the application of the FA solution.

PLASTOID® films with 80.8 mg/g of FA did not improve the amount retained in skin layers compared to other ones when the concentration of FA was halved reduced. Additionally, the effect of occlusion was investigated in this latter case, since occlusion can enhance the percutaneous absorption of some compounds [68]. However, the application of the film containing PLASTOID® in occlusive conditions did not modify FA retention and permeation, probably because folic acid is a polar molecule and occlusion seems to have a greater effect on lipid-soluble permeants [69].

4.1.3 Microneedle Roller Application on Semisolid Formulations

4.1.3.1 Hydrogels

For comparison purposes, a hydrogel composed with the same polymers and excipients as the PVA-PVP k30 film and containing the same amount of water obtained after wetting with 167 µl/cm^2, was prepared (H1, see Methods paragraph 8.1.1). Two additional formulations, with higher viscosity, were prepared: one contained a higher percentage of polymers (H2 hydrogel) and one contained also Carbopol® 934 (see Methods par 8.1). All formulations were tested in infinite dose conditions in 6 h permeation experiments in passive condition and after pre-treatment with 0.5 mm MN roller. Figure 40 shows the amount retained in epidermis (Panel A), dermis (Panel B), globally in the skin (Panel C) and the amount permeated through the skin (Panel D), in comparison with the data obtained from the FA solution (12.5 mg/ml).

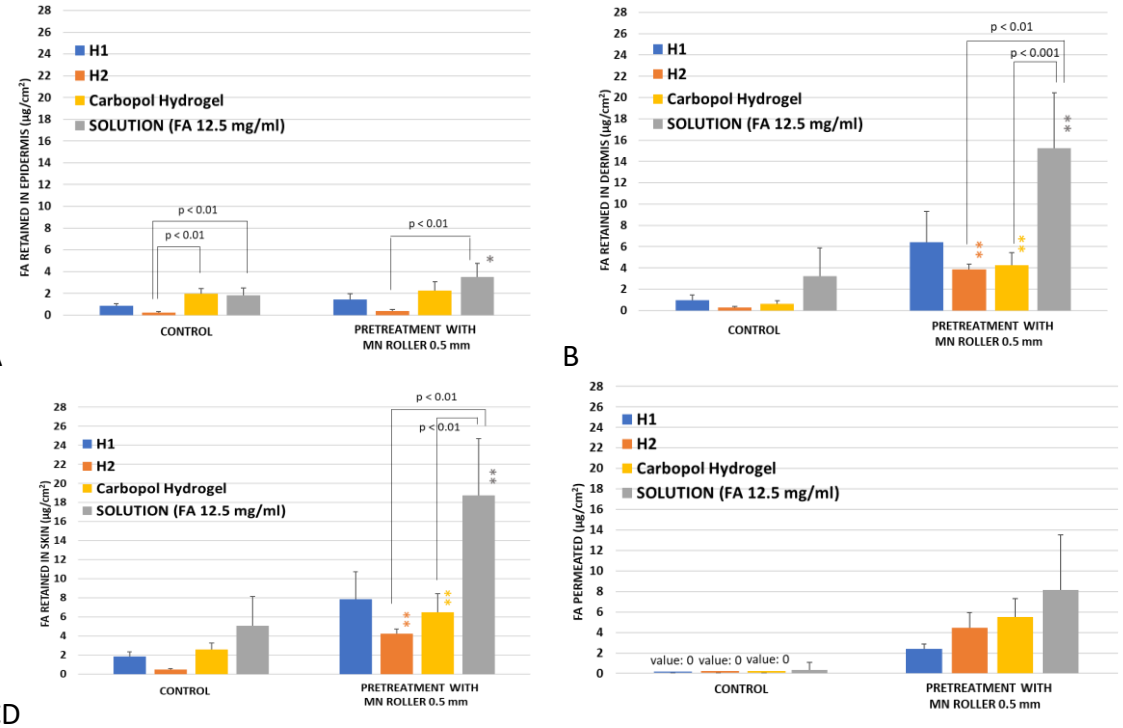

*Figure 40: Amount of FA retained in epidermis (Panel A), dermis (Panel B), globally in the skin (Panel C) and permeated through the skin (Panel D) for the hydrogels H1, H2 and for that containing Carbopol® after 6 h permeation experiment in infinite dose conditions. All the data are reported as mean ± SD; n: 2 (H1), n: 3 (H2), n:5 (Carbopol® hydrogel), n: 10 (FA solution). *: p < 0.01 and **: p < 0.001, compared to control.*

As shown in Panel A of Figure 40, the pretreatment with 0.5 mm needle length MN roller was not effective in improving the amount of FA retained in epidermis, compared to respective controls, except for the solution. Panel B shows the amount retained in dermis after 6 h *in vitro* permeation experiment, which were higher than the amount retained in epidermis. Pretreatment with 0.5 mm MN roller significative increased FA dermis retention for more viscous H2 and Carbopol® hydrogels and for the solution, compared to respective controls. Analysing the same treatment group, no significative variations were observed between the semisolid formulations; this behaviour was maintained considering the amount retained globally in the skin (Panel C). The passive application of the hydrogels did not lead to permeation (Panel D, Figure 40), while after the pretreatment with MN rollers 0.5 mm the amounts were slightly higher, but not significative different between the groups.

Based on these observations, hydrogels were not particularly effective in increasing FA retained in skin layers, thus did represent an improvement compared to the reference solution.

4.1.3.2 O/W and W/O Emulsions

From the physicochemical characteristics and the data obtained in Results paragraph 4.1.3.1, FA is a highly hydrophilic substance which therefore appears to have a great affinity for the vehicle in hydrogels, resulting in low accumulation of the drug in the skin layers. Starting from these considerations, biphasic semisolid formulations allowing the solubilization of this drug and its passage through the skin have been developed. In addition, formulations like emulsions contain surfactants which can reversibly remove the barrier resistance of the stratum corneum.

Hence, TEFOSE® O/W emulsion, stearic acid O/W emulsion and W/O emulsion were developed and tested *in vitro* in 6 h permeation experiments in infinite conditions. Figure 41 shows the amount retained in epidermis (Panel A), dermis (Panel B), globally in the skin (Panel C) and the amount permeated through the skin (Panel D), in comparison with the data obtained from the reference FA solution (12.5 mg/ml).

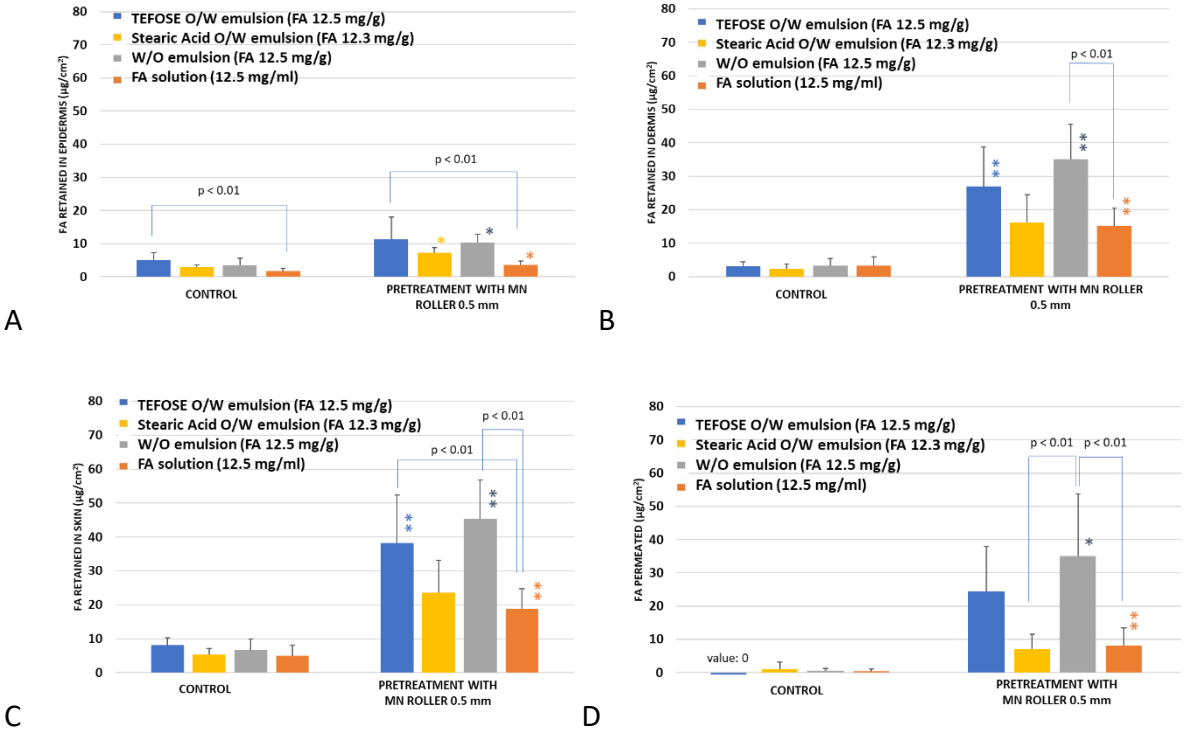

*Figure 41: Amount of FA retained in epidermis (A), dermis (B), globally in the skin (Panel C) and permeated through the skin (Panel D) after 6 h in vitro permeation experiments after the application of the emulsions in infinite dose conditions, in comparison with the application of the solution. All the data are expressed as mean ± SD; n ≥ 4. *: p < 0.01 and **: p < 0.001, compared to control.*

In general, 0.5 mm MN roller application improved epidermis and dermis retention and skin permeation compared to the respective controls, although the difference was not always statistically significant.

Considering the amount found in epidermis (Panel A), the pretreatment of the skin with 0.5 mm MN rollers produced retention significantly different from the respective control for all formulations tested, except for the TEFOSE® O/W emulsion. While considering the amount of FA found in dermis (Panel B), it was comparable for the three formulations tested in passive conditions, whereas a difference was evident after MN pre-treatment: TEFOSE® O/W and W/O emulsions resulted significantly superior to FA solution ($p < 0.01$). A similar trend was maintained considering the overall skin retention (Panel C).

The passive application of the emulsions in the skin led to a very small (or no) permeation of the drug, while the pretreatment with MN roller increased a lot the amount found in receptor fluid, except for TEFOSE® O/W emulsion, which resulted not significative different from the solution.

The latter shows a better performance compared to FA solution both in passive conditions and after MN pretreatment ($p < 0.01$).

4.1.4 Soluble Microneedle Arrays

Among the different strategies for improving dermal application, nanocrystals of folic acid, formulated as colloidal suspension (nanosuspension) were selected to overcome the problem related to solubility of this drug and to exploit of the advantages associated to nanosized components. In fact, the overall impact on the improvement of the drug's skin penetration of nanocrystals is related to an increase in the drug saturation solubility, to a faster dissolution process related to an increased particle surface area and to a greater adherence to the skin [132] [133].

Soluble microneedles containing FA nanosuspension were tested in conditions comparable to the reference formulation. In particular, two different arrays were used, with 0.5 and 0.8 mm microneedles. For comparison purposes, FA-nanosuspension disks were tested as well, both in passive conditions and after 0.5 mm MN roller pretreatment (4 passes).

Figure 42 shows the amount of FA retained in skin layers after 6 h permeation experiments (FA was never detected in receptor fluid for all the conditions tested).

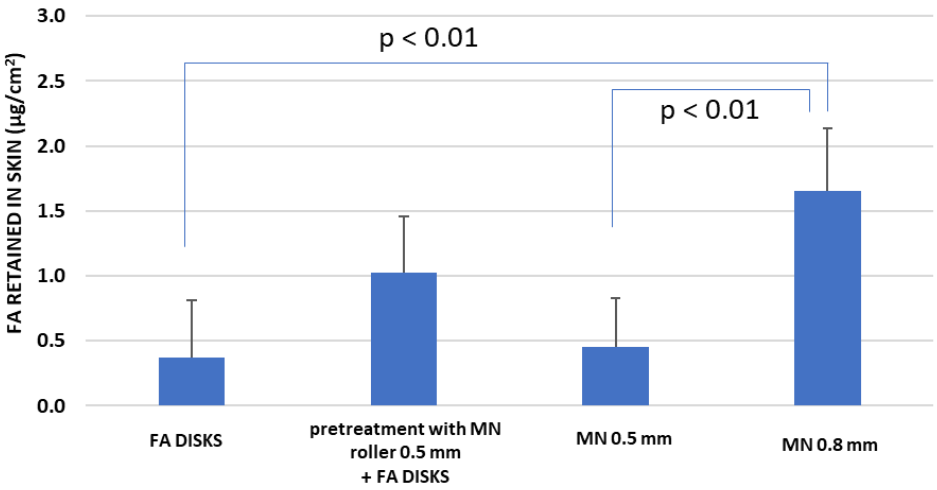

Figure 42: Amount of FA retained in the skin after 6 h permeation experiments after the application of the FA disks (with and without MN roller pretreatment) and the application of MNs 0.5 and 0.8 mm. Data expressed as mean ± SD. N:4

The results obtained demonstrate that after the application of FA-nanosuspension disks, a small amount of folic acid was anyway able to deposit in the skin, even in passive condition, probably because of the presence of nanocrystals. This amount increases in the condition of the pretreatment of the skin, due to the presence of micro wounds created in the tissue.

Considering microneedles arrays application, an increase in drug retention after the application of 0.8 mm microneedles is observed. Indeed, despite using the same amount of FA-nanosuspension/PVP dispersion for the fabrication of both 0.5 mm and 0.8 mm microneedle arrays, it is conceivable that the structural differences in the two molds may result in distinct drug deposition patterns within the array/patch. In the case of the 0.5 mm samples, the FA-nanosuspension/PVP dispersion filled the needles, and any excess formed a thin layer above them. This excess, situated in the non-invasive part of the array, could not deposit in the skin layers. In contrast, the needle tips in the 0.8 mm molds could accommodate the entire volume of FA-nanosuspension/PVP dispersion, with minimal or no excess remaining to create the aforementioned layer [132]. Therefore, when the 0.8 mm microneedle arrays were applied on the skin, a higher amount ($p < 0.01$) of the loaded drug could penetrate in the skin's layers since it was more efficiently located in the needle tips.

Very surprisingly, the result obtained by pretreating the skin with MN roller, followed by FA disks application was higher compared to the application of soluble MN of the same length, although not statistically significant. A possible explanation is that the number of micro wounds created following the 4 passes of MN roller is greater than after the application of dissolvable microneedles. Furthermore, microneedles mounted on the roller are made of stainless-steel and are probably sharper than those present in the arrays, made of PVP.

4.2 Methotrexate

To assess the similarity of *in vitro* skin distribution of FA and MTX, the TEFOSE® O/W emulsion was prepared with MTX, at the same concentration as FA (12.5 mg/g) and tested in infinite dose conditions. The bar graphs in Figure 43 report the amount of FA (expressed as µg/cm^2) retained in epidermis (Panel A), in dermis (Panel B), globally in the skin (Panel C) and permeated through the skin (Panel D).

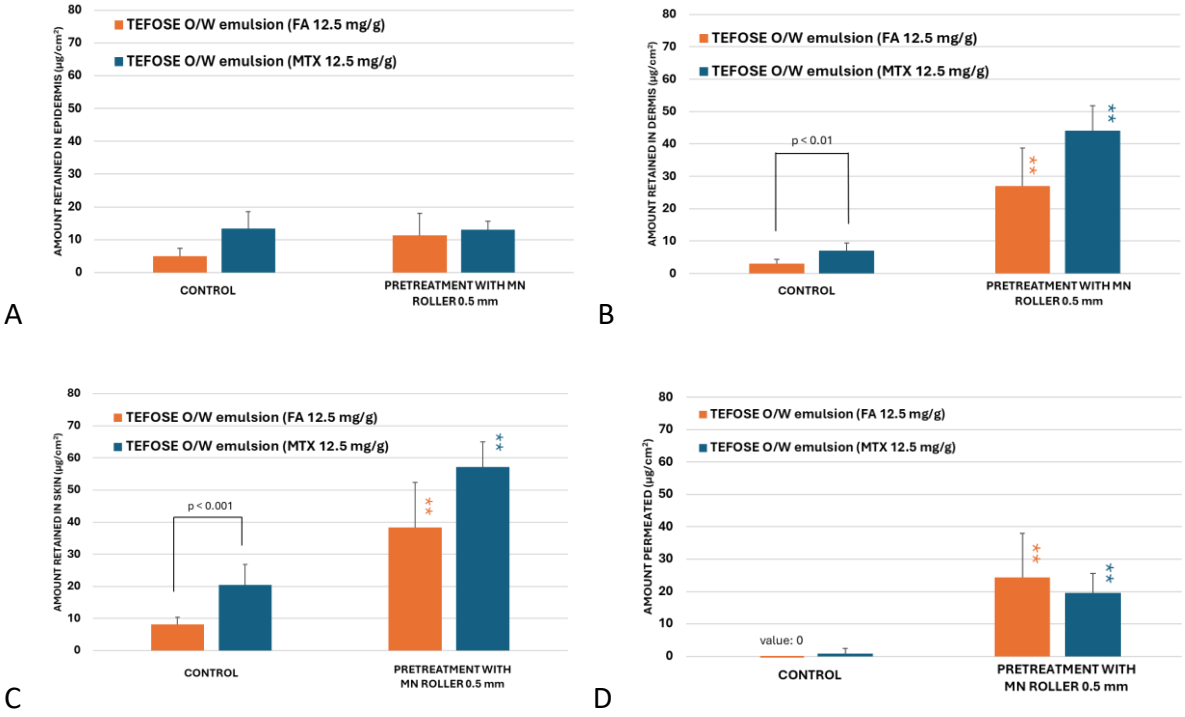

*Figure 43: Amount of FA or MTX retained in epidermis (A), dermis (B), globally in the skin (C) and permeated through the skin (D) expressed as µg/cm^2 after 6 h permeation experiments in infinite dose conditions (92 mg/cm^2) in the presence of the TEFOSE® O/W emulsion. All data are expressed as mean ± SD. N ≥ 5. *: p < 0.01 and **: p < 0.001, compared to control.*

From the results shown in Figure 43, the amount of MTX accumulated in passive condition (epidermis, dermis and overall skin) was slightly but significantly higher compared to FA – a trend that has already been observed in preliminary experiments with solution (see Results paragraph 2.0). This difference can be justified by considering the slightly different physicochemical characteristics, which lead to a slightly different interaction of the molecules with the stratum corneum. The difference between MTX and FA are less pronounced, and not statistically significant, in the presence of MN pre-treatment. Probably, the partial disruption of the stratum corneum allows for the formation of aqueous channels, that represent a preferential penetration pathway.

Considering the amount permeated, it was zero, or close to zero, in passive condition and increased to the same extent for the two drugs with MN pre-treatment.

CONCLUSIONS

Innovative formulations for the topical administration of methotrexate in a non-invasive or minimally invasive way, to treat non melanoma skin cancers, were developed. The project was carried out through 4 main objectives:

The *first objective* was to set up a suitable extraction method to quantify methotrexate in the skin (epidermis and dermis). Considering the hydrophilic nature of the molecule, the extraction procedure posed a serious problem and the use of a suitable internal standard (folic acid) resulted necessary to reach the quantitative recovery of the drug.

Given methotrexate toxicity, the attention moved to the identification of a model drug to be used for preliminary investigations (*second objective*): based on similar physicochemical characteristics, folic acid was selected and an extraction method for its quantification in skin layers was developed, using methotrexate as internal standard. Preliminary *in vitro* permeation experiments conducted applying solutions of the two drugs showed that there were no significative differences in the amounts of drug retained and permeated, confirming the possibility to use folic acid as a model drug for preliminary investigations. The high data variability might be explained by considering the different tropism of both folic acid and methotrexate for hair follicles, which are differently distributed in biological samples. The analysis conducted using the two-photon microscopy technique after a folic acid solution application seems to support its retention in the hair follicle. However, further studies will be necessary to better investigate the preferential accumulation of folic acid in hair follicles.

The *third objective* was to test a minimally invasive technique to improve skin retention of folic acid. The use of microneedle rollers was selected as a possible simple strategy to improve the drug retention in skin tissues bypassing the stratum corneum barrier. The effect of number of passes of microneedle roller was investigated, as well as the effect of needle lengths: based on data obtained, 4 passes along a single axis of microneedle roller 0.5 mm resulted as the best options to maximize drug retention and minimize drug permeation through the skin. The effect of the application time (2 or 6 hours) was also considered and 6 hours were selected as more similar to the residence time *in vivo* of a formulation applied to the skin.

Since the application of a solution is not suitable for clinical treatment, the *fourth objective* was to develop topical formulations for the delivery of folic acid to the skin. Among all, topical films mainly based on hydrophilic polymers PVA and PVP, were chosen because of the easy preparation and good technological properties. However, although the physical characteristics were satisfactory, their adhesion properties were not suitable for skin application. Films containing PLASTOID® were then formulated and tested *in vitro*, but the results were not satisfactory, not even in the presence of a pretreatment with microneedle roller.

Therefore, the attention moved to semisolid systems like hydrogels and emulsions. PVA- and PVP-based hydrogels and Carbopol® containing hydrogels were developed, characterized and tested, also in the presence of pretreatment of the skin. The results were encouraging, although worse compared to the application of a solution. Then, biphasic formulations such as O/W and W/O emulsions were considered. After their preparation, these formulations were applied on the skin, with and without the pretreatment with 4 passes of microneedle roller 0.5 mm. The results showed that one specific formulation (TEFOSE® O/W emulsion) applied after a pretreatment with microneedle roller, guaranteed a retention of drug in skin over than 35 μg/cm^2, much higher than the reference solution, without increasing significantly the amount permeated.

To overcome the solubility problems of folic acid, a nanosuspension of folic acid in water was prepared and used for fabricating soluble microneedles arrays (0.5 and 0.8 mm) made of PVP. As expected, 0.8 mm resulted more effective than 0.5 mm microneedles, although the overall amount recovered was lower compared to the previous conditions tested. For comparison purposes, the suspension used for microneedles arrays preparation was dried also in the form of discs. The application of dried discs to the skin produced a very limited skin retention of folic acid, that was only slightly improved by microneedles roller pretreatment.

Finally, the best performing formulation (TEFOSE® O/W emulsion) was replicated with the active ingredient methotrexate at the same concentration: the results obtained were comparable for the two drugs, confirming that all the data produced with folic acid can be reasonably extended to methotrexate.

The general conclusion of this work is that the topical administration of methotrexate, to be used as an alternative of intradermal injection, can be realized by combining a traditional formulation (such as an emulsion) with a minimally invasive technique, such as skin pretreatment with microneedles.

REFERENCES

[1] "'Skin Cancer', International Agency for Research on Cancer. https://www.iarc.who.int/cancer-type/skin-cancer (accessed Dec. 10, 2023)."

[2] "'Skin Cancer, Facts & Statistics'. Skin Cancer Foundation. https://www.skincancer.org/skin-cancer-information/skin-cancer-facts (accessed Oct. 15, 2023)."

[3] D. L. Narayanan, R. N. Saladi, and J. L. Fox, "Ultraviolet radiation and skin cancer," *Int. J. Dermatol.*, vol. 49, no. 9, pp. 978–986, 2010, doi: 10.1111/j.1365-4632.2010.04474.x.

[4] "P. M. Zito; R. Scharf, Keratoachantoma, StatPearls [Internet]. Treasure Island (FL): StatPearls Publishing; last update: Aug. 8, 2023."

[5] A. M. Vîlcea *et al.*, "Clinical, histopathological and immunohistochemical study of keratoacanthoma," *Rom. J. Morphol. Embryol.*, vol. 62, no. 2, pp. 445–456, Apr. 2021, doi: 10.47162/RJME.62.2.10.

[6] P. Nagarajan, "Differentiating keratoacanthoma from squamous cell carcinoma—In quest of the holy grail," *J. Cutan. Pathol.*, vol. 47, no. 4, pp. 418–420, Apr. 2020, doi: 10.1111/CUP.13640.

[7] A. Nirenberg, H. Steinman, and A. Dixon, "Keratoacanthoma: Update on the Debate," *Am. J. Dermatopathol.*, vol. 43, no. 4, pp. 305–307, Apr. 2021, doi: 10.1097/DAD.0000000000001872.

[8] "'How Dangerous is Melanoma? It's All a Matter of Timing'. Skin Cancer Foundation. https://www.skincancer.org/blog/dangerous-melanoma-matter-timing.(accessed Oct. 20, 2023)."

[9] "'Melanoma Overview. A Dangerous Skin Cancer'. Skin Cancer Foundation. https://www.skincancer.org/skin-cancer-information/melanoma. (accessed Oct. 20, 2023)."

[10] M. J. Eide *et al.*, "Identification of patients with nonmelanoma skin cancer using health maintenance organization claims data," *Am. J. Epidemiol.*, vol. 171, no. 1, pp. 123–128, 2010, doi: 10.1093/aje/kwp352.

[11] J. P. Malone, F. G. Fedok, D. A. Belchis, and M. E. Maloney, "Basal cell carcinoma metastatic to the parotid: Report of a new case and review of the literature," *Ear, Nose Throat J.*, vol. 79, no. 7, pp. 511–515, 2000, doi: 10.1177/014556130007900710.

[12] B. S. Cherpelis, C. Marcusen, and P. G. Lang, "Prognostic factors for metastasis in squamous cell carcinoma of the skin," *Dermatologic Surg.*, vol. 28, no. 3, pp. 268–273, 2002, doi: 10.1046/j.1524-4725.2002.01169.x.

[13] M. Ciążyńska *et al.*, "The incidence and clinical analysis of non-melanoma skin cancer," *Sci. Rep.*, vol. 11, no. 1, pp. 1–10, 2021, doi: 10.1038/s41598-021-83502-8.

[14] C. F. Baez *et al.*, "Investigation of three oncogenic epitheliotropic viruses shows human papillomavirus in association with non-melanoma skin cancer," *Eur. J. Clin. Microbiol. Infect. Dis.*, vol. 38, no. 6, pp. 1129–1133, Jun. 2019, doi: 10.1007/S10096-019-03508-Z/TABLES/2.

[15] T. Amaral and C. Garbe, "Non-melanoma skin cancer: new and future synthetic drug

treatments," *Expert Opin. Pharmacother.*, vol. 18, no. 7, pp. 689–699, 2017, doi: 10.1080/14656566.2017.1316372.

[16] S. Benkhaled, D. Van Gestel, C. Gomes da Silveira Cauduro, S. Palumbo, V. del Marmol, and A. Desmet, "The State of the Art of Radiotherapy for Non-melanoma Skin Cancer: A Review of the Literature," *Front. Med.*, vol. 9, no. June, pp. 1–12, 2022, doi: 10.3389/fmed.2022.913269.

[17] M. Xiang *et al.*, "A Review of Light Sources and Enhanced Targeting for Photodynamic Therapy," *Curr. Med. Chem.*, vol. 28, no. 31, pp. 6437–6457, 2021, doi: 10.2174/0929867328666210121122106.

[18] L. L. Griffin, A. Faisal, R. Ali, and J. T. Lear, "Non-melanoma skin cancer," *C. DERMATOLOGY Clin. Med.*, vol. 16, no. 1, pp. 62–67, 2016.

[19] L. R. Braathen *et al.*, "Guidelines on the use of photodynamic therapy for nonmelanoma skin cancer: An international consensus," *J. Am. Acad. Dermatol.*, vol. 56, no. 1, pp. 125–143, 2007, doi: 10.1016/j.jaad.2006.06.006.

[20] L. A. Fecher, "Systemic therapy for inoperable and metastatic basal cell cancer," *Curr. Treat. Options Oncol.*, vol. 14, no. 2, pp. 237–248, 2013, doi: 10.1007/s11864-013-0233-9.

[21] "Pfeiffer P, Hansen O, Rose C. Systemic cytotoxic therapy of basal cell carcinoma. A review of the literature. Eur J Cancer. 1990 Jan;26(1):73-7. doi: 10.1016/0277-5379(90)90262-r. PMID: 2138485."

[22] K. Moeholt, H. Aagaard, P. Pfeiffer, and O. Hansen, "Platinum-based cytotoxic therapy in basal cell carcinoma. A review of the literature," *Acta Oncol. (Madr).*, vol. 35, no. 6, pp. 677–682, 1996, doi: 10.3109/02841869609083998.

[23] A. Fahradyan, A. C. Howell, E. M. Wolfswinkel, M. Tsuha, P. Sheth, and A. K. Wong, "Updates on the management of non-melanoma skin cancer (Nmsc)," *Healthc.*, vol. 5, no. 4, pp. 9–11, 2017, doi: 10.3390/healthcare5040082.

[24] R. Dummer *et al.*, "Sonidegib and vismodegib in the treatment of patients with locally advanced basal cell carcinoma: a joint expert opinion," *J. Eur. Acad. Dermatology Venereol.*, vol. 34, no. 9, pp. 1944–1956, 2020, doi: 10.1111/jdv.16230.

[25] A. M. van Huizen *et al.*, "On which evidence can we rely when prescribing off-label methotrexate in dermatological practice?-a systematic review with GRADE approach," *J. Dermatolog. Treat.*, vol. 33, no. 4, pp. 1947–1966, 2022, doi: 10.1080/09546634.2021.1961999.

[26] T. Searle, F. R. Ali, and F. Al-Niaimi, "Intralesional methotrexate in dermatology: Diverse indications and practical considerations," *Dermatol. Ther.*, vol. 34, no. 1, Jan. 2021, doi: 10.1111/DTH.14404.

[27] F. C. Saporito and M. A. Menter, "Methotrexate and psoriasis in the era of new biologic agents," *J. Am. Acad. Dermatol.*, vol. 50, no. 2, pp. 301–309, 2004, doi: 10.1016/S0190-9622(03)00803-X.

[28] D. Aickara, A. M. Bashyam, R. O. Pichardo, and S. R. Feldman, "Topical methotrexate in

dermatology: a review of the literature," *J. Dermatolog. Treat.*, 2020, doi: 10.1080/09546634.2020.1770170.

[29] P. Rajitha, R. Biswas, M. Sabitha, and R. Jayakumar, "Methotrexate in the Treatment of Psoriasis and Rheumatoid Arthritis: Mechanistic Insights, Current Issues and Novel Delivery Approaches," *Curr. Pharm. Des.*, vol. 23, no. 24, pp. 3550–3566, 2017, doi: 10.2174/1381612823666170601105439.

[30] C. Smith, D. Srivastava, and R. I. Nijhawan, "Intralesional methotrexate for keratoacanthomas: A retrospective cohort study," *J. Am. Acad. Dermatol.*, vol. 83, no. 3, pp. 904–905, 2020, doi: 10.1016/j.jaad.2020.03.096.

[31] J. L. Melton, B. R. Nelson, D. B. Stough, M. D. Brown, N. A. Swanson, and T. M. Johnson, "Treatment of keratoacanthomas with intralesional methotrexate," *J. Am. Acad. Dermatol.*, vol. 25, no. 6, pp. 1017–1023, 1991, doi: 10.1016/0190-9622(91)70301-H.

[32] N. Aubut, J. Alain, and J. Claveau, "Intralesional Methotrexate Treatment for Keratoacanthoma Tumors: A Retrospective Case Series," *J. Cutan. Med. Surg.*, vol. 16, no. 3, pp. 212–217, 2012, doi: 10.1177/120347541201600316.

[33] M. Scalvenzi *et al.*, "Intralesional Methotrexate for the Treatment of Keratoacanthoma: The Neapolitan Experience," *Dermatol. Ther. (Heidelb).*, vol. 9, no. 2, pp. 369–372, 2019, doi: 10.1007/s13555-019-0286-1.

[34] M. G. Yoo and I. H. Kim, "Intralesional methotrexate for the treatment of keratoacanthoma: retrospective study and review of the korean literature," *Ann. Dermatol.*, vol. 26, no. 2, pp. 172–176, 2014, doi: 10.5021/AD.2014.26.2.172.

[35] N. P. Patel and A. L. Cervino, "Treatment of Keratoacanthoma: Is Intralesional Methotrexate An Option?," *http://dx.doi.org/10.1177/229255031101900209*, vol. 19, no. 2, pp. 15–18, Jun. 2011, doi: 10.1177/229255031101900209.

[36] J. M. Kremer, "Methotrexate pharmacogenomics," *Ann. Rheum. Dis.*, vol. 65, no. 9, pp. 1121–1123, 2006, doi: 10.1136/ard.2006.051789.

[37] N. M. Annest, M. J. VanBeek, C. J. Arpey, and D. C. Whitaker, "Intralesional methotrexate treatment for keratoacanthoma tumors: A retrospective study and review of the literature," *J. Am. Acad. Dermatol.*, vol. 56, no. 6, pp. 989–993, Jun. 2007, doi: 10.1016/J.JAAD.2006.12.017.

[38] J. K. Cullen, J. L. Simmons, P. G. Parsons, and G. M. Boyle, "Topical treatments for skin cancer," *Adv. Drug Deliv. Rev.*, vol. 153, pp. 54–64, 2020, doi: 10.1016/j.addr.2019.11.002.

[39] A. H. M. M. Arits *et al.*, "Photodynamic therapy versus topical imiquimod versus topical fluorouracil for treatment of superficial basal-cell carcinoma: A single blind, non-inferiority, randomised controlled trial," *Lancet Oncol.*, vol. 14, no. 7, pp. 647–654, 2013, doi: 10.1016/S1470-2045(13)70143-8.

[40] G. Siller, R. Rosen, M. Freeman, P. Welburn, J. Katsamas, and S. M. Ogbourne, "PEP005 (ingenol mebutate) gel for the topical treatment of superficial basal cell carcinoma: Results of a randomized phase IIa trial," *Australas. J. Dermatol.*, vol. 51, no. 2, pp. 99–105, 2010, doi: 10.1111/j.1440-0960.2010.00626.x.

[41] S. Aditya and S. Gupta, “Ingenol mebutate: A novel topical drug for actinic keratosis,” *Indian Dermatol. Online J.*, vol. 4, no. 3, p. 246, 2013, doi: 10.4103/2229-5178.115538.

[42] A. Collins, J. Savas, and L. Doerfler, “Nonsurgical Treatments for Nonmelanoma Skin Cancer,” *Dermatol. Clin.*, vol. 37, no. 4, pp. 435–441, 2019, doi: 10.1016/j.det.2019.05.003.

[43] B. Ramchatesingh *et al.*, “The Use of Retinoids for the Prevention and Treatment of Skin Cancers: An Updated Review,” *Int. J. Mol. Sci.*, vol. 23, no. 20, 2022, doi: 10.3390/ijms232012622.

[44] “J. L. N. Frederic H. Martini, Robert B. Tallitsch, Human Anatomy, 9th edition., Pearson Education, 2017.”

[45] J. A. McGrath and J. Uitto, “Anatomy and Organization of Human Skin,” *Rook’s Textb. Dermatology Eighth Ed.*, vol. 1, pp. 34–86, 2010, doi: 10.1002/9781444317633.ch3.

[46] J. Khavkin and D. A. F. Ellis, “Aging Skin: Histology, Physiology, and Pathology,” *Facial Plast. Surg. Clin. North Am.*, vol. 19, no. 2, pp. 229–234, 2011, doi: 10.1016/j.fsc.2011.04.003.

[47] A. L. Cunningham, A. Abendroth, C. Jones, N. Nasr, and S. Turville, “Viruses and Langerhans cells,” *Immunol. Cell Biol.*, vol. 88, no. 4, pp. 416–423, 2010, doi: 10.1038/icb.2010.42.

[48] B. H. Thiers, J. C. Maize, S. S. Spicer, and A. B. Cantor, “The effect of aging and chronic sun exposure on human Langerhans cell populations,” *Journal of Investigative Dermatology*, vol. 82, no. 3. pp. 223–226, 1984, doi: 10.1111/1523-1747.ep12260055.

[49] “Biga L. M., Anatomy & Physiology, 2019 (online version book). “https://open.oregonstate.education/aandp/chapter/5-1-layers-of-the-skin (accessed Oct. 23, 2023).”

[50] J. E. Lai-Cheong and J. A. McGrath, “Structure and function of skin, hair and nails,” *Med. (United Kingdom)*, vol. 41, no. 6, pp. 317–320, 2013, doi: 10.1016/j.mpmed.2013.04.017.

[51] E. Dellambra and G. P. Dimri, “Cellular Senescence and Skin Aging,” *Skin Aging Handbook: An Integrated Approach to Biochemistry and Product Development*. pp. 129–148, 2008, doi: 10.1016/B978-0-8155-1584-5.50011-9.

[52] “T. M. Brown; K. Krishnamurthy, Hystology, Dermis, StatPearls [Internet], last update: Nov. 14, 2022.”

[53] Y. Q. Yu, X. Yang, X. F. Wu, and Y. Bin Fan, “Enhancing Permeation of Drug Molecules Across the Skin via Delivery in Nanocarriers: Novel Strategies for Effective Transdermal Applications,” *Front. Bioeng. Biotechnol.*, vol. 9, p. 646554, Mar. 2021, doi: 10.3389/FBIOE.2021.646554/BIBTEX.

[54] D. Ramadon, M. T. C. McCrudden, A. J. Courtenay, and R. F. Donnelly, “Enhancement strategies for transdermal drug delivery systems: current trends and applications,” *Drug Deliv. Transl. Res.*, vol. 12, no. 4, pp. 758–791, 2022, doi: 10.1007/s13346-021-00909-6.

[55] T. N. T. Tran, “Cutaneous Drug Delivery: An Update,” *J. Investig. Dermatology Symp. Proc.*, vol. 16, no. 1, pp. S67–S69, 2013, doi: 10.1038/jidsymp.2013.28.

[56] S. Mitragotri, “Modeling skin permeability to hydrophilic and hydrophobic solutes based on four permeation pathways,” *J. Control. Release*, vol. 86, no. 1, pp. 69–92, Jan. 2003, doi: 10.1016/S0168-3659(02)00321-8.

[57] “B. W. Barry, ‘Drug delivery routes in skin: A novel approach,’ Adv. Drug Deliv. Rev., vol. 54, no. SUPPL., pp. 31–40, 2002, doi: 10.1016/S0169-409X(02)00113-8.”

[58] M. S. Roberts *et al.*, “Topical drug delivery: History, percutaneous absorption, and product development,” *Advanced Drug Delivery Reviews*, vol. 177. 2021, doi: 10.1016/j.addr.2021.113929.

[59] T. Garg, G. Rath, and A. K. Goyal, “Drug Delivery Comprehensive review on additives of topical dosage forms for drug delivery Comprehensive review on additives of topical dosage forms for drug delivery,” *Drug Deliv*, vol. 22, no. 8, pp. 969–987, 2015, doi: 10.3109/10717544.2013.879355.

[60] S. Karki, H. Kim, S. J. Na, D. Shin, K. Jo, and J. Lee, “Thin films as an emerging platform for drug delivery,” *Asian J. Pharm. Sci.*, vol. 11, no. 5, pp. 559–574, 2016, doi: 10.1016/j.ajps.2016.05.004.

[61] R. Guo, X. Du, R. Zhang, L. Deng, A. Dong, and J. Zhang, “Bioadhesive film formed from a novel organic-inorganic hybrid gel for transdermal drug delivery system,” *Eur. J. Pharm. Biopharm.*, vol. 79, no. 3, pp. 574–583, 2011, doi: 10.1016/j.ejpb.2011.06.006.

[62] C. Padula, S. Nicoli, P. Colombo, and P. Santi, “Single-layer transdermal film containing lidocaine: Modulation of drug release,” *Eur. J. Pharm. Biopharm.*, vol. 66, no. 3, pp. 422–428, Jun. 2007, doi: 10.1016/J.EJPB.2006.11.014.

[63] C. Padula, G. Colombo, S. Nicoli, P. L. Catellani, G. Massimo, and P. Santi, “Bioadhesive film for the transdermal delivery of lidocaine: In vitro and in vivo behavior,” *J. Control. Release*, vol. 88, no. 2, pp. 277–285, Mar. 2003, doi: 10.1016/S0168-3659(03)00015-4.

[64] S. Jacob, A. B. Nair, J. Shah, N. Sreeharsha, S. Gupta, and P. Shinu, “Emerging Role of Hydrogels in Drug Delivery Systems , Tissue Engineering and Wound Management,” 2021.

[65] G. W. Lu and P. Gao, *Emulsions an1. Lu GW, Gao P. Emulsions and Microemulsions for Topical and Transdermal Drug Delivery. Handbook of Non-Invasive Drug Delivery Systems. 2010. 59–94 p. d Microemulsions for Topical and Transdermal Drug Delivery*. 2010.

[66] A. Z. Alkilani, M. T. C. McCrudden, and R. F. Donnelly, “Transdermal drug delivery: Innovative pharmaceutical developments based on disruption of the barrier properties of the stratum corneum,” *Pharmaceutics*, vol. 7, no. 4, pp. 438–470, 2015, doi: 10.3390/pharmaceutics7040438.

[67] S. Mitragotri, “Devices for overcoming biological barriers: The use of physical forces to disrupt the barriers,” *Adv. Drug Deliv. Rev.*, vol. 65, no. 1, pp. 100–103, 2013, doi: 10.1016/j.addr.2012.07.016.

[68] F. Hafeez and H. Maibach, “Occlusion effect on in vivo percutaneous penetration of chemicals in man and monkey: Partition coefficient effects,” *Skin Pharmacol. Physiol.*, vol. 26, no. 2, pp. 85–91, 2013, doi: 10.1159/000346273.

[69] H. Zhai and H. I. Maibach, “Occlusion vs. skin barrier function,” *Ski. Res. Technol.*, vol. 8, no. 1, pp. 1–6, 2002, doi: 10.1046/j.0909-752x.2001.10311.x.

[70] V. R. Leite-Silva, M. M. De Almeida, A. Fradin, J. E. Grice, and M. S. Roberts, “Delivery of drugs applied topically to the skin,” *Expert Rev. Dermatol.*, vol. 7, no. 4, pp. 383–397, 2012, doi: 10.1586/edm.12.32.

[71] T. M. Barnes, D. Mijaljica, J. P. Townley, F. Spada, and I. P. Harrison, “Vehicles for drug delivery and cosmetic moisturizers: Review and comparison,” *Pharmaceutics*, vol. 13, no. 12, 2021, doi: 10.3390/pharmaceutics13122012.

[72] J. E. Grice, S. Ciotti, N. Weiner, P. Lockwood, S. E. Cross, and M. S. Roberts, “Relative uptake of minoxidil into appendages and stratum corneum and permeation through human skin in vitro,” *J. Pharm. Sci.*, vol. 99, no. 2, pp. 712–718, 2010, doi: 10.1002/jps.21856.

[73] T. C. De Oliveira, M. E. V Tavares, J. L. Soares-Sobrinho, and L. L. Chaves, “The role of nanocarriers for transdermal application targeted to lymphatic drug delivery: Opportunities and challenges,” *J. Drug Deliv. Sci. Technol.*, vol. 68, p. 103110, 2022, doi: 10.1016/j.jddst.2022.103110.

[74] R. R. Wakaskar, “Polymeric Micelles and their Properties,” *J. Nanomed. Nanotechnol.*, vol. 08, no. 02, 2017, doi: 10.4172/2157-7439.1000433.

[75] J. Escobar-Chavez *et al.*, “Nanocarriers for transdermal drug delivery,” *Res. Reports Transdermal Drug Deliv.*, no. November, p. 3, 2012, doi: 10.2147/rrtd.s32621.

[76] W. Y. Jeong, M. Kwon, H. E. Choi, and K. S. Kim, “Recent advances in transdermal drug delivery systems: a review,” *Biomater. Res.*, vol. 25, no. 1, pp. 1–15, 2021, doi: 10.1186/s40824-021-00226-6.

[77] E. Touitou, M. Alkabes, N. Dayan, and M. Eliaz, “Ethosomes: novel vesicular carriers for enhanced delivery,” *Pharmaceutical development and technology*, vol. 14. pp. S305–S306, 1997.

[78] 2 Aleksandra Zieli ´nska 1 *et al.*, “Polymeric Nanoparticles: Production, Characterization, Toxicology and Ecotoxicology,” *Molecules*, vol. 25, p. 3731, 2020.

[79] M. E. Lane, “Nanoparticles and the skin applications and limitations,” *J. Microencapsul.*, vol. 28, no. 8, pp. 709–716, 2011, doi: 10.3109/02652048.2011.599440.

[80] P. Ghasemiyeh and S. Mohammadi-Samani, “Solid lipid nanoparticles and nanostructured lipid carriers as novel drug delivery systems: Applications, advantages and disadvantages,” *Res. Pharm. Sci.*, vol. 13, no. 4, pp. 288–303, 2018, doi: 10.4103/1735-5362.235156.

[81] M. Nikzamir, Y. Hanifehpour, A. Akbarzadeh, and Y. Panahi, “Applications of Dendrimers in Nanomedicine and Drug Delivery: A Review,” *J. Inorg. Organomet. Polym. Mater.*, vol. 31, no. 6, pp. 2246–2261, 2021, doi: 10.1007/s10904-021-01925-2.

[82] K. S. Paudel1, M. Milewski1, C. L. Swadley1, N. K. Brogden1, P. Ghosh1, and & A. L. Stinchcomb, "Challenges and opportunities in dermal/transdermal delivery," *Ther. Deliv.*, 2010.

[83] A. Kováčik, M. Kopečná, and K. Vávrová, "Permeation enhancers in transdermal drug delivery: benefits and limitations," *Expert Opin. Drug Deliv.*, vol. 17, no. 2, pp. 145–155, 2020, doi: 10.1080/17425247.2020.1713087.

[84] P. Karande and S. Mitragotri, "Enhancement of transdermal drug delivery via synergistic action of chemicals," *Biochim. Biophys. Acta - Biomembr.*, vol. 1788, no. 11, pp. 2362–2373, 2009, doi: 10.1016/j.bbamem.2009.08.015.

[85] F. M. N. Gajraj, J. Pennant, "Eutectic Mixture of Local Anesthetics (EMLA®) Cream," *Anesth. Analg.*, pp. 574–583, 1994.

[86] E. L. Smith, A. P. Abbott, and K. S. Ryder, "Deep Eutectic Solvents (DESs) and Their Applications," *Chem. Rev.*, vol. 114, no. 21, pp. 11060–11082, 2014, doi: 10.1021/cr300162p.

[87] J. Wang *et al.*, "Deep Eutectic Systems as Novel Vehicles for Assisting Drug Transdermal Delivery," *Pharmaceutics*, vol. 14, no. 11, p. 2265, 2022, doi: 10.3390/pharmaceutics14112265.

[88] S. N. Pedro *et al.*, "Deep Eutectic Solvent Formulations and Alginate-Based Hydrogels as a New Partnership for the Transdermal Administration of Anti-Inflammatory Drugs," *Pharmaceutics*, vol. 14, no. 4, 2022, doi: 10.3390/pharmaceutics14040827.

[89] E. E. L. Tanner, K. N. Ibsen, and S. Mitragotri, "Transdermal insulin delivery using choline-based ionic liquids (CAGE)," *J. Control. Release*, vol. 286, no. April, pp. 137–144, 2018, doi: 10.1016/j.jconrel.2018.07.029.

[90] X. Wu *et al.*, "Improving dermal delivery of hydrophilic macromolecules by biocompatible ionic liquid based on choline and malic acid," *Int. J. Pharm.*, vol. 558, no. November 2018, pp. 380–387, 2019, doi: 10.1016/j.ijpharm.2019.01.021.

[91] A. Mandal *et al.*, "Treatment of psoriasis with NFKBIZ siRNA using topical ionic liquid formulations," *Sci. Adv.*, vol. 6, no. 30, pp. 1–10, 2020, doi: 10.1126/sciadv.abb6049.

[92] K. B. Ita, "Prodrugs for transdermal drug delivery – Trends and challenges," *J. Drug Target.*, vol. 24, no. 8, pp. 671–678, 2016, doi: 10.3109/1061186X.2016.1154562.

[93] S. Indermun *et al.*, "Current advances in the fabrication of microneedles for transdermal delivery," *Journal of Controlled Release*, vol. 185, no. 1. pp. 130–138, 2014, doi: 10.1016/j.jconrel.2014.04.052.

[94] T.-M. T.-M. *et al.*, "Microneedles for intradermal and transdermal drug delivery," *European Journal of Pharmaceutical Sciences*, vol. 50, no. 5. pp. 623–637, 2013.

[95] H. Katsumi *et al.*, "Development of a novel self-dissolving microneedle array of alendronate, a nitrogen-containing bisphosphonate: Evaluation of transdermal absorption, safety, and pharmacological effects after application in rats," *J. Pharm. Sci.*, vol. 101, no. 9, pp. 3230–3238, 2012, doi: 10.1002/jps.23136.

[96] Y. A. Gomaa, M. J. Garland, F. McInnes, L. K. El-Khordagui, C. Wilson, and R. F. Donnelly,

"Laser-engineered dissolving microneedles for active transdermal delivery of nadroparin calcium," *Eur. J. Pharm. Biopharm.*, vol. 82, no. 2, pp. 299–307, 2012, doi: 10.1016/j.ejpb.2012.07.008.

[97] Y. Ito, M. Hirono, K. Fukushima, N. Sugioka, and K. Takada, "Two-layered dissolving microneedles formulated with intermediate-acting insulin," *Int. J. Pharm.*, vol. 436, no. 1–2, pp. 387–393, 2012, doi: 10.1016/j.ijpharm.2012.06.047.

[98] Y. C. Kim, J. H. Park, and M. R. Prausnitz, "Microneedles for drug and vaccine delivery," *Adv. Drug Deliv. Rev.*, vol. 64, no. 14, pp. 1547–1568, 2012, doi: 10.1016/j.addr.2012.04.005.

[99] J. H. Park, S. O. Choi, S. Seo, Y. Bin Choy, and M. R. Prausnitz, "A microneedle roller for transdermal drug delivery," *European Journal of Pharmaceutics and Biopharmaceutics*, vol. 76, no. 2. pp. 282–289, 2010, doi: 10.1016/j.ejpb.2010.07.001.

[100] A. Arora, M. R. Prausnitz, and S. Mitragotri, "Micro-scale devices for transdermal drug delivery," *International Journal of Pharmaceutics*, vol. 364, no. 2. pp. 227–236, 2008, doi: 10.1016/j.ijpharm.2008.08.032.

[101] T. Han and D. B. Das, "Potential of combined ultrasound and microneedles for enhanced transdermal drug permeation: A review," *Eur. J. Pharm. Biopharm.*, vol. 89, pp. 312–328, 2015, doi: 10.1016/j.ejpb.2014.12.020.

[102] S. Mitragotri, "Current status and future prospects of needle-free liquid jet injectors," *Nat. Rev.*, vol. 5, no. Drug Discovery, pp. 543–548.

[103] C. M. Schoellhammer, D. Blankschtein, and R. Langer, "Skin permeabilization for transdermal drug delivery: Recent advances and future prospects," *Expert Opin. Drug Deliv.*, vol. 11, no. 3, pp. 393–407, 2014, doi: 10.1517/17425247.2014.875528.

[104] N. Dixit, V. Bali, S. Baboota, A. Ahuja, and J. Ali, "Iontophoresis - An Approach for Controlled Drug Delivery: A Review," *Curr. Drug Deliv.*, vol. 4, no. 1, pp. 1–10, 2006, doi: 10.2174/156720107779314802.

[105] E. D. Baron *et al.*, "Laser-assisted penetration of topical anesthetic in adults," *Arch. Dermatol.*, vol. 139, no. 10, pp. 1288–1290, 2003, doi: 10.1001/archderm.139.10.1288.

[106] D. L. Dhamecha, V. B. Rajendra, A. A. Rathi, S. V. Ghadlinge, M. Saifee, and M. H. G. Dehghan, "Physical approaches to penetration enhancement," *Int. J. Heal. Res.*, vol. 3, no. 2, pp. 57–70, 2010, doi: 10.4314/ijhr.v3i2.70269.

[107] and M. R. P. Jeong Woo Lee, Priya Gadirajub, Jung-Hwan Parkc, Mark G. Allenb, "Microsecond Thermal Ablation of Skin for Transdermal Drug Delivery," *J Control Release*, 2011.

[108] A. C. Sintov, I. Krymberk, D. Daniel, T. Hannan, Z. Sohn, and G. Levin, "Radiofrequency-driven skin microchanneling as a new way for electrically assisted transdermal delivery of hydrophilic drugs," *J. Control. Release*, vol. 89, no. 2, pp. 311–320, 2003, doi: 10.1016/S0168-3659(03)00123-8.

[109] J. C. Alva-Ensastegui, E. Morales-Avila, A. P. de la Luz, and M. J. Bernad-Bernad, "Determination of pKa values and deprotonation order of methotrexate using a

combined experimental-theoretical study and binding constants of the methotrexate-Laponite complex at different pH values," *J. Photochem. Photobiol. A Chem.*, p. 115406, 2023, doi: https://doi.org/10.1016/j.jphotochem.2023.115406.

[110] Z. Wu, X. Li, C. Hou, and Y. Qian, "Solubility of Folic Acid in Water at pH Values between 0 and 7 at Temperatures (298.15, 303.15, and 313.15) K," doi: 10.1021/je1000268.

[111] A. M. Alambiaga-Caravaca *et al.*, "Development, characterization, and ex vivo evaluation of an insert for the ocular administration of progesterone," *Int. J. Pharm.*, vol. 606, no. July, 2021, doi: 10.1016/j.ijpharm.2021.120921.

[112] C. Balaguer-Fernández, C. Padula, A. Femenía-Font, V. Merino, P. Santi, and A. López-Castellano, "Development and evaluation of occlusive systems employing polyvinyl alcohol for transdermal delivery of sumatriptan succinate," *Drug Deliv.*, vol. 17, no. 2, pp. 83–91, 2010, doi: 10.3109/10717540903509019.

[113] C. Padula, S. Nicoli, and P. Santi, "Innovative formulations for the delivery of levothyroxine to the skin," *Int. J. Pharm.*, vol. 372, no. 1–2, pp. 12–16, 2009, doi: 10.1016/j.ijpharm.2008.12.028.

[114] C. Padula, L. Pozzetti, V. Traversone, S. Nicoli, and P. Santi, "In vitro evaluation of mucoadhesive films for gingival administration of lidocaine," *AAPS PharmSciTech*, vol. 14, no. 4, pp. 1279–1283, 2013, doi: 10.1208/s12249-013-0020-8.

[115] C. Padula *et al.*, "Bioadhesive film for dermal and transdermal drug delivery," *Eur. J. Dermatology*, vol. 17, no. 4, pp. 309–312, 2007, doi: 10.1684/ejd.2007.0205.

[116] L. Giulio, C. Padula, S. Pescina, S. Nicoli, and P. Santi, "Development and validation of a HPLC–UV based method for the extraction and quantification of methotrexate in the skin," *Biomed. Chromatogr.*, p. e5349, 2022, doi: 10.1002/BMC.5349.

[117] E. S. Von Zuben, A. G. Oliveira, M. Chorilli, and M. V. Scarpa, "Development and validation of a rapid reverse-phase HPLC method for the determination of methotrexate from nanostructured liquid crystalline systems," *Pharmazie*, vol. 73, no. 3, pp. 128–132, 2018, doi: 10.1691/ph.2018.7140.

[118] E. Begas, C. Papandreou, A. Tsakalof, D. Daliani, G. Papatsibas, and E. Asprodini, "Simple and reliable HPLC method for the monitoring of methotrexate in osteosarcoma patients," *J. Chromatogr. Sci.*, vol. 52, no. 7, pp. 590–595, 2014, doi: 10.1093/chromsci/bmt081.

[119] Y. D. Li, Y. Li, N. S. Liang, F. Yang, and Z. P. Kuang, "A reversed-phase high performance liquid chromatography method for quantification of methotrexate in cancer patients serum," *J. Chromatogr. B Anal. Technol. Biomed. Life Sci.*, vol. 1002, pp. 107–112, 2015, doi: 10.1016/j.jchromb.2015.08.017.

[120] Raichurvinay and V. Kusum Devi, "Development and validation of a highly sensitive high-performance liquid chromatography (HPLC) method for the estimation of methotrexate (MTX) pure drug and marketed formulation in spiked rat plasma," *Int. J. Pharm. Pharm. Sci.*, vol. 8, no. 3, pp. 313–317, 2016.

[121] M. Uchiyama *et al.*, "Simple and sensitive HPLC method for the fluorometric determination of methotrexate and its major metabolites in human plasma by post-

column photochemical reaction," *Biomed. Chromatogr.*, vol. 26, no. 1, pp. 76–80, Jan. 2012, doi: 10.1002/BMC.1628.

[122] F. Ullah, Z. Iqbal, A. Raza, I. Khan, F. Ullah Khan, and M. Hassan, "Simultaneous determination of methotrexate and metoclopramide in physiological fluids using RP-HPLC with ultra-violet detection; application in evaluation of polymeric nanoparticles," *J. Liq. Chromatogr. Relat. Technol.*, vol. 40, no. 20, pp. 1020–1030, 2017, doi: 10.1080/10826076.2017.1399417.

[123] "PubChem, 'https://pubchem.ncbi.nlm.nih.gov/compound/Methotrexate,'(accessed Nov. 5, 2021)."

[124] "PubChem, 'https://pubchem.ncbi.nlm.nih.gov/compound/Folic-acid,'(accessed Nov. 5, 2021)."

[125] M. A. Hofsäss *et al.*, "Biowaiver Monographs for Immediate-Release Solid Oral Dosage Forms: Folic Acid," *J. Pharm. Sci.*, vol. 106, no. 12, pp. 3421–3430, 2017, doi: 10.1016/j.xphs.2017.08.007.

[126] "Younis IR. Pharmaceutical Quality Performance ofFolic Acid Supplements [master thesis]. Morgantown: West Virginia University; 2003."

[127] K. R. Bellavinha, N. M. Silva-Barcellos, J. B. Souza, J. C. Leite, and J. De Souza, "Folic acid: A biopharmaceutical evaluation," *Pharm. Dev. Technol.*, vol. 20, no. 6, pp. 730–737, Jan. 2015, doi: 10.3109/10837450.2014.920352.

[128] "PubChem, 'https://pubchem.ncbi.nlm.nih.gov/compound/Folinic-acid.'(accessed Oct. 12, 2023)."

[129] L. Binder, J. Mazál, R. Petz, V. Klang, and C. Valenta, "The role of viscosity on skin penetration from cellulose ether-based hydrogels," *Ski. Res. Technol.*, vol. 25, no. 5, pp. 725–734, 2019, doi: 10.1111/srt.12709.

[130] J. H. Park, S. O. Choi, S. Seo, Y. Bin Choy, and M. R. Prausnitz, "A microneedle roller for transdermal drug delivery," *Eur. J. Pharm. Biopharm.*, vol. 76, no. 2, pp. 282–289, 2010, doi: 10.1016/j.ejpb.2010.07.001.

[131] J. Zhang *et al.*, "Microneedle-enabled therapeutics delivery and biosensing in clinical trials," *J. Control. Release*, vol. 360, pp. 168–3659, 2023, doi: 10.1016/j.jconrel.2023.07.023.

[132] L. Casula *et al.*, "Nanosuspension-Based Dissolvable Microneedle Arrays to Enhance Diclofenac Skin Delivery," *Pharmaceutics*, vol. 15, no. 9, 2023, doi: 10.3390/pharmaceutics15092308.

[133] J. Wadhawan, P. K. Parmar, and A. K. Bansal, "Nanocrystals for improved topical delivery of medium soluble drug: A case study of acyclovir," *J. Drug Deliv. Sci. Technol.*, vol. 65, p. 102662, Oct. 2021, doi: 10.1016/J.JDDST.2021.102662.